

1 **Comparative geochemical study on Furongian–earliest Ordovician (Toledanian)**  
2 **and Ordovician (Sardic) felsic magmatic events in south-western Europe:**  
3 **underplating of hot mafic magmas linked to the opening of the Rheic Ocean**

4

5 J. Javier Álvaro<sup>a\*</sup>, Teresa Sánchez-García<sup>b</sup>, Claudia Puddu<sup>c</sup>, Josep Maria Casas<sup>d</sup>,  
6 Alejandro Díez-Montes<sup>e</sup>, Montserrat Liesa<sup>f</sup> & Giacomo Oggiano<sup>g</sup>

7

8 <sup>a</sup> *Instituto de Geociencias (CSIC-UCM), Dr. Severo Ochoa 7, 28040 Madrid, Spain,*  
9 *jj.alvaro@csic.es*

10 <sup>b</sup> *Instituto Geológico y Minero de España, Ríos Rosas 23, 28003 Madrid, Spain,*  
11 *t.sanchez@igme.es*

12 <sup>c</sup> *Dpto. Ciencias de la Tierra, Universidad de Zaragoza, 50009 Zaragoza, Spain,*  
13 *claudiapuddugeo@gmail.com*

14 <sup>d</sup> *Dpt. de Dinàmica de la Terra i de l'Oceà, Universitat de Barcelona, Martí Franquès*  
15 *s/n, 08028 Barcelona, Spain, casas@ub.edu*

16 <sup>e</sup> *Instituto Geológico y Minero de España, Plaza de la Constitución 1, 37001*  
17 *Salamanca, Spain, al.diez@igme.es*

18 <sup>f</sup> *Dept. de Mineralogia, Petrologia i Geologia aplicada, Universitat de Barcelona, Martí*  
19 *Franquès s/n, 08028 Barcelona, Spain, mliesa@ub.edu*

20 <sup>g</sup> *Dipartimento di Scienze della Natura e del Territorio, 07100 Sassari, Italy,*  
21 *giacoggi@uniss.it*

22

23 \* Corresponding author

24

25 **ABSTRACT**

26

27 A geochemical comparison of Early Palaeozoic felsic magmatic episodes throughout  
28 the south-western European margin of Gondwana is made, and includes (i) Furongian–  
29 Early Ordovician (Toledanian) activities recorded in the Central Iberian and Galicia-Trás-  
30 os-Montes Zones of the Iberian Massif, and (ii) Early–Late Ordovician (Sardic) activities  
31 in the eastern Pyrenees, Occitan Domain (Albigeois, Montagne Noire and Mouthoumet  
32 massifs) and Sardinia. Both phases are related to uplift and denudation of an inherited  
33 palaeorelief, and stratigraphically preserved as distinct angular discordances and  
34 paraconformities involving gaps of up to 22 m.y. The geochemical features of the  
35 Toledanian and Sardic, felsic-dominant activities point to a predominance of magmatic  
36 byproducts derived from the melting of metasedimentary rocks, rich in SiO<sub>2</sub> and K<sub>2</sub>O  
37 and with peraluminous character. Zr/TiO<sub>2</sub>, Zr/Nb, Nb/Y and Zr vs. Ga/Al ratios, and  
38 REE and  $\epsilon_{\text{Nd}(t)}$  values suggest the contemporaneity, for both phases, of two  
39 geochemical scenarios characterized by arc and extensional features evolving to  
40 distinct extensional and rifting conditions associated with the final outpouring of mafic  
41 tholeiitic-dominant lava flows. The Toledanian and Sardic magmatic phases are linked  
42 to neither metamorphism nor penetrative deformation; on the contrary, their  
43 unconformities are associated with foliation-free open folds subsequently affected by  
44 the Variscan deformation. The geochemical and structural framework precludes  
45 subduction generated melts reaching the crust in a magmatic arc to back-arc setting,  
46 but favours partial melting of sediments and/or granitoids in a continental lower crust  
47 triggered by the underplating of hot mafic magmas related to the opening of the Rheic  
48 Ocean.

49 **Keywords:** granite, orthogneiss, geochemistry, Cambrian, Ordovician, Gondwana.

50

51

## 52 1. Introduction

53

54 A succession of Early–Palaeozoic magmatic episodes, ranging in age from Furongian  
55 (former “late Cambrian”) to Late Ordovician, is widespread along the south-western  
56 European margin of Gondwana. Magmatic pulses are characterized by preferential  
57 development in different palaeogeographic areas and linked to the development of  
58 stratigraphic unconformities, but they are related to neither metamorphism nor  
59 penetrative deformation (Gutiérrez Marco et al., 2002; Montero et al., 2007). In the  
60 Central Iberian Zone of the Iberian Massif (representing the western branch of the  
61 Ibero-Armorican Arc; Fig. 1A–B), this magmatism is mainly represented by the Ollo de  
62 Sapo Formation, which has long been recognized as a Furongian–Early Ordovician  
63 (495–470 Ma) assemblage of felsic-dominant volcanic, subvolcanic and plutonic  
64 igneous rocks. This magmatic activity is contemporaneous with the development of the  
65 Toledanian Phase, which places Lower Ordovician (upper Tremadocian–Floian) rocks  
66 onlapping an inherited palaeorelief formed by Ediacaran–Cambrian rocks and involving  
67 a sedimentary gap of ca. 22 m.y. This unconformity can be correlated with the  
68 “Furongian gap” identified in the Ossa-Morena Zone of the Iberian Massif and the Anti-  
69 Atlas Ranges of Morocco (Álvaro et al., 2007, 2018; Álvaro and Vizcaíno, 2018;  
70 Sánchez-García et al., 2019), and with the “lacaune normande” in the central and  
71 North-Armorican Domains (Le Corre et al., 1991).

72 Another felsic-dominant magmatic event, although younger (Early–Late Ordovician)  
73 in age, has been recognized in some massifs situated along the eastern branch of the  
74 Variscan Ibero-Armorican Arc, such as the Pyrenees, the Occitan Domain and Sardinia  
75 (Fig. 1A, C–E). This magmatism is related to the Sardinic unconformity, where  
76 Furongian–Lower Ordovician rocks are unconformably overlain by those attributed to  
77 the Sandbian–lower Katian (former Caradoc). The Sardinic Phase is related to both: (i) a  
78 sedimentary gap of ca. 16–20 m.y., and an unconformity that geometrically ranges  
79 from 90° (angular discordance) to 0° (paraconformity) (Barca and Cherchi, 2004;

80 Funneda and Oggiano, 2009; Álvaro et al., 2016, 2018; Casas et al., 2019); and (ii) a  
81 Mid Ordovician development of cleavage-free folds lacking any contemporaneous  
82 metamorphism (for an updated revision, see Casas et al., 2019). The gap is 16-20 m.y.  
83 and the magmatic activity took place during a time span of about 25-30 m.y. (from 475  
84 to 445 Ma) so, both ranges can be considered as broadly contemporaneous.

85 Although a general consensus exists to associate this Furongian–Ordovician  
86 magmatism with the opening of the Rheic Ocean and the drift of Avalonia from  
87 northwestern Gondwana (Díez Montes et al., 2010; Nance et al., 2010; Thomson et al.,  
88 2010; Álvaro et al., 2014a), the origin of this magmatism has received different  
89 interpretations. In the Central Iberian Zone, for instance, several geodynamic models  
90 have been proposed, such as: (i) subduction-related melts reaching the crust in a  
91 magmatic arc to back-arc setting (Valverde-Vaquero and Dunning, 2000; Castro et al.,  
92 2009); (ii) partial melting of sediments or granitoids in a continental lower crust affected  
93 by the underplating of hot mafic magmas during an extensional regime (Bea et al.,  
94 2007; Montero et al., 2009; Díez Montes et al., 2010); and (iii) post-collisional  
95 decompression melting of an earlier thickened continental crust, and without significant  
96 mantle involvement (Villaseca et al., 2016). In the Occitan Domain (southern French  
97 Massif Central and Mouthoumet massifs) and the Pyrenees, Marini (1988), Pouclet et  
98 al. (2017) and Puddu et al. (2019) have suggested a link to mantle thermal anomalies.  
99 Navidad et al. (2018) proposed that the Pyrenean magmatism was induced by  
100 progressive crustal thinning and uplift of lithospheric mantle isotherms. In Sardinia,  
101 Oggiano et al. (2010), Carmignani et al. (2001), Gaggero et al. (2012) and Cruciani et  
102 al. (2018) have suggested that a subduction scenario, mirroring an Andean-type active  
103 margin, caused the main Mid–Ordovician magmatic activity. In the Alps, the Sardinic  
104 counterpart is also interpreted as a result of the collision of the so-called Qaidam Arc  
105 with the Gondwanan margin, subsequently followed by the accretion of the Qilian Block  
106 (Von Raumer and Stampfli, 2008; Von Raumer et al., 2013, 2015). This geodynamic  
107 interpretation is mainly suggested for the Alpine Briançonnais-Austroalpine basement,

108 where the volcanosedimentary complexes postdating the Sardinic tectonic inversion and  
109 folding stage portray a younger arc-arc oblique collision (450 Ma) of the eastern tail of  
110 the internal Alpine margin with the Hun terrane, succeeded by conspicuous exhumation  
111 in a transform margin setting (430 Ma) (Zurbruggen et al., 1997; Schaltegger et al.,  
112 2003; Franz and Romer, 2007; Von Raumer and Stampfli, 2008; Von Raumer et al.,  
113 2013; Zurbruggen, 2015, 2017).

114 Until now the Toledanian and Sardinic magmatic events had been studied on different  
115 areas and interpreted separately, without taking into account their similarities and  
116 differences. In this work, the geochemical affinities of the Furongian–Early Ordovician  
117 (Toledanian) and Early–Late Ordovician (Sardinic) felsic magmatic activities recorded in  
118 the Central Iberian and Galicia-Trás-os-Montes Zones, Pyrenees, Occitan Domain and  
119 Sardinia are compared. The re-appraisal is based on 17 new samples from the  
120 Pyrenees, Montagne Noire and Sardinia, completing the absence of analysis in these  
121 areas and wide-ranging a dataset of 93 previously published geochemical analyses  
122 throughout the study region in south-western Europe. This comparison may contribute  
123 to a better understanding of the meaning and origin of this felsic magmatism, and thus,  
124 to discuss the geodynamic scenario of this Gondwana margin (Fig. 1A) during  
125 Cambrian–Ordovician times, bracketed between the Cadomian and Variscan  
126 orogenies.

127

## 128 **2. Emplacement and age of magmatic events**

129

130 This section documents the emplacement (summarized in Fig. 2) and age (Fig. 3) of  
131 the Toledanian and Sardinic magmatic events throughout the south-western basement  
132 European Variscan Belt, in the northwestern margin of Gondwana during Cambro–  
133 Ordovician times.

134

### 135 **2.1. Iberian Massif**

136

137 In the Ossa Morena and southern Central Iberian Zones of the Iberian Massif (Fig. 1A–  
138 B), the so-called Toledanian Phase is recognized as an angular discordance that  
139 separates variably tilted Ediacaran–Cambrian Series 2 rifting volcanosedimentary  
140 packages from overlying passive-margin successions. The Toledanian gap comprises,  
141 at least, most of the Furongian and basal Ordovician, but the involved erosion can  
142 incise into the entire Cambrian and the upper Ediacaran Cadomian basement  
143 (Gutiérrez-Marco et al., 2019; Álvaro et al., 2019; Sánchez-García et al., 2019).  
144 Recently, Sánchez-García et al. (2019) have interpreted the Toledanian Phase as a  
145 break-up (or rift/drift) unconformity with the Armorican Quartzite (including the Purple  
146 Series and Los Montes Beds; McDougall et al., 1987; Gutiérrez-Alonso et al., 2007;  
147 Shaw et al., 2012, 2014) sealing an inherited Toledanian palaeorelief (Fig. 2).

148 The phase of uplift and denudation of an inherited palaeorelief composed of upper  
149 Ediacaran–Cambrian rocks is associated with the massive outpouring of felsic-  
150 dominant calc-alkaline magmatic episodes related to neither metamorphic nor cleavage  
151 features. This magmatic activity is widely distributed throughout several areas of the  
152 Iberian Massif, such as the Cantabrian Zone and the easternmost flank of the West  
153 Asturian-Leonese Zone, where sills and rhyolitic lava flows and volcanoclastics mark  
154 the base of the Armorican Quartzite (dated at ca. 477.5 Ma; Gutiérrez-Alonso et al.,  
155 2007, 2016), and the lower Tremadocian Borrachón Formation of the Iberian Chains  
156 (Álvaro et al., 2008). Similar ages have been reported from igneous rocks of the Basal  
157 Allochthonous Units and the Schistose Domain in the Galicia-Trás-os-Montes Zone  
158 (500–462 Ma; Valverde-Vaquero et al., 2005, 2007; Montero et al., 2009; Talavera et  
159 al., 2008, 2013; Dias da Silva et al., 2012, 2014; Díez Fernández et al., 2012; Farias et  
160 al., 2014) and different areas of the Central Iberian Zone, including the contact  
161 between the Central Iberian and Ossa-Morena Zones, where the Carrascal and  
162 Portalegre batoliths are intruded and the felsic volcanosedimentary Urra Formation  
163 marks the unconformity that separates Cambrian and Ordovician strata (494–470 Ma,

164 Solá et al., 2008; Antunes et al., 2009; Neiva et al., 2009; Romão et al., 2010; Rubio-  
165 Ordóñez et al., 2012; Villaseca et al., 2013) (Fig. 1B).

166 The most voluminous Toledanian-related volcanic episode is represented by the  
167 Ollo de Sapo Formation, which crops out throughout the northeastern Central Iberian  
168 Zone. It mainly consists of felsic volcanosedimentary and volcanic rocks, interbedded  
169 at the base of the Lower Ordovician strata and plutonic bodies. The Ollo de Sapo  
170 volcanosedimentary Formation has long been recognized as an enigmatic Furongian–  
171 Early Ordovician (495–470 Ma) magmatic event exposed along the core of a 600 km-  
172 long antiform (labelled as 77 in Fig. 1B) (Valverde-Vaquero and Dunning, 2000; Bea et  
173 al., 2006; Montero et al., 2007, 2009; Zeck et al., 2007; Castiñeiras et al., 2008a; Díez  
174 Montes et al., 2010; Navidad and Castiñeiras, 2011; Talavera et al., 2013; López-  
175 Sánchez et al., 2015; Díaz-Alvarado et al., 2016; Villaseca et al., 2016; García-Arias et  
176 al., 2018). The peak of magmatic activity was reached at ca. 490–485 Ma and its most  
177 recognizable characteristic is the presence of abundant megacrysts of K-feldspar,  
178 plagioclase and blue quartz. There is no evident space-time relationship in its  
179 distribution (for a discussion, see López-Sánchez et al., 2015) and, collectively, the  
180 Ollo de Sapo Formation rocks record a major tectonothermal event whose expression  
181 can be found in most of the Variscan massifs of continental Europe including the  
182 Armorican and Bohemian massifs (e.g., von Quadt, 1997; Kröner and Willmer, 1998;  
183 Linnemann et al., 2000; Tichomirowa et al., 2001; Friedl et al., 2004; Mingram et al.,  
184 2004; Teipel et al., 2004; Ballèvre et al., 2012; El Korh et al., 2012; Tichomirowa et al.,  
185 2012; for a summary, see Casas and Murphy, 2018). The large volume of magmatic  
186 rocks located in the European Variscan Belt led some authors to propose the existence  
187 of a siliceous Large Igneous Province (LIP) (Díez Montes et al., 2010; Gutiérrez-Alonso  
188 et al., 2016), named Ibero-Armorican LIP by García-Arias et al. (2018).

189 The Sardic Phase has been proposed marking a stratigraphic discontinuity close to  
190 the Middle–Upper Ordovician boundary interval in some areas of the Central Iberian  
191 (e.g., Buçaco and the Truchas Syncline; Martínez Catalán et al., 1992; Días da Silva et

192 al., 2016) and the Morais Allochthonous Complex of the Galicia-Trás-os-Montes Zones  
193 (Días da Silva, 2014; Días da Silva et al., 2014, 2016). In the Truchas Syncline, the  
194 significance of the discontinuity (or discontinuities) was questioned by a biostratigraphic  
195 study of conodonts and the re-interpretation of some of these scouring surfaces as the  
196 result of Hirnantian glaciogenic incisions (Sarmiento et al., 1999). The pre-Hirnantian  
197 discontinuities have been interpreted as linked to the development of “horsts and half-  
198 grabens of local extent” , as a result of which “tilting and gentle folding of the Lower-  
199 Middle Ordovician strata, due to the rotation of individual half-grabens and horsts,  
200 create the Sardinic unconformity in Iberia” (Da Silva et al., 2016: pp. 1131 and 1143).  
201 However, the presence of synsedimentary listric faults associated with local outpouring  
202 of a basic volcanism, related to extensional pulses in the Ordovician passive-margin  
203 platform fringing Northwest Gondwana, cannot be associated with the Sardinic Phase.  
204 As summarized in this work, the Sardinic Phase is characterized by generalized cortical  
205 uplift, denudation of exposed uplifted areas under subaerial exposure, stratigraphic  
206 gaps of about 25–30 m.y., broad intrusion of felsic granitic plutons (now orthogneisses  
207 after Variscan deformation and metamorphism) with calc-alkaline affinity, and record of  
208 alluvial-to-fluvial deposits overlapping the unconformity. These are the features that  
209 characterize the Ordovician Sardinic Phase, not the record of Ordovician volcanism and  
210 of local listric faults (e.g., Casas et al., 2010, 2019; Álvaro et al., 2016).

211 In contrast, the Sardinic aftermath is represented by a basic-dominant volcanic  
212 activity, mainly of tholeiitic affinity, and lining rifting branches highlighting the onset of  
213 listric-fault networks; this event could be geodynamically compared with some  
214 processes recorded in the Central Iberian and the Galician-Trás-os-Montes Zones, but  
215 not with the Sardinic Phase. Therefore, the presence of the Sardinic Phase in Iberia was  
216 already ruled out by the information published during the last two decades, and should  
217 not be maintained except if the above-reported tectonothermal events are really found  
218 in Iberia. The presence of an Ordovician volcanism associated with listric faults is not  
219 an argument to support the record of the Sardinic Phase.



220

## 221 **2.2. Central and Eastern Pyrenees**

222

223 In the central and eastern Pyrenees (Fig. 1D), earliest Ordovician volcanic-free  
224 passive-margin conditions, represented by the Jujols Group (Padel et al., 2018), were  
225 succeeded by a late Early–Mid Ordovician phase of uplift and erosion that led to the  
226 onset of the Sardinic unconformity (Fig. 2). Uplift was associated with magmatic activity,  
227 which continued until Late Ordovician times. An extensional interval took place then  
228 developing normal faults that controlled the sedimentation of post–Sardinic siliciclastic  
229 deposits infilling palaeorelief depressions. Acritarchs recovered in the uppermost part  
230 of the Jujols Group suggest a broad Furongian–earliest Ordovician age (Casas and  
231 Palacios, 2012), conterminous with a maximum depositional age of ca. 475 Ma, based  
232 on the age of the youngest detrital zircon populations (Margalef et al., 2016). On the  
233 other hand, a ca. 459 Ma U–Pb age for the Upper Ordovician volcanic rocks overlying  
234 the Sardinic Unconformity has been proposed in the eastern Pyrenees (Martí et al.,  
235 2019), and ca. 452–455 Ma in the neighbouring Catalan Coastal Ranges, which  
236 represent the southern prolongation of the Pyrenees (Navidad et al., 2010; Martínez et  
237 al., 2011). Thus, a time gap of about 16–23 m.y. can be related to the Sardinic Phase in  
238 the eastern Pyrenees and the neighbouring Catalan Coastal Ranges.

239 Coeval with the late Early–Mid Ordovician phase of generalized uplift and  
240 denudation, a key magmatic activity led to the intrusion of voluminous granitoids, about  
241 500 to 3000 m thick and encased in strata of the Ediacaran–Lower Cambrian  
242 Canaveilles Group (Fig. 2). These granitoids constitute the protoliths of the large  
243 orthogneissic laccoliths that punctuate the backbone of the central and eastern  
244 Pyrenees. These are, from west to east (Fig. 1D), the Aston (467–470 Ma ; Denèle et  
245 al., 2009; Mezger and Gerdes, 2016), Hospitalet (about 472 Ma, Denèle et al., 2009),  
246 Canigó (472–462 Ma, Cocherie et al., 2005; Navidad et al., 2018), Roc de Frausa  
247 (477–476 Ma; Cocherie et al., 2005; Castiñeiras et al., 2008b) and Albera (about 470

248 Ma; Liesa et al., 2011) massifs, which comprise a dominant Floian–Dapingian age. It is  
249 noticeable the fact that only a minor representation of coeval basic magmatic rocks are  
250 outcropped. The acidic volcanic equivalents have been documented in the Albera  
251 massif, where subvolcanic rhyolitic porphyroid rocks have yielded similar ages to those  
252 of the main gneissic bodies at about 474–465 Ma (Liesa et al., 2011). Similar acidic  
253 byproducts are represented by the rhyolitic sills of Pierrefite (Calvet et al., 1988).

254 The late Early–Mid Ordovician (“Sardic”) phase of uplift was succeeded by a Late  
255 Ordovician extensional interval responsible for the opening of (half-)grabens infilled  
256 with the basal Upper Ordovician alluvial-to-fluvial conglomerates (La Rabassa  
257 Conglomerate Formation). At map scale, a set of NE-SW trending normal faults  
258 abruptly controlling the thickness of the basal Upper Ordovician formations can be  
259 recognized in the La Cerdanya area (Casas and Fernández, 2007; Casas, 2010).  
260 Sharp variations in the thickness of the Upper Ordovician strata have been  
261 documented by Hartevelt (1970) and Casas and Fernández (2007). Drastic variations  
262 in grain size and thickness can be attributed to the development of palaeotopographies  
263 controlled by faults and subsequent erosion of uplifted palaeoreliefs, with subsequent  
264 infill of depressed areas by alluvial fan and fluvial deposits, finally sealed by Silurian  
265 sediments (Puddu et al., 2019). A Late Ordovician magmatic pulse contemporaneously  
266 yielded a varied set of magmatic rocks. Small granitic bodies are encased in the  
267 Canaveilles strata of the Canigó massif. They constitute the protoliths of the Cadí  
268 (about 456 Ma; Casas et al., 2010), Casemí (446 to 452 Ma; Casas et al., 2010), Núria  
269 (ca. 457 Ma; Martínez et al., 2011) and Canigó G-1 type (ca. 457 Ma; Navidad et al.,  
270 2018) gneisses.

271 The lowermost part of the Canaveilles Group (the so-called Balaig Series) host  
272 metre-scale thick bodies of metadiorite sills related to an Upper Ordovician protolith,  
273 (ca. 453 Ma, SHRIMP U–Pb in zircon; Casas et al., 2010). Coeval calc-alkaline  
274 ignimbrites, andesites and volcanoclastic rocks are interbedded in the Upper Ordovician  
275 succession of the Bruguera and Ribes de Freser areas (Robert and Thiebaut, 1976;

276 Ayora, 1980; Robert, 1980; Martí et al., 1986, 2019). In the Ribes area, a granitic body  
277 with granophyric texture, dated at ca. 458 Ma by Martínez et al. (2011), intruded at the  
278 base of the Upper Ordovician succession. In the La Pallaresa dome, some metre-scale  
279 rhyodacitic to dacitic subvolcanic sills, Late Ordovician in age (ca. 453 Ma, Clariana et  
280 al., 2018), occur interbedded within the pre-unconformity strata and close to the base  
281 of the Upper Ordovician.

282

### 283 **2.3. Occitan Domain: Albigeois, Montagne Noire and Mouthoumet massifs**

284

285 The parautochthonous framework of the southern French Massif Central, named  
286 Occitan Domain by Pouclet et al. (2017), includes among others, from south to north,  
287 the Mouthoumet, Montagne Noire and Albigeois massifs. The domain represents the  
288 southeastern prolongation of the Variscan South Armorican Zone (including  
289 southwestern Bretagne and Vendée). Since Gèze (1949) and Arthaud (1970), the  
290 southern edge of the French Massif Central has been traditionally subdivided, from  
291 north to south, into the northern, axial and southern Montagne Noire (Fig. 1C). The  
292 Palaeozoic succession of the northern and southern sides includes sediments ranging  
293 from late Ediacaran to Silurian and from Terreneuvian (Cambrian) to Visean in age,  
294 respectively. These successions are affected by large scale, south-verging recumbent  
295 folds that display a low to moderate metamorphic grade. Their emplacement took place  
296 in Late Visean to Namurian times (Engel et al., 1980; Feist and Galtier, 1985; Echlter  
297 and Malavieille, 1990). The Axial Zone consists of plutonic, migmatitic and  
298 metamorphic rocks forming a regional ENE-WSW oriented dome (Fig. 1C), where four  
299 principal lithological units can be recognized (i) schists and micaschists, (ii) migmatitic  
300 orthogneisses, (iii) metapelitic metatexites, and (iv) diatexites and granites (Cocherie,  
301 2003; Faure et al., 2004; Roger et al., 2004, 2015; Bé Mézème, 2005; Charles et al.,  
302 2009; Rabin et al., 2015). The Rosis micaschist synform subdivides the eastern Axial

303 Zone into the Espinouse and Caroux sub-domes, whereas the southwestern edge of  
304 the Axial Zone comprises the Nore massif.

305 In the Occitan Domain, two main Cambro–Ordovician felsic events can be identified  
306 giving rise to the protoliths of (i) the Larroque metarhyolites in the northern Montagne  
307 Noire and Albigeois, thrust southward from Rouergue; and (ii) the migmatitic  
308 orthogneisses that form the Axial Zone of the Montagne Noire (Fig. 2).

309 (i) The Larroque volcanosedimentary Complex is a thick (500–1000 m) package of  
310 porphyroclastic metarhyolites located on the northern Montagne Noire (Lacaune  
311 Mountains), Albigeois (St-Salvi-de-Carcavès and St-Sernin-sur-Rance nappes) and  
312 Rouergue; the Variscan setting of the formation is allochthonous in the Albigeois and  
313 parautochthonous in the rest. This volcanism is encased in the so-called “Série schisto-  
314 gréseuse verte” (see Guérangé-Lozes et al., 1996; Guérangé-Lozes and Alabouvette,  
315 1999) (Pouclet et al., 2017) (Fig. 2). The Larroque volcanic rocks consist of deformed  
316 porphyroclastic rhyolites rich in largely fragmented, lacunous (rhyolitic) quartz and  
317 alkali feldspar phenocrysts. The metarhyolites occur as porphyritic lava flows, sills and  
318 other associated facies, such as aphyric lava flows, porphyritic and aphyric pyroclastic  
319 flows of welded or unwelded ignimbritic types, fine to coarse tephra deposits, and  
320 epiclastic and volcanoclastic deposits. These rocks are named “augen gneiss” or  
321 augengneiss and do not display a high-grade gneiss paragenesis but a general lower  
322 grade metamorphic mineralogy. The Occitan augengneisses mimic the Ollo de Sapo  
323 facies from the Central Iberian Zone because of their large bluish quartz phenocrysts.  
324 Based on geochemical similarities and contemporaneous emplacement, Pouclet et al.  
325 (2017) suggested that this event also supplied the Davejean acidic volcanic rocks in  
326 the Mouthoumet Massif, which represent the southern prolongation of the Montagne  
327 Noire (Fig. 2), and the Génis rhyolitic unit of the western Limousin sector.

328 (ii) Some migmatitic orthogneisses make up the southern Axial Zone, from the  
329 western Cabardès to the eastern Caroux domes. The orthogneisses, derived from  
330 Ordovician metagranites bearing large K-feldspar phenocrysts, were emplaced at

331 about 471 Ma (Somail Orthogneiss, Cocherie et al., 2005), 456 to 450 Ma (Pont de  
332 Larn and Gorges d'Héric gneisses, Roger et al., 2004) and ca. 455 Ma (Sain Eutrope  
333 gneiss, Pitra et al., 2012). They intruded a metasedimentary pile, traditionally known as  
334 "Schistes X" and formally named St. Pons-Cabardès Group (Fig. 2). The latter consists  
335 of schists, greywackes, quartzites and subsidiary volcanic tuffs and marbles (Demange  
336 et al., 1996; Demange, 1999; Alabouvette et al., 2003; Roger et al., 2004; Cocherie et  
337 al., 2005). The group is topped by the Sériès Tuff, dated at about 545 Ma (Lescuyer  
338 and Cocherie, 1992), which represents a contemporaneous equivalent of the  
339 Cadomian Rivernous rhyolitic tuff (542.5 to 537.1 Ma) from the Lodève inlier of the  
340 northern Montagne Noire (Álvaro et al., 2014b, 2018; Padel et al., 2017). Age of  
341 migmatization has been inferred from U–Pb dates on monacite from migmatites and  
342 anatectic granites at 333 to 327 Ma (Bé Mézème, 2005; Charles et al., 2008); as a  
343 result, the 330–325 Ma time interval can represent a Variscan crustal melting event in  
344 the Axial Zone.

345 As in the Pyrenees, the Middle Ordovician is absent in the Occitan Domain. Its gap  
346 allows distinction between a Lower Ordovician pre-unconformity sedimentary package  
347 para- to unconformably overlain by an Upper Ordovician–Silurian succession (Álvaro et  
348 al., 2016; Pouclet et al., 2017).

349

#### 350 **2.4. Sardinia**

351

352 In Sardinia the Cambro–Ordovician magmatism is well represented in the external  
353 (southern) and internal (northern) nappe zones of the exposed Variscan Belt (Fig. 1E),  
354 and ranges in age from late Furongian to Late Ordovician. A Furongian–Tremadocian  
355 (ca. 491–480 Ma) magmatic activity, predating the Sardic phase, is mostly represented  
356 by felsic volcanic and subvolcanic rocks encased in the San Vito sandstone Formation.  
357 The Sardic-related volcanic products differ from one nappe to another: intermediate  
358 and basic (mostly metandesites and andesitic basalts) are common in the nappe

359 stacking of the central part of the island (Barbagia and Goceano), whereas felsic  
360 metavolcanites prevail in the southeastern units. Their age is bracketed between 465  
361 and 455 Ma (Giacomini et al., 2006; Oggiano et al., 2010; Pavanetto et al., 2012;  
362 Cruciani et al., 2018) and matches the Sardinic gap based on biostratigraphy (Barca et  
363 al., 1988).

364 Teichmüller (1931) and Stille (1939) were the first to recognize in southwestern  
365 Sardinia an intra-Ordovician stratigraphic hiatus. Its linked erosive unconformity is  
366 supported by a correlatable strong angular discordance in the Palaeozoic basement of  
367 the Iglesias-Sulcis area, External Zone (Carmignani et al., 2001). This major  
368 discontinuity separates the Cambrian–Lower Ordovician Nebida, Gonnese and Iglesias  
369 groups (Pillola et al., 1998) from the overlying coarse-grained (“Puddinga”) Monte  
370 Argentu metasediments (Leone et al., 1991, 2002; Laske et al., 1994). The gap  
371 comprises a chronostratigraphically constrained minimum gap of about 18 m.y. that  
372 includes the Floian and Dapingian (Barca et al., 1987, 1988; Pillola et al., 1998; Barca  
373 and Cherchi, 2004) (Fig. 2). The hiatus is related to neither metamorphism nor  
374 cleavage, though some E–W folds have been documented in the Gonnese Anticline  
375 and the Iglesias Syncline (Cocco et al., 2018), which are overstepped by the  
376 “Puddinga” metaconglomerates. Both the E–W folds and the overlying  
377 metaconglomerates were subsequently affected by Variscan N–S folds (Cocco and  
378 Funneda, 2011, 2017). Sardinic-related volcanic rocks are not involved in this area, but  
379 Sardinic-inherited palaeoreliefs are lined with breccia slides that include metre- to  
380 decametre-scale carbonate boulders (“Olistoliti”), some of them hosting  
381 synsedimentary faults contemporaneously mineralized with ore bodies (Boni and  
382 Koeppel, 1985; Boni, 1986; Barca, 1991; Caron et al., 1997). The lower part of the  
383 unconformably overlying Monte Argentu Formation deposited in alluvial to fluvial  
384 environments (Martini et al., 1991; Loi et al., 1992; Loi and Dabard, 1997).

385 A similar gap was reported by Calvino (1972) in the Sarrabus-Gerrei units of the  
386 External Nappe Zone. The so-called “Sarrabese Phase” is related to the onset of thick,

387 up to 500 m thick, volcanosedimentary complexes and volcanites (Barca et al., 1986;  
388 Di Pisa et al., 1992) with a Darriwilian age for the protoliths of the metavolcanic rocks  
389 (465.4 to 464 Ma; Giacomini et al., 2006; Oggiano et al., 2010). In the Iglesiente-Sulcis  
390 region (Fig. 1E), Carmignani et al. (1986, 1992, 1994, 2001) suggested that the  
391 “Sardic-Sarrabese phase” should be associated with the compression of a Cambro–  
392 Ordovician back-arc basin that originated the migration of the Ordovician volcanic arc  
393 toward the Gondwanan margin.

394 Some gneissic bodies, interpreted as the plutonic counterpart of metavolcanic rocks,  
395 are located in the Bithia unit (e.g., the Monte Filau area, 458 to 457 Ma, surrounded by  
396 a Mid–Ordovician andalusite thermal aureole; Pavanetto et al., 2012; Costamagna et  
397 al., 2016) and in the internal units (Lodè orthogneiss, ca. 456 Ma; Tanaunella  
398 orthogneiss, ca. 458 Ma, Helbing and Tiepolo, 2005; Golfo Aranci orthogneiss, ca. 469  
399 Ma, Giacomini et al., 2006).

400 The Sardic palaeorelief is sealed by Upper Ordovician transgressive deposits. The  
401 sedimentary facies show high variability, but the –mostly terrigenous– sediments vary  
402 from grey fine- to medium-sized sandstones, to muddy sandstones and mudstones.  
403 They are referred to the Katian Punta Serpeddì and Orroledu formations (Pistis et al.,  
404 2016). This post–Sardic sedimentary succession is coeval with a new magmatic  
405 pulsation represented by alkaline to tholeiitic within-plate basalts (Di Pisa et al., 1992;  
406 Gaggero et al., 2012).

407

### 408 **3. Geochemical data**

409

#### 410 **3.1. Materials and methods**

411

412 The rocks selected for geochemical analysis (231 samples; see tectonostratigraphic  
413 location in Fig. 1 and stratigraphic emplacement in Fig. 2) have recorded different  
414 degrees of hydrothermalism and metamorphism, as a result of which only the most

415 immobile elements have been considered. The geochemical calculations, in which the  
416 major elements take part, have been made from values recalculated to 100 in volatile  
417 free compositions; Fe is reported as  $\text{FeO}_t$ .

418 The geochemical dataset of the Central Iberian Zone includes 152 published  
419 geochemical data, from which 85 are plutonic and 67 volcanic and volcanoclastic rocks  
420 from the Ollo de Sapo Formation (Galicia, Sanabria and Guadarrama areas), and the  
421 contact between the Central Iberian and Ossa Morena Zones (Urra Formation and  
422 Portalegre and Carrascal granites). Other data were yielded from six volcanic rocks of  
423 the Galicia-Trás-os-Montes Zone (Saldanha area) (Fig. 1B; Repository Data).

424 The dataset of the eastern Pyrenees consists of 38 samples, six of which are upper  
425 Lower Ordovician volcanic rocks, and seven upper Lower Ordovician plutonic rocks,  
426 together with nine Upper Ordovician volcanic and 14 Upper Ordovician plutonic rocks  
427 (Repository Data). New data reported below include two samples of subvolcanic sills  
428 intercalated in the pre-Sardic unconformity succession (Clariana et al., 2018; Margalef,  
429 unpubl.; Table 1).

430 The study samples from the Occitan Domain comprise six metavolcanic rocks, four  
431 from the Larroque volcanosedimentary Complex in the Albigeois and northern  
432 Montagne Noire and two from the Mouthoumet massif (Pouclet et al., 2017)  
433 (Repository Data), and four new samples for the Axial Zone gneisses (Table 1).

434 In the Sardinian dataset, 25 published analyses are selected: five correspond to the  
435 Golfo Aranci orthogneiss (Giacomini et al., 2006), six to metavolcanics from the central  
436 part of the island (Giacomini et al., 2006; Cruciani et al., 2013), and five to  
437 metavolcanics and one to gneisses from the Bithia unit (Cruciani et al., 2018)  
438 (Repository Data). Ten new analyses are added from the Monte Filau and Capo  
439 Spartivento gneisses of the Bithia unit, and from the Punta Bianca gneisses embedded  
440 within the migmatites of the High-grade Metamorphic complex of the Inner Zone (Table  
441 1).



442 Whole-rock major and trace elements and rare earth element (REE) compositions  
443 were determined at ACME Laboratories, Vancouver, Canada. LiBO<sub>2</sub> fusion followed by  
444 X-ray fluorescence spectroscopy (XRF) analysis was used to determine major  
445 elements. Rare earth and refractory elements were measured by ICP–MS following a  
446 lithium metaborate/tetraborate fusion and nitric acid digestion on 0.2 g of sample. For  
447 base metals, 0.5 g of sample was digested in Aqua Regia at 95 °C and analyzed by  
448 inductively coupled plasma - atomic emission spectrometry (ICP–AES). Analyses of  
449 standards and duplicate samples indicate precision to better than 1 % for major oxides,  
450 and 3–10 % for minor and trace elements.

451 Additional Sm–Nd isotopic analyses were performed at Centro de Geocronología y  
452 Geoquímica Isotópica from the Complutense University, Madrid. They were carried out  
453 in whole-rock powders using a <sup>150</sup>Nd–<sup>149</sup>Sm tracer by isotope dilution-thermal ionization  
454 mass spectrometry (ID–TIMS). The samples were first dissolved through oven  
455 digestion in sealed Teflon bombs with ultra pure reagents to perform two-stage  
456 conventional cation-exchange chromatography for separation of Sm and Nd (Strelow,  
457 1960; Winchester, 1963), and subsequently analysed using a Sector 54 VG-Micromass  
458 multicollector spectrometer. The measured <sup>143</sup>Nd/<sup>144</sup>Nd isotopic ratios were corrected  
459 for possible isobaric interferences from <sup>142</sup>Ce and <sup>144</sup>Sm (only for samples with  
460 <sup>147</sup>Sm/<sup>144</sup>Sm < 0.0001) and normalized to <sup>146</sup>Nd/<sup>144</sup>Nd = 0.7219 to correct for mass  
461 fractionation. The Lajolla Nd international isotopic standard was analysed during  
462 sample measurement, and gave an average value of <sup>143</sup>Nd/<sup>144</sup>Nd = 0.5114840 for 9  
463 replicas, with an internal precision of ± 0.000032 (2σ). These values were used to  
464 correct the measured ratios for possible sample drift. The estimated error for the  
465 <sup>147</sup>Sm/<sup>144</sup>Nd ratio is 0.1%.

466 A general classification of the analyzed samples, following Winchester and Floyd  
467 (1977), can be seen in Figure 4A–B, and the geographical coordinates of the new  
468 samples in Table 1. For geochemical comparison (summarized in Table 2), two large  
469 groups or suites are differentiated in order to check the similarities and differences

470 between the magmatic rocks, and to infer a possible geochemical trend following a  
471 palaeogeographic SW–NE transect. The description reported below follows the same  
472 palaeogeographic and chronological order.

473

### 474 **3.2. Furongian–to–Mid Ordovician Suite**

475

476 In the Central Iberian and Galicia-Trás-os-Montes Zones, the Furongian–to–Mid  
477 Ordovician magmatic activity is pervasive. Their main representative is the Ollo de  
478 Sapo Formation, which includes volcanic and subvolcanic rocks (67 samples) as well  
479 as plutonic rocks (85 samples) (data from Murphy et al., 2006; Díez-Montes, 2007;  
480 Montero et al., 2007, 2009; Solá, 2007; Solá et al., 2008; Talavera, 2009; Villaseca et  
481 al., 2016). From the Parautochthon Schistose Domain of the Galicia-Trás-os Montes  
482 Zone, six samples of rhyolite tuffs of the Saldanha Formation (Dias da Silva et al.,  
483 2014) are selected, which share geochemical features with the Ollo de Sapo  
484 Formation. In summary, five facies are differentiated in the Central Iberian and Galicia-  
485 Trás-os Montes Zones: the Ollo de Sapo orthogneisses, some leucogneisses,  
486 metagranites and volcanic rocks, and the San Sebastián orthogneiss (for a  
487 geochemical characterization, see Table 2).

488 In the central and eastern Pyrenees, an Early–Mid Ordovician magmatic activity  
489 gave rise to the intrusion of voluminous (about 500–3000 m in size) aluminous granitic  
490 bodies, encased into the Canaveilles beds (Álvaro et al., 2018; Casas et al., 2019).  
491 They constitute the protoliths of the large orthogneissic laccoliths that form the core of  
492 the domal massifs scattered throughout the backbone of the Pyrenees. Rocks of the  
493 Canigó, Roc de Frausa and Albera massifs have been taken into account in this work,  
494 in which volcanic rocks of the Pierrefite and Albera massifs, and the so-called G2 and  
495 G3 orthogneisses by Guitard (1970) are also included. All subgroups vary  
496 compositionally from subalkaline andesite to rhyolite, as illustrated in the Pearce's

497 (1996) diagram of Figure 5 (data compiled from Vilà et al., 2005; Castiñeiras et al.,  
498 2008b; Liesa et al., 2011; Navidad et al., 2018).

499 Although most rocks in this area are acidic, it is remarkable the presence of minor  
500 mafic bodies (Cortalet and Marialles metabasites, not studied in this work), which could  
501 indicate a mantle connection with parental magmas during the Mid and Late  
502 Ordovician. As well, it should be noted that there are no andesitic rocks in the area.

503 In the Occitan Domain, six samples of the Larroque volcanosedimentary Complex  
504 (Early Tremadocian in age) represent basin floors and subaerial explosive and effusive  
505 rhyolites (Pouclet et al., 2017). The porphyroclastic rocks of the Larroque metarhyolites  
506 were sampled in the Saint-Géraud and Larroque areas from the Saint-Sernin-sur-  
507 Rance nappe and the Saint-André klippe above the Saint-Salvi-de-Carcavès nappe  
508 (Pouclet et al., 2017).

509 In the Middle Ordovician rocks of Sardinia, 11 samples are selected, five of which  
510 correspond to orthogneisses of the Aranci Gulf, in the Inner Zone of the NE island  
511 (Giacomini et al., 2006), completed with six volcanic rocks of the External Zone  
512 (Giacomini et al., 2006; Cruciani et al., 2018) (Table 2).

513

### 514 **3.3 Upper Ordovician Suite**

515

516 In the central and eastern Pyrenees, four Upper Ordovician subgroups are  
517 distinguished based on their field occurrence and geochemical and geochronological  
518 features: the *G1*-type orthogneisses *sensu* Guitard (1970); the Cadí and Casemí  
519 orthogneisses and the metavolcanic rocks that include the Ribes de Freser rhyolites;  
520 the Els Metges volcanic tuffs; and the rhyolites from Andorra and Pallaresa areas (the  
521 latter dated at ca. 453 Ma; Clariana et al., 2018) (Table 2). The suite is completed with  
522 the Somail orthogneisses of the Axial Montagne Noire (dated at ca. 450 Ma at Gorges  
523 d'Héric; Roger et al., 2004) and the orthogneisses from the Sardinian External Zone

524 (dated at ca. 458–457 Ma at Monte Filau; Pavanetto et al., 2012) and the volcanic rocks  
525 from the Sardinian Nappe Zone (Table 2).

526

#### 527 **4. Geochemical framework**

528

529 A geochemical comparison between the Furongian–Ordovician felsic rocks of all the  
530 above-reported groups offers the opportunity to characterize the successive sources of  
531 crustal-derived melts along the south-western European margin of Gondwana.

532 The geochemical features point to a predominance of materials derived from the  
533 melting of metasedimentary rocks, rich in  $\text{SiO}_2$  and  $\text{K}_2\text{O}$  (average  $\text{K}_2\text{O}/\text{Na}_2\text{O} = 2.25$ )  
534 and peraluminous ( $0.4 < C_{\text{norm}} < 4.5$  and  $0.94 < A/\text{CNK} < 3.12$ ), with only three samples  
535 with  $A/\text{CNK} < 1$  (samples 100786 of the Casemí subgroup, and T26 and T27 of the San  
536 Sebastián subgroup).

537 The result of plotting the REE content vs. average values of continental crust  
538 (Rudnick and Gao, 2004; Fig. 6) yields a flat spectra and a base level shared by most  
539 of the considered groups. The total content in REE is moderate to high (average REE =  
540 176 ppm, ranging between 482.2 and 26.0 ppm; Fig. 7), with a maximum in the  
541 subgroup of the Middle Ordovician volcanic rocks from Sardinia (average REE = 335  
542 ppm, *VOL-SMO*), and with LREE values more fractionated than HREE ones, and  
543 negative anomalies of Eu, which would indicate a characteristic process of magmatic  
544 evolution with plagioclase fractionation. These features are common in peraluminous  
545 granitoids.

546 All subgroups display similar chondritic normalized REE patterns (Fig. 7), with an  
547 enrichment in LREE relative to HREE, which should indicate the involvement of crustal  
548 materials in their parental magmas. Nevertheless, some variations can be highlighted,  
549 such as the lesser fractionation in REE content of some subgroups. These are the  
550 leucogneisses from the Iberian massif (*LG*,  $\text{La}/\text{Yb}_n = 2.01$ ), the Upper Ordovician  
551 orthogneisses from Sardinia (*OG-SUO*,  $\text{La}/\text{Yb}_n = 2.94$ ), the Casemí orthogneisses

552 (La/Yb<sub>n</sub> = 4.42) and the Middle Ordovician volcanic rocks from Sardinia (*OG-SUO*,  
553 La/Yb<sub>n</sub> = 2.94). This may be interpreted as a greater degree of partial fusion in the  
554 origin of their parental magmas (Rollinson, 1993).

555 There are three geochemical groups displaying (Gd/Yb)<sub>n</sub> values > 2, and (La/Yb)<sub>n</sub>  
556 values ≥ 9. These groups are *OSS* (Central Iberian Zone), *VOL-OD* (Occitan Domain)  
557 and *G1* (Pyrenees), and share higher alkalinity features.

558 Some *V1* rocks from the Pyrenees (Pierrefite Formation) show no negative  
559 anomalies in Eu. Their parental magmas could have been derived from deeper origins  
560 and related to residual materials of the lower continental crust, in areas of production of  
561 K-rich granites (Taylor and McLennan, 1989).

562 The spider diagrams (Fig. 8), however, exhibit strong negative anomalies in Nb, Sr  
563 and Ti, which indicate a distinct crustal affiliation (Díez-Montes, 2007). Only the San  
564 Sebastián orthogneisses (*OSS*) show distinct discrepancies in respect of the remaining  
565 samples from the Ollo de Sapo Formation. They display lower negative anomalies in  
566 Nb and a more alkaline character by comparison with the rest of the Ollo de Sapo  
567 rocks, which point to alkaline affinities and greater negative anomalies in Nb.

568 Despite some small differences in the chemical ranges of some major elements,  
569 most felsic Ordovician rocks from the Iberian massif (Central Iberian and Galicia-Trás-  
570 os Montes Zones), eastern Pyrenees, Occitan Domain and Sardinia share a common  
571 chemical pattern. The Lower–Middle Ordovician rocks of the eastern Pyrenees show  
572 less variation in the content of Zr and Nb (Fig. 8B). The volcanic rocks of these groups  
573 show a different REE behaviour, which would indicate different sources. Two groups  
574 are distinguished in Figure 7, one with greater enrichment in REE and negative  
575 anomaly of Eu, and another with lesser content of HREE and without Eu negative  
576 anomalies.

577 Figure 9 illustrates how the average of all the considered groups approximates the  
578 mean values of the Rudnick and Gao's (2003) upper continental crust (UCC). In this  
579 figure, small deviations can be observed, some of them toward lower continental crust

580 (LCC) values and others toward bulk continental crust (BCC), indicating variations in  
581 their parental magmas but with quite similar spectra. Overall chondrite-normalized  
582 patterns are close to the values that represent the upper continental crust, with slight  
583 enrichments in the Th/Nb, Th/La and Th/Yb ratios.

584 Finally, in the Occitan volcanic rocks (*VOL-OD*) the rare earth elements are enriched  
585 and fractionated ( $33.2 \text{ ppm} < \text{La} < 45.6 \text{ ppm}$ ;  $11.2 < \text{La/Yb} < 14.5$ ). The upper  
586 continental crust normalized diagram exhibits negative anomalies of Ti, V, Cr, Mn and  
587 Fe associated with oxide fractionation, of Zr and Hf linked to zircon fractionation, and of  
588 Eu related to plagioclase fractionation. The profiles are comparable to the Vendean  
589 Saint-Gilles rhyolitic ones. The Th vs. Rb/Ba features are also similar to those of the  
590 Saint-Gilles rhyolites, and the Iberian Ollo de Sapo and Urra rhyolites (Solá et al.,  
591 2008; Díez Montes et al., 2010).

592

#### 593 **4. Discussion**

594

##### 595 **4.1 Inferred tectonic settings**

596

597 In order to clarify the evolution of geotectonic environments, the data have been  
598 represented in different discrimination diagrams. The Zr/TiO<sub>2</sub> ratio (Lentz, 1996; Syme,  
599 1998) is a key index of compositional evolution for intermediate and felsic rocks. In the  
600 Syme diagram (Fig. 10), most rocks from the Central Iberian Zone represent a  
601 characteristic arc association, although there are some contemporaneous samples  
602 characterized by extensional-related values ( $\text{Zr/Ti} = 0.10$ , *LG*). The rocks of the  
603 Middle–Ordovician San Sebastián orthogneisses (*OSS*) show values of  $\text{Zr/Ti} = 0.08$ ,  
604 intermediate between extensional and arc conditions. This could be interpreted as a  
605 sharp change in geotectonic conditions toward the Mid Ordovician (Fig. 10A). For a  
606 better comparison, the samples of the San Sebastián orthogneisses (*OSS*) and the  
607 granites (*GRA*) have been distinguished with a shaded area in all the diagrams, since

608 they have slightly different characteristics to the rest of the samples from the Ollo de  
609 Sapo group. The samples *G1* (Pyrenees) and *VOL* (Central Iberian Zone) broadly  
610 share similar values, as a result of which, the three latter groups (*OSS*, *G1* and *VOL*)  
611 arrange following a good correlation line. The same trend seems to be inferred in the  
612 eastern Pyrenees (Fig. 10B), where the Middle Ordovician subgroups display arc  
613 features, but half of the Upper Ordovician subgroups show extensional affinities (*G1*  
614 and Casemí orthogneisses). In the case of the Occitan orthogneisses (Fig. 10C), they  
615 show arc characters, which contrast with the contemporaneous volcanic rocks  
616 displaying extensional values with  $Zr/Ti = 0.10$ . This disparity between plutonic and  
617 volcanic rocks could be interpreted as different conditions for the origin of these  
618 magmas. In Sardinia (Fig. 10D), the same evolution from arc to extensional conditions  
619 is highlighted for the Upper Ordovician samples, although some Middle Ordovician  
620 volcanic rocks already shared extensional patterns ( $Zr/Ti = 0.09$ ). In summary, there  
621 seems to be a geochemical evolution in the Ordovician magmas grading from arc to  
622 extensional environments.

623 In the Nb–Y tectonic discriminating diagram of Pearce et al. (1984) (Fig. 11), most  
624 samples plot in the volcanic arc-type, though some subgroups project in the within-  
625 plate and anomalous ORG. The majority of samples display very similar Zr/Nb and  
626 Nb/Y ratios, typical of island arc or active continental margin rhyolites (Díez-Montes et  
627 al., 2010). Only some samples plot separately: *OSS* samples with highest Nb contents  
628 (>20 ppm), and some volcanic rocks of the Occitan Domain (average Nb =16.87 ppm).  
629 In the eastern Pyrenees, the Middle Ordovician rocks plot in the volcanic arc field,  
630 whereas the Upper Ordovician ones point in the ORG type, except the Casemí  
631 samples. This progress of magmatic sources agrees with the evolution seen in Figure  
632 10. In the Occitan Domain, *VOL-OD* samples share values with those of the San  
633 Sebastián orthogneiss, while *OG-OD* shares values with those of *OG* from the Central  
634 Iberian Zone.

635 The Zr vs. Nb diagram (Leat et al., 1986; modified by Piercey, 2011) (Fig. 12)  
636 illustrates how magmas evolved toward richer values in Zr and Nb, which is consistent  
637 with what it is observed in the Syme diagram (Fig. 10). Figure 12A documents how  
638 most samples show a general positive correlation. These different groups correspond  
639 to the OSS and Portalegre granites, highlighted in the figure. The two groups indicate a  
640 tendency toward alkaline magmas. Some samples, such as the Pyrenean *G1*, some  
641 Occitan *VOL-OD* samples and some Sardinian *OG-UOS* samples share the same  
642 affinity, clearly distinguished from the general geochemical trend exhibited by the  
643 Central Iberian Zone.

644 On a Zr vs. Ga/Al diagram (Whalen et al., 1987) (Fig. 13), the samples depict an  
645 intermediate character between anorogenic or alkaline (A-type) and orogenic (I&S-  
646 type). In the Central Iberian Zone, samples from the San Sebastián orthogneisses and  
647 Portalegre granites show characters of A-type granites, while the remaining samples  
648 display affinities of I&S-type granites. For the Central Iberian Zone, a clear magmatic  
649 shift toward more extensional geotectonic environments is characterized. For the  
650 eastern Pyrenees, we find the same situation as in the Central Iberian Zone, with a  
651 magmatic evolution toward A-granite type characteristics, indicating more extensional  
652 geotectonic environments. In the Occitan Domain, the samples show a clear I&S  
653 character. In the Sardinian case, the same seems to happen as in the Central Iberian  
654 Zone: the Upper Ordovician orthogneisses suggest a more extensional character.

655 In summary, all the reported diagrams point to a magmatic evolution through time,  
656 grading from arc to extensional geotectonic environments (with increased Zr/Ti ratios)  
657 and to granite type-A characters. This geotectonic framework is consistent with that  
658 illustrated in Figure 10. The geochemical characters of these rocks show a rhyodacite  
659 to dacite composition, peraluminous and calc-alkaline K-rich character, and an arc-  
660 volcanic affinity for most of samples, but without intermediate rocks associated with  
661 andesitic types. Hence a change in time is documented toward more alkaline magmas.

662



## 663 4.2 Interpretation of $\epsilon\text{Nd}$ values

664

665  $\epsilon\text{Nd}_{(t)}$  values are useful to interpret the nature of magmatic sources. Most samples of  
666 the above-reported groups show no significant differences in isotopic  $\epsilon\text{Nd}_{(t)}$  values, and  
667  $\text{Nd}_{\text{CHUR}}$  model ages (Fig. 14). Some exceptions are related to granites from the  
668 southern Central Iberian Zone, which display positive values (from +2.6 to -2.4) and  
669  $T_{\text{DM}}$  values from 0.90 to 3.46 Ga. These granites, space-related with calcalkaline  
670 diorites and gabbros, were interpreted by Solá et al. (2008) as the result of  
671 underplating and temporal storage of mantle-derived magmas as a potential source for  
672 the intrusive “orogenic melts” during Early Palaeozoic extension.

673 Some samples from (i) the Central Iberian Zone, such as VI-3 (Leucogneiss subgroup)  
674 and PORT2 and PORT15 (Granite subgroup); (ii) the eastern Pyrenees, such as 99338  
675 (G1 subgroup) and 100786 samples (Casemí subgroup); and (iii) the Sardinian CS5,  
676 CS8 and CC5 samples (Upper Ordovician Orthogneiss subgroup) display anomalous  
677  $T_{\text{DM}}$  values and  $^{147}\text{Sm}/^{144}\text{Nd}$  ratios  $> 0.17$  (Table 2; Fig. 14), a character relatively  
678 common in some felsic rocks (DePaolo, 1988; Martínez et al., 2011). According to  
679 Stern et al. (2012), these values should not be considered, but a possible explanation  
680 for these high ratios may be related to the M-type tetrad effect (e.g., Irber, 1999;  
681 Monecke et al., 2007; Ibrahim et al., 2015), which affects REE fractionation in highly  
682 evolved felsic rocks due to the interaction with hydrothermal fluids. This process can be  
683 reflected as an enrichment of Sm related to Nd. Other authors, however, explain this  
684 enrichment as a result of both magmatic evolution (e.g., McLennan, 1994; Pan, 1997)  
685 and weathering processes after exhumation (e.g., Masuda and Akagi, 1989; Takahasi  
686 et al., 2002).

687 In the granites of the southern Central Iberian Zone and the volcanic rocks of  
688 Sardinia, positive values in  $\epsilon\text{Nd}_{(t)}$  could be interpreted as a more primitive nature of  
689 their parental magmas, even though the samples with highest  $T_{\text{DM}}$  values are those  
690 that display higher  $^{147}\text{Sm}/^{144}\text{Nd}$  ratios ( $> 0.17$ ; Table 2).

691 The volcanic rocks of the Central Iberian Zone display some differences following a  
692 N-S transect, being  $\epsilon\text{Nd}_{(t)}$  values less variable in the north ( $\epsilon\text{Nd}_{(t)}$ :  $-4.0$  to  $-5.0$ ) than in  
693 the south ( $\epsilon\text{Nd}_{(t)}$ :  $-1.6$  to  $-5.5$ ). The isotopic signature of the Urra volcanoclastic rocks is  
694 compatible with magmas derived from young crustal rocks, with intermediate to felsic  
695 igneous compositions (Solá et al., 2008). The volcanic rocks of the northern Central  
696 Iberian Zone could be derived from old crustal rocks (Montero et al., 2007). The  
697 isotopic composition of the granitoids from the southern Central Iberian Zone has more  
698 primitive characters than those of the northern Central Iberian Zone, suggesting  
699 different sources for both sides (Talavera et al., 2013). OSS shows lower inheritance  
700 patterns, more primitive Sr–Nd isotopic composition than other rocks of the Ollo de  
701 Sapo suite, and an age some 15 m.y. younger than most meta-igneous rocks of the  
702 Sanabria region (Montero et al., 2009), likely reflecting a greater mantle involvement in  
703 its genesis (Díez-Montes et al., 2008).

704 According to Talavera et al. (2013), the Cambro–Ordovician rocks of the Galicia-  
705 Trás-os-Montes Zone schistose area and the magmatic rocks of the northern Central  
706 Iberian Zone are contemporary. Both metavolcanic and metagranitic rocks almost  
707 share the same isotopic compositions.

708 The Upper Ordovician orthogneisses from the Occitan Domain show very little  
709 variation in  $\epsilon\text{Nd}_{(t)}$  values ( $-3.5$  to  $-4.0$ ), typical of magmas derived from young crustal  
710 rocks. The variation in TDM values is also small (1.4 to 1.8 Ga) indicating similar  
711 crustal residence times to other rock groups.

712 In Sardinia,  $\epsilon\text{Nd}_{(t)}$  values present a greater variation ( $-1.6$  to  $-3.3$ ), but they are also  
713 included in the typical continental crustal range. As noted above, anormal TDM values  
714 (between 1.2 to 4.5 Ga) may be due to post-magmatic hydrothermal alteration  
715 processes.

716

## 717 **5. Geodynamic setting**

718

719 In the Iberian Massif, the Ediacaran–Cambrian transition was marked by  
720 paraconformities and angular discordances indicating the passage from Cadomian  
721 volcanic arc to rifting conditions. The axis of the so-called Ossa-Morena Rift lies along  
722 the homonymous Zone (Quesada, 1991; Sánchez-García et al., 2003, 2008, 2010)  
723 close to the remains of the Cadomian suture (Murphy et al., 2006). Rifting conditions  
724 were accompanied by a voluminous magmatism that changed from peraluminous acid  
725 to bimodal (Sánchez-García et al., 2003, 2008, 2016, 2019). Some authors (Álvaro et  
726 al., 2014; Sánchez-García et al., 2019) propose that this rift resulted from a SW-to-NE  
727 inward migration, toward innermost parts of Gondwana, of rifting axes from the Anti-  
728 Atlas in Morocco to the Ossa-Morena Zone in the Iberian Massif. According to this  
729 proposal the rifting developed later (in Cambro–Ordovician times) in the Iberian,  
730 Armorican and Bohemian massifs.

731 The Furongian–Ordovician transition to drifting conditions is associated, in the  
732 Iberian Massif, Occitan Domain, Pyrenees and Sardinia, with a stepwise magmatic  
733 activity contemporaneous with the record of the Toledanian and Sardic unconformities.  
734 These, related to neither metamorphism nor penetrative deformations, are linked to  
735 uplift, erosion and irregularly distributed mesoscale deformation that gave rise to  
736 angular unconformities up to 90°. The time span involved in these gaps is similar (22  
737 m.y. in the Iberian Massif, 16–23 m.y. in the Pyrenees and 18 m.y. in Sardinia). This  
738 contrasts with the greater time span displayed by the magmatic activity (30–45 m.y.),  
739 which started before the unconformity formation (early Furongian in the Central Iberian  
740 Zone vs. Floian in the Pyrenees, Occitan Domain and Sardinia), continued during the  
741 unconformity formation (Furongian and early Tremadocian in the Central Iberian Zone  
742 vs. Floian–Darriwilian in the Pyrenees, Occitan Domain and Sardinia), and ended  
743 during the sealing of the uplifted and eroded palaeorelief (Tremadocian–Floian  
744 volcanoclastic rocks at the base of the Armorican Quartzite in the Central Iberian Zone  
745 vs. Sandbian–Katian volcanic rocks at the lowermost part of the Upper Ordovician  
746 successions in the Pyrenees, Occitan Domain and Sardinia; Gutiérrez-Alonso et al.,

747 2007, 2016; Navidad et al., 2010; Martínez et al., 2011; Álvaro et al., 2016; Martí et al.,  
748 2019). In the Pyrenees, Upper Ordovician magmatism and sedimentation coexist with  
749 normal faults controlling marked thickness changes of the basal Upper Ordovician  
750 succession and cutting the lower part of this succession, the Sardinian unconformity and  
751 the underlying Cambro–Ordovician sequence (Puddu et al., 2018, 2019).

752 Although the Toledanian and Sardinian Phases reflect similar geodynamic conditions in  
753 two distinct palaeogeographic areas, at present forming the western and eastern  
754 branches of the Variscan Ibero-Armorican Arc, they display different peaks in magmatic  
755 activity with a minor chronological overlapping (Fig. 3). This may reflect a SW-to-NE  
756 “zip-like” propagation of the latest Ediacaran–Terreneuvian rifting axes in the so-called  
757 Atlas-Ossa Morena Rift.

758

#### 759 *Toledanian Phase*

760

761 The Early Ordovician (Toledanian) magmatism of the Central Iberian Zone evolved to a  
762 typical passive-margin setting, with geochemical features dominated by acidic rocks,  
763 peraluminous and rich in K, and lacking any association with basic or intermediate  
764 rocks. Some of the orthogneisses of the Galicia-Trás-os-Montes Zone basal and  
765 allochthonous complex units share these same patterns. This fact has been interpreted  
766 by some authors as a basin environment subject to important episodes of crustal  
767 extension (Martínez-Catalán et al., 2007; Díez-Montes et al., 2010). In contrast,  
768 Villaseca et al. (2016) interpreted this absence as evidence against rifting conditions,  
769 though the absence of contemporary basic magmatism may be explained by the partial  
770 fusion of a thickened crust, through recycling of Neoproterozoic crustal materials. The  
771 thrust of a large metasedimentary sequence could generate dehydration and  
772 metasomatism of the rocks above this sequence, triggering partial fusion at different  
773 levels, although the increase in peraluminosity with the basicity of the orthogneisses is  
774 against any AFC process involving mantle materials. However, this increase in

775 peraluminosity with the basicity has not been revealed in the samples studied above.  
776 Following Villaseca et al.'s (2016) model, a flat subduction of the southern part of the  
777 Central Iberian Zone would have taken place under its northern prolongation, whereas  
778 the reflection of such a subduction is not evident in the field. The calc-alkaline signature  
779 of this magmatism has also been taken into account as proof of its relationship with  
780 volcanic-arc environments (Valverde-Vaquero and Dunning, 2000). However, calc-  
781 alkaline features may be also interpreted as a result of a variable degree of continental  
782 crustal contamination and/or previously enriched mantle source (Sánchez-García et al.,  
783 2003, 2008, 2016, 2019; Díez-Montes et al., 2010). Finally, other granites not  
784 considered here of Tremadocian age have been reported in the southern Central  
785 Iberian Zone, such as the Oledo massif and the Beira Baixa-Central Extremadura,  
786 which display a I-type affinity (Antunes et al., 2009; Rubio Ordóñez et al., 2012). These  
787 granites could represent different sources for the Ordovician magmatism in the Central  
788 Iberian Zone.

789 Sánchez-García et al. (2019) have proposed that the anomaly that produced the  
790 large magmatism throughout the Iberian Massif could have migrated from the rifting  
791 axis to inwards zones and the acid, peraluminous, K-rich rocks of Mid Ordovician in  
792 age should represent the initial stages of a new rifting pulse, resembling the  
793 peraluminous rocks of the Early Rift Event *sensu* Sánchez-García et al. (2003) from the  
794 Cambrian Epoch 2 of the Ossa-Morena Rift.

795 In the parautochthon of the Galicia-Trás-os-Montes Zone, the appearance of  
796 tholeiitic and alkaline-peralkaline magmatism in the Mid Ordovician would signal the  
797 first steps toward extensional conditions (Díez Fernández et al., 2012; Dias da Silva et  
798 al., 2016). In the Montagne Noire and the Mouthoumet massifs contemporaneous  
799 tholeiitic lavas indicate a similar change in the tectonic regimen (Álvaro et al., 2016).  
800 This gradual change in geodynamic conditions is also marked by the appearance of  
801 rocks with extensional characteristics in some of subgroups considered here, such as  
802 the Central Iberian Zone (San Sebastián orthogneisses), eastern Pyrenees (Casemí

803 orthogneisses, and G1), volcanic rocks of the Occitan Domain, and the orthogneisses  
804 and volcanic rocks from Sardinia.

805

806 *Sardic Phase*

807

808 In the eastern Pyrenees, two peaks of Ordovician magmatic activity are observed  
809 (Casas et al., 2019). Large Lower–Middle Ordovician peraluminous granite bodies are  
810 known representing the protoliths of numerous gneissic bodies with laccolithic  
811 morphologies. In the Canigó massif, the Upper Ordovician granite bodies (protoliths of  
812 Cadí, Casemí, G1) are encased in sediments of the Canaveilles and Jujols groups.  
813 During this time span, there was generalized uplift and erosion that culminated with the  
814 onset of the Sardic unconformity. The Sardic Phase was succeeded by an extensional  
815 interval related to the formation of normal faults affecting the pre–unconformity strata  
816 (Puddu et al., 2018, 2019). The volcanic arc signature can be explained by crustal  
817 recycling (Navidad et al., 2010; Casas et al., 2010; Martínez et al., 2011), as in the  
818 case of the Toledanian Phase in the Central Iberian Zone, although, according to  
819 Casas et al. (2019), the Pyrenees and the Catalan Coastal Ranges were probably  
820 fringing the Gondwana margin in a different position than that occupied by the Iberian  
821 Massif. As a whole, the Ordovician magmatism in the Pyrenees lasted about 30 m.y.,  
822 from ca 477 to 446 Ma, in a time span contemporaneous with the formation of the  
823 Sardic unconformity (Fig. 2). Recently, Puddu et al. (2019) proposed that a thermal  
824 doming, bracketed between 475 and 450 Ma, could have stretched the Ordovician  
825 lithosphere. The emersion and denudation of the inherited Cambrian–Ordovician  
826 palaeorelief would have given rise to the onset of the Sardic unconformity. According to  
827 these authors, thermal doming triggered by hot mafic magma underplating may also be  
828 responsible for the late Early–Late Ordovician coeval magmatic activity.

829 In the Occitan Domain, there was a dramatic volcanic event in early Tremadocian  
830 times, with the uprising of basin floors and the subsequent effusion of abundant

831 rhyolitic activities under subaerial explosive conditions (Larroque volcanosedimentary  
832 Complex in the Montagne Noire, and Davejean acidic volcanic counterpart in the  
833 Mouthoumet Massif). Pouclet et al., (2017) interpreted this as a delayed Ollo de Sapo-  
834 style outpouring where a massive crustal melting required a rather significant heat  
835 supply. Asthenospheric upwelling leading to the interplay of lithospheric doming,  
836 continental break-up, and a decompressionally driven mantle melting can explain such  
837 a great thermal anomaly. The magmatic products accumulated on the mantle-crust  
838 contact would provide enough heat transfer for crustal melting (Huppert and Sparks,  
839 1988). Subsequently, a post-Sardic reactivation of rifting conditions is documented in  
840 the Cabrières klippes (southern Montagne Noire) and the Mouthoumet massif. There, a  
841 Late Ordovician fault-controlled subsidence linked to the record of rift-related tholeiites  
842 (Roque de Baudies and Villerouge formations) were contemporaneous with the record  
843 of the Hirnantian glaciation (Álvarez et al., 2016). Re-opening of rifting branches  
844 (Montagne Noire and Mouthoumet massifs) was geometrically recorded as overlapping  
845 patterns and final sealing of Sardic palaeoreliefs by Silurian and Lower Devonian  
846 strata.

847 Sardinia illustrates an almost complete record of the Variscan Belt (Carmignani et  
848 al., 1994; Rossi et al., 2009). Some plutonic orthogneisses of the Inner Zone belong to  
849 this cycle, such as the orthogneisses of Golfo Aranci (Giacomini et al., 2006). Gaggero  
850 et al. (2012) described three magmatic cycles. The first cycle is well represented in the  
851 Sarrabus unit by Furongian–Tremadocian volcanic and subvolcanic interbeds within a  
852 terrigenous succession (San Vito Formation) which is topped by the Sardic  
853 unconformity. Some plutonic orthogneisses of the Inner Zone belong to this cycle, such  
854 as the orthogneisses of Golfo Aranci (Giacomini et al., 2006) and the PB orthogneiss of  
855 Punta Bianca). The second Mid–Ordovician cycle, about 50 m.y. postdating the  
856 previous cycle, is of an arc-volcanic type with calc-alkaline affinity and acidic-to-  
857 intermediate composition. The acidic metavolcanites are referred in the literature as  
858 “porphyroids”, which crop out in the External Nappe Zone and some localities of the

859 Inner Zone. The intermediate to basic derivatives are widespread in Central Sardinia  
860 (Serra Tonnai Formation). Some plutonic rocks (Mt. Filau orthogneisses and Capo  
861 Spartivento) of the second cycle are discussed above. The third cycle consists of  
862 alkalic meta-epiclastites interbedded in post-Sandbian strata and metabasites marking  
863 the Ordovician/Silurian contact and reflecting rifting conditions. In this work only the first  
864 two cycles are considered. Giacomini et al. (2006) cite coeval mafic rocks of felsic  
865 magmatism of Mid Ordovician age (Cortesogno et al., 2004; Palmeri et al., 2004;  
866 Giacomini et al., 2005), although they interpret a subduction scenario of the Hun terrain  
867 below Corsica and Sardinia in the Mid Ordovician.

868

#### 869 *Origin of intracrustal siliceous melts*

870

871 In this scenario, the key to generate large volumes of acidic rocks in an intraplate  
872 context would be the existence of a lower-middle crust, highly hydrated, in addition to a  
873 high heat flow, possibly caused by mafic melts (Bryan et al., 2002; Díez-Montes, 2007).  
874 This could be the scenario initiated by the arrival of a thermal anomaly in a subduction-  
875 free area (Sánchez-García et al., 2003, 2008, 2019; Álvaro et al., 2016). The formation  
876 of large volumes of intracrustal siliceous melts could act as a viscous barrier,  
877 preventing the rise of mafic magmas within volcanic environments, and causing the  
878 underplating of these magmas at the contact between the lower crust and the mantle  
879 (Huppert and Sparks, 1988; Pankhurst et al., 1998; Bindeman and Valley, 2003). The  
880 cooling of these magmas could lead to crustal thickening and in this case, the volcanic  
881 arc signature can be explained by crustal recycling (Navidad et al., 2010; Díez-Montes  
882 et al., 2010; Martínez et al., 2011).

883 Sánchez-García et al. (2019) have proposed that the anomaly that produced the  
884 large magmatism throughout the Iberian Massif could have migrated from the rifting  
885 axis to inwards zones and the acid, peraluminous, K-rich rocks of Mid Ordovician in  
886 age should represent the initial stages of a new rifting pulse, resembling the



887 peraluminous rocks of the Early Rift Event *sensu* Sánchez-García et al. (2003) from the  
888 Cambrian Epoch 2 of the Ossa-Morena Rift. In the parautochthon of the Galicia-Trás-  
889 os-Montes Zone, the appearance of tholeiitic and alkaline-peralkaline magmatism in  
890 the Mid Ordovician would signal the first steps toward extensional conditions (Díez  
891 Fernández et al., 2012; Dias da Silva et al., 2016). In the Montagne Noire and the  
892 Mouthoumet massifs contemporaneous tholeiitic lavas indicate a similar change in the  
893 tectonic regimen (Álvaro et al., 2016). This change in geodynamic conditions is also  
894 marked by the appearance of rocks with extensional characteristics in some of  
895 subgroups considered here, such as the Central Iberian Zone (San Sebastián  
896 orthogneisses), eastern Pyrenees (Casemí orthogneisses, and G1), volcanic rocks of  
897 the Occitan Domain, and the orthogneisses and volcanic rocks from Sardinia. In the  
898 Pyrenees, Puddu et al. (2019) proposed that a thermal doming, between 475 and 450  
899 Ma, should have stretched the Ordovician lithosphere leading to emersion and  
900 denudation of a Cambrian–Ordovician palaeorelief, and giving rise to the onset of the  
901 Sardinic unconformity. According to these authors, thermal doming triggered by hot mafic  
902 magma underplating may also be responsible for the late Early–Late Ordovician coeval  
903 magmatic activity

904 A major continental break-up, leading to the so-called Tremadocian Tectonic Belt,  
905 was suggested by Pouclet et al. (2017), which initiated by upwelling of the  
906 asthenosphere and tectonic thinning of the lithosphere. Mantle-derived mafic magmas  
907 were underplated at the mantle-crust transition zone and intruded the crust. These  
908 magmas provided heat for crustal melting, which supplied the rhyolitic volcanism. After  
909 emptying the rhyolitic crustal reservoirs, the underlying mafic magmas finally rose and  
910 reached the surface. According to Pouclet et al. (2017), the acidic magmatic output  
911 associated with the onset of the Larroque metarhyolites resulted in massive crustal  
912 melting requiring a rather important heat supply. Asthenospheric upwelling leading to  
913 lithospheric doming, continental break-up, and a decompressionally driven mantle

914 melting can explain such a great thermal anomaly. Magmatic products accumulated on  
915 the mantle-crust contact providing enough heat transfer for crustal melting.

916

## 917 **6. Conclusions**

918

919 A geochemical comparison of 231 plutonic and volcanic samples of two major suites,  
920 Furongian–Mid Ordovician and Late Ordovician in age, from the Central Iberian and  
921 Galicia-Trás-os-Montes Zones of the Iberian Massif and in the eastern Pyrenees,  
922 Occitan Domain (Albigeois, Montagne Noire and Mouthoumet massifs) and Sardinia  
923 points to a predominance of materials derived from the melting of metasedimentary  
924 rocks, peraluminous and rich in  $\text{SiO}_2$  and  $\text{K}_2\text{O}$ . The total content in REE is moderate to  
925 high. Most felsic rocks display similar chondritic normalized REE patterns, with an  
926 enrichment of LREE relative to HREE, which should indicate the involvement of crustal  
927 materials in their parental magmas.

928  $\text{Zr}/\text{TiO}_2$ ,  $\text{Zr}/\text{Nb}$ ,  $\text{Nb}/\text{Y}$  and  $\text{Zr}$  vs.  $\text{Ga}/\text{Al}$  ratios, and REE and  $\epsilon_{\text{Nd}}$  values reflect  
929 contemporaneous arc and extensional scenarios, which progressed to distinct  
930 extensional conditions finally associated with outpouring of mafic tholeiitic-dominant  
931 rifting lava flows. Magmatic events are contemporaneous with the formation of the  
932 Toledanian (Furongian–Early Ordovician) and Sardic (Early–Late Ordovician)  
933 unconformities, related to neither metamorphism nor penetrative deformation. The  
934 geochemical and structural framework precludes subduction generated melts reaching  
935 the crust in a magmatic arc to back-arc setting. On the contrary, it favours partial  
936 melting of sediments and/or granitoids in a continental lower crust triggered by the  
937 underplating of hot mafic magmas related to the opening of the Rheic Ocean as a  
938 result of asthenospheric upwelling.

939

## 940 **7. Acknowledgements**

941

942 The authors thank the constructive and useful revisions made by Laura Gaggero  
943 (Genoa, Italy) and Jochen Mezger (Fairbanks, USA). This paper is a contribution to  
944 projects CGL2017-87631-P and PGC2018-093903-B-C22 from Spanish Ministry of  
945 Science and Innovation. We acknowledge support of the publication fee by the CSIC  
946 Open Access Publication Support Initiative through its Unit of Information Resources  
947 for Research (URICI).

948

949 **Data availability** - All data included in the paper and the Repository Data.

950

951 **Author contributions** - JJA, TSG and JMC: Methodology (Lead), Supervision (Lead),  
952 Writing – Original Draft (Lead), Writing – Review & Editing (Lead); CP, ADM, ML & GO:  
953 Methodology (Supporting), Supervision (Supporting), Writing – Original Draft  
954 (Supporting), Writing – Review & Editing (Supporting).

955

956 **Competing interests** - No competing interests

957

## 958 **References**

959

960 Alabouvette, B., Demange, M., Guérangé-Lozes, J., Ambert, P., 2003. Notice  
961 explicative de la carte géologique de Montpellier au 1/250 000. BRGM, Orléans.

962 Álvaro, J.J., Vizcaïno, D., 2018. The Furongian break-up (rift-drift) transition in the Anti-  
963 Atlas, Morocco. *J. Iberian Geol.* 44, 567–587.

964 Álvaro, J.J., Ferretti, F., González-Gómez, C., Serpagli, E., Tortello, M. F., Vecoli, M.,  
965 Vizcaïno, D., 2007. A review of the Late Cambrian (Furongian) palaeogeography in  
966 the western Mediterranean region, NW Gondwana. *Earth-Sci. Rev.* 85, 47–81.

967 Álvaro, J.J., Ezzouhairi, H., Ribeiro, M.L., Ramos, J.F., Solá, A.R., 2008. Early  
968 Ordovician volcanism of the Iberian Chains (NE Spain) and its influence on  
969 preservation of shell concentrations. *Bull. Soc. géol. France* 179(6), 569–581.

- 970 Álvaro, J.J., Bellido, F., Gasquet, D., Pereira, F., Quesada, C., Sánchez-García, T.,  
971 2014a. Diachronism of late Neoproterozoic–Cambrian arc-rift transition of North  
972 Gondwana: a comparison of Morocco and the Iberian Ossa-Morena Zone. *J. Afr.*  
973 *Earth Sci.* 98, 113–132.
- 974 Álvaro, J.J., Bauluz, B., Clausen, S., Devaere, L., Gil Imaz, A., Monceret, E., Vizcaïno,  
975 D., 2014b. Stratigraphy of the Cambrian–Lower Ordovician volcanosedimentary  
976 complexes, northern Montagne Noire, France. *Stratigraphy* 11, 83–96.
- 977 Álvaro, J.J., Colmenar, J., Monceret, E., Pouclet, A., Vizcaïno, D., 2016. Late  
978 Ordovician (post–Sardic) rifting branches in the North Gondwanan Montagne Noire  
979 and Mouthoumet massifs of southern France. *Tectonophysics* 681, 111–123.
- 980 Álvaro, J.J., Casas, J.M., Clausen, S., Quesada, C., 2018. Early Palaeozoic  
981 geodynamics in NW Gondwana. *J. Iberian Geol.* 44, 551–565.
- 982 Álvaro, J.J., Cortijo, I., Jensen, S., Lorenzo, S., Palacios, T., Pieren, A., 2019. Updated  
983 stratigraphic framework and biota of the Ediacaran and Terreneuvian in the Alcudia-  
984 Toledo Mountains of the Central Iberian Zone, Spain. *Est. Geol.* 75(2), e093.
- 985 Álvaro, J.J., Casas, J.M., Quesada, C., 2020. Reconstructing the pre-Variscan puzzle  
986 of Cambro–Ordovician basement rocks in the southwestern European margin of  
987 Gondwana. In: *Pannotia to Pangaea: Neoproterozoic and Paleozoic Orogenic*  
988 *Cycles in the Circum-Atlantic Regional* (Murphy, J.B., Strachan, R., Quesada, C.,  
989 eds.). *Geol. Soc., London, Spec. Publ.* 503, <https://doi.org/10.1144/SP503-2020-89>.
- 990 Antunes, I.M.H.R., Neiva, A.M.R., Silva, M.M.V.G., Corfu, F., 2009. The genesis of I-  
991 and S-type granitoid rocks of the Early Ordovician Oledo pluton, Central Iberian  
992 Zone (central Portugal). *Lithos* 111, 168–185.
- 993 Arthaud, F., 1970. Etude tectonique et microtectonique comparée de deux domaines  
994 hercyniens: les nappes de la Montagne Noire (France) et l'anticlinorium de  
995 l'Iglesiente (Sardaigne). PhD, Univ. Montpellier.
- 996 Ayora, C., 1980. Les concentrations métal-liques de la Vall de Ribes. PhD, Univ.  
997 Barcelona.

- 998 Ballèvre, M., Fourcade S., Capdevila, R., Peucat, J.J., Cocherie, A., Mark Fanning, C.,  
999 2012. Geochronology and geochemistry of Ordovician felsic volcanism in the  
1000 Southern Armorican Massif (Variscan belt, France): Implications for the breakup of  
1001 Gondwana. *Gondwana Res.* 21, 1019–1036.
- 1002 Barca, S., 1991. Phénomènes de resédimentation et flysch hercynien à faciès Culm  
1003 dans le “synclinal du Sarrabus” (SE de la Sardaigne, Italie). *C. R. Acad. Sci., Paris*  
1004 313(2), 1051–1057.
- 1005 Barca, S., Cherchi, A., 2004. Regional geological setting. In: Barca, S., Cherchi, A.  
1006 (eds.), *Sardinian Palaeozoic Basement and its Meso–Cainozoic Cover (Italy)*. 32nd  
1007 *Int. Geol. Congress. Field Trip Guide Book–P39 (5)*, 3–8.
- 1008 Barca, S., Carmignani, L., Maxia, M., Oggiano, G., Pertusati, P.C., 1986. The Geology  
1009 of Sarrabus. In: *Guide-Book to the Excursion on the Paleozoic Basement of Sardinia*  
1010 (Carmignani, L., Coccozza, T., Ghezzi, C., Pertusati, P.C., Ricci, C.A., eds.). *IGCP*  
1011 *Newsl., Spec. Iss.* 5, 51–60.
- 1012 Barca, S., Coccozza, T., Del Rio, M., Pillola, G.L., Pittau Demelia, P., 1987. Datation de  
1013 l’Ordovicien inférieur par *Dictyonema flabelliforme* et acritarches dans la partie  
1014 supérieure de la formation “cambrienne” de Cabitza (SW de la Sardaigne, Italie):  
1015 conséquences géodynamiques. *C. R. Acad. Sci., Paris* 305(2), 1109–1113.
- 1016 Barca, S., Del Rio, M., Pittau Demelia, P., 1988. New geological and stratigraphical  
1017 data and discovery of Lower Ordovician acritarchs in the San Vito Sandstone of the  
1018 Genn’Argiolas Unit (Sarrabus, Southeastern Sardinia). *Riv. It. Paleontol. Stratigr.* 94,  
1019 339–360.
- 1020 Bea, F., Montero, P., Talavera, C., Zinger, T., 2006. A revised Ordovician age for the  
1021 Miranda do Douro orthogneiss, Portugal. Zircon U–Pb ion-microprobe and LA–  
1022 ICPMS dating. *Geol. Acta* 4, 395–401.
- 1023 Bea, F., Montero, P., González Lodeiro, F., Talavera, C., 2007. Zircon inheritance  
1024 reveals exceptionally fast crustal magma generation processes in Central Iberia  
1025 during the Cambro–Ordovician. *J. Petrol.* 48, 2327–2339

- 1026 Bé Mézème, E., 2005. Contribution de la géochronologie U–Th–Pb sur monazite à la  
1027 compréhension de la fusion crustale dans la chaîne Hercynienne française et  
1028 implication géodynamique. PhD, Univ. Orléans.
- 1029 Bindeman, I.N., Valley, J.W., 2003. Rapid generation of both high- and low- $\delta^{18}\text{O}$ , large-  
1030 volume silicic magmas at the Timber Mountain/Oasis Valley caldera complex,  
1031 Nevada. *Geol. Soc. Am. Bull.* 115(5), 581–595.
- 1032 Boni, M., 1986. The Permo–Triassic vein and paleokarst ores in southwest Sardinia:  
1033 contribution of fluid inclusion studies to their genesis and paleoenvironment. *Mineral.*  
1034 *Deposita* 21, 53–62.
- 1035 Boni, M., Koepfel, V., 1985. Ore-lead isotope pattern from the Iglesias-Sulcis area  
1036 (SW Sardinia) and the problem of remobilization of metals. *Mineral. Deposita* 20,  
1037 185–193.
- 1038 Bryan, S.E., Riley, T.R., Jerram, D.A., Stephens, Ch.J., Leat, Ph.T., 2002. Silicic  
1039 volcanism: An undervalued component of large igneous provinces and volcanic  
1040 rifted margins. In: *Volcanic Rifted Margins* (Menzies, M.A., Klemperer, S.L., Ebinger,  
1041 C.J., Baker, J., eds.). *Geol. Soc. Am., Spec. Pap.* 362, 99–120.
- 1042 Calvet, P., Lapierre, H., Chavet, J., 1988. Diversité du volcanisme Ordovicien dans la  
1043 région de Pierrefitte (Hautes Pyrénées): rhyolites calco-alcalines et basaltes  
1044 alcalins. *C. R. Acad. Sci., Paris* 307, 805–812.
- 1045 Calvino, F., 1972. Note Illustrative della Carta Geologica d'Italia, Foglio 227 –  
1046 Muravera. Servizio Geologico d'Italia, Roma, 60 p.
- 1047 Carmignani, L., Cocozza, T., Ghezzi, C., Pertusati, P.C., Ricci, C.A., 1986. Guide-  
1048 book to the Excursion on the Palaeozoic Basement of Sardinia. IGCP Project no. 5,  
1049 *Newsl. Spec. Iss.*, 1–102.
- 1050 Carmignani, L., Pertusati, P.C., Barca, S., Carosi, R., Di Pisa, A., Gattiglio, M., et al.,  
1051 1992. Struttura della Catena Ercinica in Sardegna. Guida all'escursione del Gruppo  
1052 Informali di Geologia Strutturale in Sardegna, 24–29 (Maggio), 1–177.

- 1053 Carmignani, L., Carosi, R., Di Pisa, A., Gattiglio, M., Musumeci, G., Oggiano, G. et al.,  
1054 1994. The Hercynian chain in Sardinia (Italy). *Geodin. Acta* 7, 31–47.
- 1055 Carmignani, L., Oggiano, G., Barca, S., Conti, P., Salvadori, I., Eltrudis, A. et al. 2001.  
1056 *Geologia della Sardegna. Note illustrative della Carta Geologica della Sardegna a*  
1057 *scala 1:200.000. Memorie Descrittive della Carta Geologica d'Italia, Servizio*  
1058 *Geologico* 60, 1–283. Istituto Poligrafico e Zecca dello Stato, Roma.
- 1059 Caron, C., Lancelot, J., Omenetto, P., Orgeval, J.J., 1997. Role of the Sardic tectonic  
1060 phase in the metallogensis of SW Sardinia (Iglesiente): lead isotope evidence.  
1061 *European J. Miner.* 9, 1005–1016.
- 1062 Casas, J.M., 2010. Ordovician deformations in the Pyrenees: new insights into the  
1063 significance of pre–Variscan ('sardic') tectonics. *Geol. Mag.* 147, 674–689.
- 1064 Casas, J.M., Fernández, O., 2007. On the Upper Ordovician unconformity in the  
1065 Pyrenees: New evidence from the La Cerdanya area. *Geol. Acta* 5, 193–198.
- 1066 Casas, J.M., Murphy, J.B. 2018. Unfolding the arc: the use of pre-orogenic constraints  
1067 to assess the evolution of the Variscan belt in Western Europe. *Tectonophysics* 736,  
1068 47–61.
- 1069 Casas, J.M., Palacios, T., 2012. First biostratigraphical constraints on the pre–Upper  
1070 Ordovician sequences of the Pyrenees based on organic-walled microfossils. *C. R.*  
1071 *Geosci.* 344, 50–56.
- 1072 Casas, J.M., Castiñeiras, P., Navidad, M., Liesa, M., Carreras, J., 2010. New insights  
1073 into the Late Ordovician magmatism in the Eastern Pyrenees: U–Pb SHRIMP zircon  
1074 data from the Canigó massif. *Gondwana Res.* 17, 317–324.
- 1075 Casas, J.M., Álvaro, J.J., Clausen, S., Padel, M., Puddu, C., Sanz-López, J., Sánchez-  
1076 García, T., Navidad, M., Castiñeiras, P., Liesa, M., 2019. Palaeozoic basement of  
1077 the Pyrenees. In: *The Geology of Iberia: A Geodynamic Approach* (Quesada, C.,  
1078 Oliveira, J.T., eds.). *Regional Geology Reviews*, vol. 2, 229–259. Springer,  
1079 Heidelberg.

- 1080 Castiñeiras, P., Villaseca, C., Barbero, L., Martín-Romera, C., 2008a. SHRIMP U–Pb  
1081 zircon dating of anatexis in high-grade migmatite complexes of Central Spain:  
1082 implications in the Hercynian evolution of Central Iberia. *Int. J. Earth Sci.* 97, 35–50.
- 1083 Castiñeiras, P., Navidad, M., Liesa, M., Carreras, J., Casas, J.M., 2008b. U–Pb zircon  
1084 ages (SHRIMP) for Cadomian and Lower Ordovician magmatism in the Eastern  
1085 Pyrenees: new insights in the pre–Variscan evolution of the northern Gondwana  
1086 margin. *Tectonophysics* 46, 228–239.
- 1087 Castro, A., García-Casco, A., Fernández, C., Corretgé, L.G., Moreno-Ventas, I., Gerya,  
1088 T., Löw, I., 2009. Ordovician ferrosilicic magmas: experimental evidence for  
1089 ultrahigh temperatures affecting a metagreywacke source. *Gondwana Res.* 16, 622–  
1090 632
- 1091 Charles, N., Faure, M., Chen, Y., 2008. The emplacement of the Montagne Noire axial  
1092 zone (French Massif Central): New insights from petro-textural, geochronological  
1093 and AMS studies. *22ème Réunion des Sciences de la Terre, Nancy*, 155.
- 1094 Charles, N., Faure, M., Chen, Y., 2009. The Montagne Noire migmatitic dome  
1095 emplacement (French Massif Central): New insights from petrofabric and AMS  
1096 studies. *J. Struct. Geol.* 31, 1423–1440.
- 1097 Clariana, P., Valverde-Vaquero, P., Rubio-Ordóñez, A., Beranoaguirre, A., García-  
1098 Sansegundo, J., 2018. Pre–Variscan tectonic events and Late Ordovician  
1099 magmatism in the Central Pyrenees: U–Pb age and Hf in zircon isotopic signature  
1100 from subvolcanic sills in the Pallaresa massif. *J. Iberian Geol.* 44, 589–601.
- 1101 Cocco, F., Funedda, A., 2011. New data on the pre–Middle Ordovician deformation in  
1102 SE Sardinia: a preliminary note. *Rend. online Soc. Geol. It.* 15, 34–36.
- 1103 Cocco, F., Funedda, A., 2017. The Sardinic Phase: field evidence of Ordovician tectonics  
1104 in SE Sardinia. *Italy. Geol. Mag.* 156, 25–38.
- 1105 Cocco, F., Oggiano, G., Funedda, A., Loi, A., Casini, L., 2018. Stratigraphic, magmatic  
1106 and structural features of Ordovician tectonics in Sardinia (Italy): a review. *J. Iberian  
1107 Geol.* 44, 619–639.



- 1108 Cocherie, A., 2003. Datation avec le SHRIMP II du métagranite oeilé du Somail-  
1109 Montagne Noire. C. R. technique ANA-ISO/NT, BRGM.
- 1110 Cocherie, A., Baudin, T., Guerrot, C., Autran, A., Fanning, M.C., Laumonier, B., 2005.  
1111 U-Pb zircon (ID-TIMS and SHRIMP) evidence for the early Ordovician intrusion of  
1112 metagranites in the late Proterozoic Canaveilles Group of the Pyrenees and the  
1113 Montagne Noire (France). Bull. Soc. géol. France 176, 269–282.
- 1114 Cortesogno, L., Gaggero, L., Oggiano, G., Paquette, J.L., 2004. Different tectono-  
1115 thermal evolution paths in eclogitic rocks from the Axial Zone of the Variscan Chain  
1116 in Sardinia (Italy) compared with the Ligurian Alps. *Ofioliti* 29, 125–144.
- 1117 Costamagna, L.G., Elter, F.M., Gaggero, L., Mantovani, F., 2016. Contact  
1118 metamorphism in Middle Ordovician arc rocks (SW Sardinia, Italy): New  
1119 paleogeographic constraints. *Lithos* 264, 577–593.
- 1120 Cruciani, G., Franceschelli, M., Musumeci, G., Spano, M.E., Tiepolo, M., 2013. U-Pb  
1121 zircon dating and nature of metavolcanics and metarkoses from the Monte Grighini  
1122 Unit: new insights on Late Ordovician magmatism in the Variscan belt in Sardinia,  
1123 Italy. *Int. J. Earth Sci.* 102, 2077–2096.
- 1124 Cruciani, G., Franceschelli, M., Puxeddu, M., Tiepolo, M., 2018. Metavolcanics from  
1125 Capo Malfatano, SW Sardinia, Italy: New insight on the age and nature of  
1126 Ordovician volcanism in the Variscan foreland zone. *Geol. J.* 53(4), 1573–1585.
- 1127 Demange, M., 1999. Evolution tectonique de la Montagne noire: un modèle en  
1128 transpression. C. R. Acad. Sci., Paris 329, 823–829.
- 1129 Demange, M., Guérangé-Lozes, J., Guérangé, B., 1996. Notice explicative de la feuille  
1130 de Lacaune (987) au 1:50 000. BRGM, Orléans.
- 1131 Denèle, Y., Barbey, P., Deloule, E., Pelleter, E., Olivier, Ph., Gleizes, G., 2009. Middle  
1132 Ordovician U-Pb age of the Aston and Hospitalet orthogneissic laccoliths: their role  
1133 in the Variscan evolution of the Pyrenees. Bull. Soc. géol. France 180, 209–221.
- 1134 DePaolo, D.J., 1981. Neodymium isotopes in the Colorado Front Range and crust-  
1135 mantle evolution in the Proterozoic. *Nature* 291, 193–196.

- 1136 DePaolo, D.J., 1988. Neodymium isotope geochemistry. An introduction. *Minerals and*  
1137 *Rocks Series* 20, 1–187. Springer-Verlag, Berlin.
- 1138 DePaolo, D.J., Wasserburg, G.J., 1976. Nd isotopic variations and petrogenetic  
1139 models. *Geophys. Res. Lett.* 3(5), 249–252.
- 1140 Dias da Silva, Í., 2014. Geología de las Zonas Centro Ibérica y Galicia-Tras-os-Montes  
1141 en la parte oriental del Complejo de Morais, Portugal/España. *Serie Nova Terra* 45,  
1142 1–424.
- 1143 Dias da Silva, I., Valverde-Vaquero, P., González-Clavijo, E., Díez-Montes, A.,  
1144 Martínez-Catalán, J.R., 2012. Structural and stratigraphical significance of U–Pb  
1145 ages from the Saldanha and Mora volcanic complexes (NE Portugal, Iberian  
1146 Variscides). *Géol. France* 1, 105–106.
- 1147 Dias da Silva Í., Valverde-Vaquero, P., González Clavijo E., Díez-Montes A., Martínez  
1148 Catalán J.R., 2014. Structural and stratigraphical significance of U–Pb ages from the  
1149 Mora and Saldanha volcanic complexes (NE Portugal, Iberian Variscides). In:  
1150 Schulmann, K., Martínez Catalán, J. R., Lardeaux, J. M., Janousek, V., Oggiano, G.,  
1151 (eds.), *The Variscan Orogeny: Extent, Timescale and the Formation of the*  
1152 *European Crust*. Geol. Soc., London, Spec. Publ. 405, 115–135.
- 1153 Dias da Silva, I., Díez Fernández, R., Díez Montes, A., González Clavijo, E., Foster,  
1154 D.A., 2016. Magmatic evolution in the N-Gondwana margin related to the opening of  
1155 the Rheic Ocean – evidence from the Upper Parautochthon of the Galicia-Trás-os-  
1156 Montes Zone and from the Central Iberian Zone (NW Iberian Massif). *Int. J. Earth*  
1157 *Sci.* 105, 1127–1151.
- 1158 Díaz-Alvarado, J., Fernández, C., Chichorro, M., Castro, A., Pereira, M.F., 2016.  
1159 Tracing the Cambro–Ordovician ferrosilicic to calc-alkaline magmatic association in  
1160 Iberia by *in situ* U–Pb SHRIMP zircon geochronology (Gredos massif, Spanish  
1161 Central System batholith). *Tectonophysics* 681, 95–110.

- 1162 Díez Balda, M.A., Vegas, R., González Lodeiro, F., 1990. Part IV. Central Iberian Zone.  
1163 Structures. In: (Dallmeyer, R.D. & Martínez García, E. (eds.), Pre-Mesozoic Geology  
1164 of Iberia. Springer-Verlag, Berlin, pp. 172–188.
- 1165 Díez Fernández, R., Castiñeiras, P., Gómez Barreiro, J., 2012. Age constraints on  
1166 Lower Paleozoic convection system: Magmatic events in the NW Iberian Gondwana  
1167 margin. *Gondwana Res.* 21, 1066–1079.
- 1168 Díez-Montes, A., 2007. La Geología del Dominio “Ollo de Sapo” en las Comarcas de  
1169 Sanabria y Terra do Bolo. PhD, Univ. Salamanca. Laboratorio Xelóxico de Laxe,  
1170 Serie Nova Terra no. 34, A Coruña.
- 1171 Díez Montes, A., Martínez Catalán, J.R., Bellido Mulas, F., 2010. Role of the Ollo de  
1172 Sapo massive felsic volcanism of NW Iberia in the Early Ordovician dynamics of  
1173 northern Gondwana. *Gondwana Res.* 17, 363–376.
- 1174 Di Pisa, A., Gattiglio, M., Oggiano, G., 1992. Pre-Hercynian magmatic activity in the  
1175 nappe zone (internal and external) of Sardinia: evidence of two within plate basaltic  
1176 cycles. In: Contributions to the Geology of Italy with Special Regard to the Paleozoic  
1177 Basements (Carmingnani, L., Sassi, F.P., eds.). *Newsl. IGCP 276*, 107–116.
- 1178 Echtler, H., Malavieille, J., 1990. Extensional tectonics, basement uplift and Stephano–  
1179 Permian collapse basin in a late Variscan metamorphic core complex (Montagne  
1180 Noire, southern Massif Central). *Tectonophysics* 177, 125–138.
- 1181 El Korh, A., Schmidt, S.Th., Ballèvre, M., Ulianov, A., Bruguier, O., 2012. Discovery of  
1182 an albite gneiss from the Ile de Groix (Armorican Massif, France): geochemistry and  
1183 LA–ICP–MS U–Pb geochronology of its Ordovician protolith. *Int. J. Earth Sci.* 101,  
1184 1169–1190.
- 1185 Engel, W., Feist, R., Franke, W., 1980. Le Carbonifère anté-stéphanien de la Montagne  
1186 Noire: rapports entre mise en place des nappes et sédimentation. *Bull. BRGM* 2,  
1187 341–389.
- 1188 Elter, F.M., Francescherelli, M., Ghezzi, C., Memmi, I., Ricci, C.A., 1986. The geology  
1189 of northern Sardinia. *IGCP Project n. 5 Newsletter, Spec. Iss.* 87–102.

- 1190 Farias, P., Ordoñez-Casado, B., Marcos, A., Rubio-Ordóñez, A., Fanning, C.M., 2014.  
1191 U–Pb zircon SHRIMP evidence for Cambrian volcanism in the Schistose Domain  
1192 within the Galicia-Trás-os-Montes Zone (Variscan Orogen, NW Iberian Peninsula).  
1193 *Geol. Acta* 12(3), 209–218.
- 1194 Faure, M., Ledru, P., Lardeaux, J.M., Matte, P., 2004. Paleozoic orogenies in the  
1195 French Massif Central. A cross section from Béziers to Lyon. 32nd Int. Geol.  
1196 Congress Florence (Italy), Field-trip guide book, 40 p.
- 1197 Feist, R., Galtier, J., 1985. Découverte de flores d'âge namurien probable dans le  
1198 flysch à olistolithes de Cabrières (Hérault). Implications sur la durée de la  
1199 sédimentation synorogénique dans la Montagne Noire (France Méridionale). *C. R.*  
1200 *Acad. Sci., Paris* 300, 207–212.
- 1201 Franz, L., Romer, R.L., 2007. Caledonian high-pressure metamorphism in the Strona-  
1202 Ceneri-Zone (Southern Alps of southern Switzerland and northern Italy). *Swiss J.*  
1203 *Geosci.* 100, 457–467.
- 1204 Friedl, G., Finger, F., Paquette, J.L., von Quadt, A., McNaughton, N.J., Fletcher, I.R.,  
1205 2004. Pre–Variscan geological events in the Austrian part of the Bohemian Massif  
1206 deduced from U–Pb zircon ages. *Int. J. Earth Sci.* 93, 802–823
- 1207 Funedda, A., Oggiano, G., 2009. Outline of the Variscan basement of Sardinia. In: *The*  
1208 *Silurian of Sardinia. Volume in Honour of Enrico Serpagli (Corradini, C., Ferretti, A.,*  
1209 *Štorch, P., eds.). Rend. Soc. Paleontol. It.* 3, 23–35.
- 1210 Gaggero L., Oggiano G., Funedda A., Buzzi L., 2012. Rifting and arc-related Early  
1211 Paleozoic volcanism along the North Gondwana margin: Geochemical and  
1212 geological evidence from Sardinia (Italy). *J. Geol.* 120, 273–292.
- 1213 García-Arias, M., Díez-Montes, A., Villaseca, C., Blanco-Quintero, I.F. 2018. The  
1214 Cambro–Ordovician Ollo de Sapo magmatism in the Iberian Massif and its Variscan  
1215 evolution: A review. *Earth-Sci. Rev.* 176, 345–372.
- 1216 Gèze, B., 1949. Etude géologique de la Montagne Noire et des Cévennes  
1217 méridionales. *Mém. Soc. géol. France* 62, 1–215.

- 1218 Giacomini, F, Bomparola, R.M., Ghezzi, C., 2005. Petrology and geochronology of  
1219 metabasites with eclogite facies relics from NE Sardinia: constraints for the  
1220 Palaeozoic evolution of Southern Europe. *Lithos* 82, 221–248
- 1221 Giacomini, F., Bomparola, R.M., Ghezzi, C., Gulbrandsen, H., 2006. The geodynamic  
1222 evolution of the Southern European Variscides: constraints from the U/Pb  
1223 geochronology and geochemistry of the lower Palaeozoic magmatic-sedimentary  
1224 sequences of Sardinia (Italy). *Contrib. Miner. Petr.* 152, 19–42.
- 1225 Guérangé-Lozes, J., Alabouvette, B., 1999. Notice explicative, Carte géol. France (1/50  
1226 000), feuille Saint-Sernin-sur-Rance (960). BRGM, Orléans, 84 p.
- 1227 Guérangé-Lozes, J., Alsac, C., 1986. Les nappes varisques de l'Albigeois cristallin.  
1228 *Lithostratigraphie, volcanisme et déformations. Géol. France* 3, 309–337.
- 1229 Guérangé-Lozes, J., Guérangé, B., Mouline, M.P., Delsahut, B., 1996. Notice  
1230 explicative, Carte géol. France (1/50 000), feuille Réalmont (959). BRGM, Orléans,  
1231 78 p.
- 1232 Guitard, G., 1970. Le métamorphisme hercynien mésozonal et les gneiss ocellés du  
1233 massif du Canigou (Pyrénées orientales). *Mém. BRGM* 63, 1–353.
- 1234 Gutiérrez-Alonso, G., Fernández-Suárez, J., Gutiérrez-Marco, J.C., Corfu, F., Murphy,  
1235 J.B., Suárez Martínez, S., 2007. U–Pb depositional age for the upper Barrios  
1236 Formation (Armorican Quartzite facies) in the Cantabrian zone of Iberia: implications  
1237 for stratigraphic correlation and paleogeography. In: *The Evolution of the Rheic  
1238 Ocean: from Avalonian–Cadomian Active Margin to Alleghenian–Variscan Collision*  
1239 (Linnemann, R.D., Nance, P., Kraft, G.Z., eds.). *Geol. Soc. Am.*, London, 287–296.
- 1240 Gutiérrez-Alonso, G., Gutiérrez-Marco, J.C., Fernández-Suárez, J., Bernárdez, E.,  
1241 Corfu, F., 2016. Was there a super-eruption on the Gondwanan coast 477 Ma ago?  
1242 *Tectonophysics* 681, 85–94.
- 1243 Gutiérrez-Marco, J.C., Robardet, M., Rábano, I., Sarmiento, G., San José Lancha,  
1244 M.A., Herranz Araújo, P., Pieren Vidal, A., 2002. Ordovician. In: *The Geology of  
1245 Spain*, (Gibbons, W., Moreno, T., eds.), 31–49, Geological Society, London

- 1246 Gutiérrez-Marco, J.C., Piçarra, J.M., Meireles, C.A., Cózar, P., García-Bellido, D.C.,  
1247 Pereira, Z. et al., 2019. Early Ordovician–Devonian Passive margin stage in the  
1248 Gondwanan units of the Iberian massif. In: *The Geology of Iberia: A Geodynamic*  
1249 *Approach* (Quesada, C., Oliveira, J.T., eds.). *Regional Geology Reviews*, vol. 2, 75–  
1250 98. Springer, Heidelberg.
- 1251 Hartevelt, J.J.A., 1970. Geology of the upper Segre and Valira valleys, central  
1252 Pyrenees, Andorra/Spain. *Leid. Geol. Meded.* 45, 167–236.
- 1253 Helbing, H., Tiepolo, M., 2005. Age determination of Ordovician magmatism in NE  
1254 Sardinia and its bearing on Variscan basement evolution. *J. Geol. Soc.* 162, 689–  
1255 700.
- 1256 Huppert, H.E., Sparks, R.S.J., 1988. The generation of granitic magmas by intrusion of  
1257 basalt into continental crust. *J. Petrol.* 29, 599–624.
- 1258 Ibrahim, M.E., El-Kalioby, B.A., Aly, G.M., El-Tohamy, A.M., Watanabe, K., 2015.  
1259 Altered granitic rocks, Nusab El Balgum Area, Southwestern Desert, Egypt.  
1260 Mineralogical and geochemical aspects of REEs. *Ore Geol. Rev.* 70, 252–261.
- 1261 Irber, W., 1999. The lanthanide tetrad effect and its correlation with K/Rb, Eu/Eu\*,  
1262 Sr/Eu, Y/Ho, and Zr/Hf of evolving peraluminous granite suites. *Geochim.*  
1263 *Cosmochim. Acta* 63, 489–508.
- 1264 Jégouzo, P., Peucat, J.J., Audren, C., 1986. Caractérisation et signification  
1265 géodynamique des orthogneiss calco-alcalins d'âge ordovicien de Bretagne  
1266 méridionale. *Bull. Soc. géol. France* 2, 839–848.
- 1267 Kröner, A., Willner, A.P., 1998. Time of formation and peak of Variscan HP–HT  
1268 metamorphism of quartz-feldspar rocks in the central Erzgebirge, Saxony, Germany.  
1269 *Contrib. Mineral. Petrol.* 132, 1–20
- 1270 Lancelot, J. Allegret, A., Iglesias Ponce de León, M., 1985. Outline of Upper  
1271 Precambrian and Lower Paleozoic evolution of the Iberian Peninsula according to  
1272 U–Pb dating of zircons. *Earth Planet. Sci. Lett.* 74, 325–337.

- 1273 Laske, R., Bechstädt, T., Boni, M., 1994. The post–Sardic Ordovician series. In:  
1274 Sedimentological, stratigraphical and ore deposits field guide of the autochthonous  
1275 Cambro–Ordovician of Southeastern Sardinia (Bechstädt, T., Boni, M., eds.).  
1276 Memorie descrittive della carta geologica d'Italia 48, 115–146.
- 1277 Laumonier, B., Abad, A., Alonso, J.L., Baudelot, S., Bessière, G., Besson, M., Bouquet,  
1278 C., Bourrouilh, R., Brula, P., Carreras, J., Centène, A., Courjault-Radé, R.,  
1279 Courtessole, R., Fauconnier, D., García-Sanseguendo, J., Guitard, G., Moreno-Eiris,  
1280 E., Perejón, A., Vizcaïno, D., 1996. Le Paléozoïque Inférieur. In: Barnolas A, Chiron  
1281 JC (eds) Synthèse géologique et géophysique des Pyrénées. Tome 1: Cycle  
1282 hercynien. Cambro-Ordovicien. BRGM-ITGE, Orléans-Madrid. p 157–209.
- 1283 Leat, P.T., Jackson, S.E., Thorpe, R.S., Stillman, C.J., 1986. Geochemistry of bimodal  
1284 basalt-subalkaline/peralkaline rhyolite provinces within the Southern British  
1285 Caledonides. J. Geol. Soc. 143, 259–273.
- 1286 Le Corre, C., Auvray, B., Ballèvre, M., Robardet, M., 1991. Le Massif Armoricaïn. Sci.  
1287 Géol., Bull. 44, 31–103.
- 1288 Lentz, D., 1996. U, Mo and REE mineralization in late-tectonic granite pegmatites,  
1289 south-west Grenville Province, Canada. Ore Geol. Rev. 11, 197–227.
- 1290 Leone, F., Hamman, W., Laske, R., Serpagli, E., Villas, E., 1991. Lithostratigraphic  
1291 units and biostratigraphy of the post–Sardic Ordovician sequence in south-west  
1292 Sardinia. Boll. Soc. Paleontol. It. 30, 201–235.
- 1293 Leone, F., Ferretti, A., Hammann, W., Loi, A., Pillola, G.L., Serpagli, E., 2002. A  
1294 general view of the post–Sardic Ordovician sequence from SW Sardinia. Rend. Soc.  
1295 Paleontol. It. 1, 51–68.
- 1296 Lescuyer, J.L., Cocherie, A., 1992. Datation sur monozircons des métadacites de  
1297 Sériès: arguments pour un âge protérozoïque terminal des “schistes X” de la  
1298 Montagne Noire (Massif central français). C. R. Acad. Sci., Paris (sér. 2) 314, 1071–  
1299 1077.

- 1300 Liesa, M., Carreras, J., Castiñeiras, P., Casas, J.M., Navidad, M., Vilà, M., 2011. U–Pb  
1301 zircon age of Ordovician magmatism in the Albera Massif (Eastern Pyrenees). *Geol.*  
1302 *Acta* 9, 1–9.
- 1303 Linnemann, U., Gehmlich, M., Tichomirowa, M., Buschmann, B., Nasdala, L., Jonas, P.  
1304 et al. 2000. From Cadomian subduction to early Palaeozoic rifting: the evolution of  
1305 Saxo-Thuringia at the margin of Gondwana in the light of single zircon  
1306 geochronology and basin development (Central European Variscides, Germany). In:  
1307 *Orogenic Processes: Quantification and Modelling in the Variscan Belt* (Franke, W.,  
1308 Haak, V., Oncken, O., Tanner, D., eds.). *Geol. Soc., London, Spec. Publ.* 179, 131–  
1309 153.
- 1310 Loi, A., Dabard, M.P., 1997. Zircon typology and geochemistry in the palaeogeographic  
1311 reconstruction of the Late Ordovician of Sardinia (Italy). *Sediment. Geol.* 112, 263–  
1312 279.
- 1313 Loi, A., Barca, S., Chauvel, J.J., Dabard, M.P., Leone, F., 1992. Analyse de la  
1314 sédimentation post-phase sarde les dépôts initiaux à placers du SE de la Sardaigne.  
1315 *C. R. Soc. géol. France (sér. 2)* 315, 1357–1364.
- 1316 López-Sánchez, M.A., Iriondo, A., Marcos, A., Martínez, F.J., 2015. A U–Pb zircon age  
1317 ( $479 \pm 5$  Ma) from the uppermost layers of the Ollo de Sapo Formation near Viveiro  
1318 (NW Spain): implications for the duration of rifting-related Cambro–Ordovician  
1319 volcanism in Iberia. *Geol. Mag.* 152, 341–350.
- 1320 Ludwig, K.R., Turi, B., 1989. Paleozoic age of the Capo Spartivento Orthogneiss,  
1321 Sardinia, Italy. *Chem. Geol.* 79, 147–153.
- 1322 Margalef, A., Castiñeiras, P., Casas, J.M., Navidad, M., Liesa, M., Linnemann, U.,  
1323 Hofmann, M., Gärtner, A., 2016. Detrital zircons from the Ordovician rocks of the  
1324 Pyrenees: Geochronological constraints and provenance. *Tectonophysics* 681, 124–  
1325 134.



- 1326 Marini, F., 1988. "Phase" sarde et distension ordovicienne du domaine sud-varisque,  
1327 effets de point chaud? Une hypothèse fondée sur les données nouvelles du  
1328 volcanisme albigeois. C. R. Acad. Sci., Paris (sér. 2) 306, 443–450.
- 1329 Martí, J., Muñoz, J.A., Vaquer, R., 1986. Les roches volcaniques de l'Ordovicien  
1330 supérieur de la région de Ribes de Freser-Rocabruna (Pyrénées catalanes):  
1331 caractères et signification. C. R. Acad. Sci., Paris 302, 1237–1242.
- 1332 Martí, J., Solari, L., Casas, J.M., Chichorro, M., 2019. New late Middle to early Late  
1333 Ordovician U–Pb zircon ages of extension-related felsic volcanic rocks in the  
1334 Eastern Pyrenees (NE Iberia): tectonic implications. *Geol. Mag.* 156(10), 1783–  
1335 1792.
- 1336 Martínez, F., Iriondo, A., Dietsch, C., Aleinikoff, J.N., Peucat, J.J., Cirès, J., Reche, J.,  
1337 Capdevila, R., 2011. U–Pb SHRIMP–RG zircon ages and Nd signature of lower  
1338 Paleozoic rifting-related magmatism in the Variscan basement of the Eastern  
1339 Pyrenees. *Lithos* 127, 10–23.
- 1340 Martínez Catalán, J.R., Hacar Rodríguez, M.P., Villar Alonso, P., Pérez-Estaún, A.,  
1341 González Lodeiro, F., 1992. Lower Paleozoic extensional tectonics in the limit  
1342 between the West Asturian-Leonese and Central Iberian Zones of the Variscan  
1343 Fold-Belt in NW Spain. *Geologische Rundschau* 81(2), 546–560.
- 1344 Martínez Catalán, J.R., Arenas, R., Díaz García, F., Gómez Barreiro, J., González  
1345 Cuadra, P., Abati, J. et al. 2007. Space and time in the tectonic evolution of the  
1346 northwestern Iberian Massif. Implications for the comprehension of the Variscan  
1347 belt. In: 4–D Framework of Continental Crust (Hatcher, R.D.Jr., Carlson, M.P.,  
1348 McBride, J.H., Martínez Catalán, J.R., eds.). *Geol. Soc. Am., Mem.* 200, 403–423.
- 1349 Martini, I.P., Tongiorgi, M., Oggiano, G., Cocozza, T., 1991. Ordovician alluvial fan to  
1350 marine shelf transition in SW Sardinia, Western Mediterranean Sea: tectonically  
1351 ("Sardic" phase") influenced clastic sedimentation. *Sediment. Geol.* 72, 97–115.
- 1352 Masuda, A., Akagi, T., 1989. Lanthanide tetrad effect observed in leucogranites from  
1353 China. *Geochem. J.* 23, 245–253.

- 1354 McDougall, N., Brenchley, P.J., Rebelo, J.A., Romano, M., 1987. Fans and fan deltas –  
1355 precursors to the Armorican Quartzite (Ordovician) in western Iberia. *Geol. Mag.*  
1356 124, 347–359.
- 1357 McLennan, S.M., 1994. Rare earth element geochemistry and the “tetrad” effect.  
1358 *Geochim.Cosmochim. Acta* 58, 2025–2033.
- 1359 Medina, J., Rodríguez Alonso, M.D., Alonso Gavilán, G., 1998. Sedimentação em  
1360 plataforma siliciclástica do Grupo das Beiras (CXG) na região de Caramulo -  
1361 Buçaco (Portugal Central). *Comun. Inst. Geol. Min.* 85, 39–71.
- 1362 Meireles, C., Sequeira, A.J.D., Castro, P., Ferreira, N.I., 2013. New data on the  
1363 lithostratigraphy of Beiras Group (Schist Greywacke Complex) in the region of Góis-  
1364 Arganil- Pampilhosa da Serra (Central Portugal). *Cuad. Lab. Xeol. Laxe*, 37, 105–  
1365 124.
- 1366 Mezger, J., Gerdes, A., 2016. Early Variscan (Visean) granites in the core of central  
1367 Pyrenean gneiss domes: implications from laser ablation U–Pb and Th–Pb studies.  
1368 *Gondwana Res.* 29, 181–198.
- 1369 Mingram, B., Kröner, A., Hegner, E., Krentz, O., 2004. Zircon ages, geochemistry, and  
1370 Nd isotopic systematics of pre–Variscan orthogneisses from the Erzgebirge, Saxony  
1371 (Germany), and geodynamic interpretation. *Int. J. Earth Sci.* 93, 706–727.
- 1372 Monecke, T., Dulski, P., Kempe, U., 2007. Origin of convex tetrads in rare earth  
1373 element patterns of hydrothermally altered siliceous igneous rocks from the  
1374 Zinnwald Sn–W deposit, Germany. *Geochim. Cosmochim. Acta* 71, 335–353.
- 1375 Montero, P., Bea, F., González-Lodeiro, F., Talavera, C., Whitehouse, M.J., 2007.  
1376 Zircon ages of the metavolcanic rocks and metagranites of the Ollo de Sapo Domain  
1377 in central Spain: implications for the Neoproterozoic to Early Palaeozoic evolution of  
1378 Iberia. *Geol. Mag.* 144, 963–976.
- 1379 Montero, P., Talavera, C., Bea, F., Lodeiro, F.G., Whitehouse, M.J., 2009. Zircon  
1380 geochronology of the Ollo de Sapo Formation and the age of the Cambro–  
1381 Ordovician rifting in Iberia. *J. Geol.* 117, 174–191.

- 1382 Murphy, J.B., Gutiérrez-Alonso, G., Nance, R.D., Fernández-Suárez, J., Keppie, J.D.,  
1383 Quesada, C. et al., 2006. Origin of the Rheic Ocean: rifting along a Neoproterozoic  
1384 suture? *Geology* 34, 325–328.
- 1385 Nance, R.D., Gutiérrez-Alonso, G., Keppie, J.D., Linnemann, U., Murphy, J.B.,  
1386 Quesada, C. et al., 2010. Evolution of the Rheic Ocean. *Gondwana Res.* 17, 194–  
1387 222.
- 1388 Navidad, M., Castiñeiras, P., 2011. Early Ordovician magmatism in the northern  
1389 Central Iberian Zone (Iberian Massif): new U–Pb (SHRIMP) ages and isotopic Sr–  
1390 Nd data. 11th ISOS, Alcalá de Henares, May 2011.
- 1391 Navidad, M., Castiñeiras, P., Casas, J.M., Liesa, M., Fernández-Suárez, J., Barnolas,  
1392 A., Carreras, J., Gil-Peña, I., 2010. Geochemical characterization and isotopic ages  
1393 of Caradocian magmatism in the northeastern Iberia: insights into the Late  
1394 Ordovician evolution of the northern Gondwana margin. *Gondwana Res.* 17, 325–  
1395 337.
- 1396 Navidad, M., Castiñeiras, P., Casas, J.M., Liesa, M., Belousova, E., Proenza, J.,  
1397 Aiglsperger, T., 2018. Ordovician magmatism in the Eastern Pyrenees: Implications  
1398 for the geodynamic evolution of northern Gondwana. *Lithos* 314–315, 479–496.
- 1399 Neiva, A.M.R., Williams, I.S., Ramos, J.M.F., Gomes, M.E.P., Silva, M.M.V.G.,  
1400 Antunes, I.M.H.R., 2009. Geochemical and isotopic constraints on the petrogenesis  
1401 of Early Ordovician granodiorite and Variscan two-mica granites from the Gouveia  
1402 area, central Portugal. *Lithos* 111, 186–202.
- 1403 Oggiano, G., Gaggero, L., Funedda, A., Buzzi, L., Tiepolo, M., 2010. Multiple early  
1404 Paleozoic volcanic events at the northern Gondwana margin: U–Pb age evidence  
1405 from the southern Variscan branch (Sardinia, Italy). *Gondwana Res.* 17, 44–58.
- 1406 Padel, M., Álvaro, J.J., Clausen, S., Guillot, F., Pujol, M., Chichorro, M., Monceret, E.,  
1407 Pereira, M.F., Vizcaíno, D., 2017. U–Pb laser ablation ICP–MS zircon dating across  
1408 the Ediacaran–Cambrian transition of the Montagne Noire, southern France. *C. R.*  
1409 *Geosci.* 349, 380–390.

- 1410 Padel, M., Clausen, S., Álvaro, J.J., Casas, J.M., 2018. Review of the Ediacaran–  
1411 Lower Ordovician (pre-Sardic) stratigraphic framework of the Eastern Pyrenees,  
1412 southwestern Europe. *Geol. Acta* 16, 339–355
- 1413 Palme, H., O'Neill, H.S.C., 2004. Cosmochemical estimates of mantle composition. In:  
1414 *Treatise on Geochemistry 2* (Holland, H.D., Turekian, K.K., eds.), 1–38. Elsevier-  
1415 Pergamon, Oxford.
- 1416 Palmeri, R., Fanning, M., Franceschelli, M., Memmi, I., Ricci, C.A., 2004. SHRIMP  
1417 dating of zircons in eclogite from the Variscan basement in northeastern Sardinia  
1418 (Italy). *N. Jb. Miner., Mh.* 6, 275–288.
- 1419 Pan, Y., 1997. Controls on the fractionation of isovalent trace elements in magmatic  
1420 and aqueous systems: evidence from Y/Ho, Zr/Hf, and lanthanide tetrad effect – a  
1421 discussion of the article by M. Bau, 1996. *Contrib. Mineral. Petrol.* 128, 405–408.
- 1422 Pankhurst, R.J., Rapela, C.W., Saavedra, J., Baldo, E., Dahlquist, J., Pascua, I.,  
1423 Fanning, C.M., 1998. The Famatinian magmatic arc in the central Sierras  
1424 Pampeanas, and Early to Middle Ordovician continental arc on the Gondwana  
1425 margin. In: *The Proto-Andean Margin of Gondwana* (Pankhurst, R.J., Rapela, C.E.,  
1426 eds.). *Geol. Soc., London, Spec. Publ.* 142, 343–367.
- 1427 Pavanetto, P., Funedda, A., Northrup, C. J., Schmitz, M., Crowley, J., Loi, A., 2012.  
1428 Structure and U–Pb zircon geochronology in the Variscan foreland of SW Sardinia,  
1429 Italy. *Geol. J.* 47, 426–445.
- 1430 Pearce, J.A., 1996. Sources and settings of granitic rocks. *Episodes* 19, 120–125.
- 1431 Pearce, J.A., Harris, N.B.W., Tindle, A.G., 1984. Trace element discrimination  
1432 diagrams for the tectonic interpretation of granitic rocks. *J. Petrol.* 25, 956–983.
- 1433 Pereira, M.F., Solá, A.R., Chichorro, M., Lopes, L., Gerdes, A., Silva, J.B., 2012. North-  
1434 Gondwana assembly, break-up and paleogeography: U–Pb isotope evidence from  
1435 detrital and igneous zircons of Ediacaran and Cambrian rocks of SW Iberia.  
1436 *Gondwana Res.* 22(3–4), 866–881.

- 1437 Piercey, S.J., 2011. The setting, style, and role of magmatism in the formation of  
1438 volcanogenic massive sulphide deposits. *Miner. Deposita* 46, 449–471.
- 1439 Pistis, M., Loi, A., Dabard, M.P., 2016. Influence of relative sea-level variations on the  
1440 genesis of palaeoplacers, the examples of Sarrabus (Sardinia, Italy) and the  
1441 Armorican Massif (western France). *C. R. Geosci.* 348(2), 150–157.
- 1442 Pillola, G.L., Leone, F., Loi, A., 1998. The Cambrian and Early Ordovician of SW  
1443 Sardinia. *Gior. Geol. (ser. 3), Spec. Iss.* 60, 25–38.
- 1444 Pitra, P., Poujol, M., Den Driessche, J.V., Poilvet, J. C., Paquette, J.L., 2012. Early  
1445 Permian extensional shearing of an Ordovician granite: the Saint-Eutrope “C/S-like”  
1446 orthogneiss (Montagne Noire, French Massif Central). *C. R. Geosci.* 344, 377–384.
- 1447 Pouclet, A., Álvaro, J.J., Bardintzeff, J.M., Gil Imaz, A., Monceret, E., Vizcaïno D.,  
1448 2017. Cambrian–Early Ordovician volcanism across the South Armorican and  
1449 Occitan Domains of the Variscan Belt in France: Continental break-up and rifting of  
1450 the northern Gondwana margin. *Geosci. Frontiers* 8, 25–64.
- 1451 Puddu, C., Álvaro J.J., Casas, J.M., 2018. The Sardic unconformity and the Upper  
1452 Ordovician successions of the Ribes de Freser area, Eastern Pyrenees. *J. Iberian  
1453 Geol.* 44, 603–617.
- 1454 Puddu, C., Álvaro, J.J., Carrera, N., Casas, J.M., 2019. Deciphering the Sardic  
1455 (Ordovician) and Variscan deformations in the Eastern Pyrenees. *J. Geol. Soc.*  
1456 176(6), 1191–1206.
- 1457 Quesada, C., 1991. Geological constraints on the Paleozoic tectonic evolution of  
1458 tectonostratigraphic terranes in the Iberian Massif. *Tectonophysics* 185, 225–245.
- 1459 Rabin, M., Trap, P., Carry, N. Fréville, K. Cenki-Tok, B. Lobjoie, C. Gonçalves, P.,  
1460 Marquer, D., 2015. Strain partitioning along the anatectic front in the Variscan  
1461 Montagne Noire massif (southern French Massif Central). *Tectonics* 34, 1709–1735.
- 1462 Robert, J. F. 1980. Étude géologique et métallogénique du val de Ribas sur le versant  
1463 espagnol des Pyrénées catalanes. PhD, Univ. Franche-Comté.

- 1464 Robert, J.F., Thiebaut, J., 1976. Découverte d'un volcanisme acide dans le Caradoc de  
1465 la région de Ribes de Freser (Prov. de Gérone). C. R. Acad. Sci., Paris 282, 2050–  
1466 2079.
- 1467 Roger, F., Respaut, J.P., Brunel, M., Matte, Ph., Paquette, J.L., 2004. Première  
1468 datation U–Pb des orthogneiss ocellés de la zone axiale de la Montagne Noire (Sud  
1469 du Massif central): nouveaux témoins du magmatisme ordovicien dans la chaîne  
1470 varisque. C. R. Geosci. 336, 19–28
- 1471 Roger, F., Teyssier, C., Respaut, J.P., Rey, P.F., Jolivet, M., Whitney, D.L., Paquette,  
1472 J.L., Brunel, M., 2015. Timing of formation and exhumation of the Montagne Noire  
1473 double dome, French massif Central. Tectonophysics 640–641, 53–69.
- 1474 Rollison, H.R., 1993. Using Geochemical Data: Evaluation, Presentation, Interpretation.  
1475 Longman Group, London, 352 p.
- 1476 Romão, J., Dunning, G., Marcos, A., Dias, R., Ribeiro, A., 2010. O lacólito granítico de  
1477 Mação-Penhascoso: idade e as suas implicações (SW da Zona Centro-Ibérica). e-  
1478 Terra 16, 1–4.
- 1479 Rossi, P., Oggiano, G., Cocherie, A., 2009. A restored section of the “southern  
1480 Variscan realm” across the Corsica-Sardinia microcontinent. C. R. Geosci. 34, 224–  
1481 238.
- 1482 Rubio-Ordóñez, A., Valverde-Vaquero, P., Corretgé, L. G., Cuesta-Fernández, A.,  
1483 Gallastegui, G., Fernández-González, M., Gerdès, A., 2012. An Early Ordovician  
1484 tonalitic-granodioritic belt along the Schistose-Greywacke Domain of the Central  
1485 Iberian Zone (Iberian Massif, Variscan Belt). Geol. Mag. 149, 927–939.
- 1486 Rudnick, R.L., Gao, S., 2003. Composition of the Continental Crust. In: Treatise on  
1487 Geochemistry (Holland, H.D., Turekian, K.K., eds.), vol. 3, 1–64. Elsevier-  
1488 Pergamon, Oxford.
- 1489 Sánchez-García, T., Bellido, F., Quesada, C., 2003. Geodynamic setting and  
1490 geochemical signatures of Cambrian–Ordovician rift-related igneous rocks (Ossa-  
1491 Morena Zone, SW Iberia). Tectonophysics 365, 233–255.

- 1492 Sánchez-García, T., Quesada, C., Bellido, F., Dunning, G., González de Tánago, J.,  
1493 2008. Two-step magma flooding of the upper crust during rifting: the Early Paleozoic  
1494 of the Ossa-Morena Zone (SW Iberia). *Tectonophysics* 461, 72–90.
- 1495 Sánchez-García, T., Bellido, F., Pereira, M.F., Chichorro, M., Quesada, C., Pin, Ch.,  
1496 Silva, J.B., 2010. Rift-related volcanism predating the birth of the Rheic Ocean  
1497 (Ossa-Morena zone, SW Iberia). *Gondwana Res.* 17, 392–407.
- 1498 Sánchez-García, T., Quesada, C., Bellido, F., Dunning, G.R., Pin, Ch., Moreno-Eiris,  
1499 E., Perejón, A., 2016. Age and characteristics of the Loma del Aire unit (SW Iberia):  
1500 Implications for the regional correlation of the Ossa-Morena Zone. *Tectonophysics*  
1501 681, 58–72.
- 1502 Sánchez-García, T., Chichorro, M., Solá, R., Álvaro, J.J., Díez Montes, A., Bellido, F. et  
1503 al. 2019. The Cambrian–Early Ordovician Rift Stage in the Gondwanan Units of the  
1504 Iberian Massif. In: *The Geology of Iberia: A Geodynamic Approach* (Quesada, C.,  
1505 Oliveira, J.T., eds.). *Regional Geol. Rev.* 1, 27–74.
- 1506 Sarmiento, G.N., Gutiérrez-Marco, J.C., Robardet, M., 1999. Conodontos ordovícicos  
1507 del noroeste de España. Aplicación al modelo de sedimentación de la región  
1508 limítrofe entre las zonas Asturoccidental-Leonesa y Centroibérica durante el  
1509 Ordovícico Superior. *Rev. Soc. Geol. España* 12, 477–500.
- 1510 Schaltegger, U., Abrecht, J., Corfu, F., 2003. The Ordovician orogeny in the Alpine  
1511 basement: constraints from geochronology and geochemistry in the Aar Massif  
1512 (Central Alps). *Schweizerische Miner. Petrogr. Mitteil.* 83, 183–195.
- 1513 Shaw, J., Johnston, S., Gutiérrez-Alonso, G., Weil, A.B., 2012. Oroclines of the  
1514 Variscan orogen of Iberia: paleocurrent analysis and paleogeographic implications.  
1515 *Earth Planet. Sci. Lett.* 329–330, 60–70.
- 1516 Shaw, J., Gutiérrez-Alonso, G., Johnston, S., Pastor Galán, D., 2014. Provenance  
1517 variability along the early Ordovician north Gondwana margin: paleogeographic and  
1518 tectonic implications of U–Pb detrital zircon ages from the Armorican Quartzite of  
1519 the Iberian Variscan belt. *Geol. Soc. Am. Bull.* 126(5–6), 702–719.

- 1520 Solá, A.R., 2007. Relações Petrogeoquímicas dos Maciços Graníticos do NE  
1521 Alentejano. PhD, Univ. Coimbra.
- 1522 Solá, A.R., Pereira, M.F., Williams, I.S., Ribeiro, M.L., Neiva, A.M.R., Montero, P., Bea,  
1523 F., Zinger, T., 2008. New insights from U–Pb zircon dating of Early Ordovician  
1524 magmatism on the northern Gondwana margin: the Urra formation (SW Iberian  
1525 Massif, Portugal). *Tectonophysics* 461, 114–129.
- 1526 Stern, R.J., 2002. Crustal evolution in the East African Orogen: a neodymium isotopic  
1527 perspective. *J. African Earth Sci.* 34, 109–117.
- 1528 Stille, H., 1939. Bemerkungen betreffend die “Sardische” Faultung und den Ausdruck  
1529 “Ophiolitisch”. *Zeits. Deuts. Gess. Geowiss.* 91, 771–773.
- 1530 Sun, S.S., McDonough, W.F., 1989. Chemical and isotopic systematics of oceanic  
1531 basalts: implications for mantle composition and processes. In: *Magmatism in the*  
1532 *Ocean Basins* (Saunders, A.D., Norry, M.J., eds.). *Geol. Soc., Spec. Publ.* 42, 13–  
1533 345.
- 1534 Syme, E.C., 1998. Ore-Associated and Barren Rhyolites in the central Flin Flon Belt:  
1535 Case Study of the Flin Flon Mine Sequence. Manitoba Energy and Mines, Open File  
1536 Report OF98–9, 1–32
- 1537 Takahashi, Y., Yoshida, H., Sato, N., Hama, K., Yusa, Y., Shimizu, H., 2002. W- and  
1538 M-type tetrad effects in REE patterns for water-rock systems in the Tono uranium  
1539 deposit, central Japan. *Chem. Geol.* 184, 311–335.
- 1540 Talavera, C., 2009. Pre–Variscan magmatism of the Central Iberian Zone: chemical  
1541 and isotope composition, geochronology and geodynamic significance. PhD, Univ.  
1542 Granada.
- 1543 Talavera, C., Bea F, Montero P., Whitehouse, M., 2008. A revised Ordovician age for  
1544 the Sisargas orthogneiss, Galicia (Spain). Zircon U–Pb ion-microprobe and LA–  
1545 ICPMS dating. *Geol. Acta* 8, 313–317.

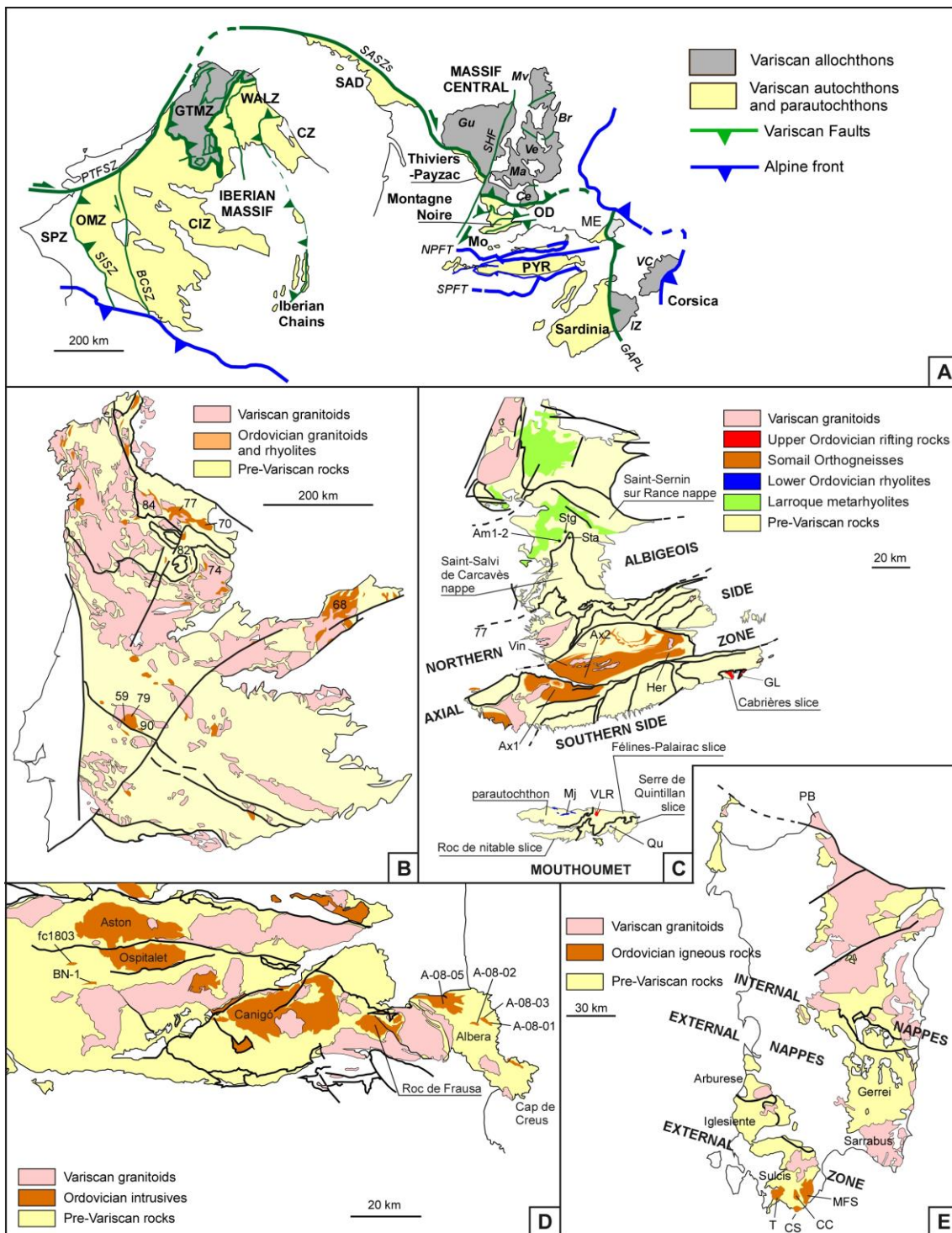


- 1546 Talavera, C., Montero, P., Bea, F., González Lodeiro, F., Whitehouse, M., 2013. U–Pb  
1547 Zircon geochronology of the Cambro–Ordovician metagranites and metavolcanic  
1548 rocks of central and NW Iberia. *Int. J. Earth. Sci.* 102, 1–23.
- 1549 Taylor, S.R., McLennan, S.M., 1985. *The Continental Crust: Its Composition and*  
1550 *Evolution*. Blackwell, London, 312 pp.
- 1551 Teichmüller, R., 1931. Zur Geologie des Thyrrhenisgebietes, Teil 1: Alte und junge  
1552 Krustenbewegungen im südlichen Sardinien. *Abh. Der wissen. Gess. Göttingen*  
1553 (Math.-Phys. Kl) 3, 857–950.
- 1554 Teipel, U., Eichhorn, R., Loth, G., Rohrmüller, J., Höll, R., Kennedy, A., 2004. U–Pb  
1555 SHRIMP and Nd isotopic data from the western Bohemian Massif (Bayerischer  
1556 Wald, Germany): Implications for Upper Vendian and Lower Ordovician magmatism.  
1557 *Int. J. Earth Sci.* 93, 782–801.
- 1558 Thompsom, M.D., Grunow, A.M., Ramezani, J., 2010. Cambro–Ordovician  
1559 paleogeography of the Southeastern New England Avalon Zone: Implications for  
1560 Gondwana breakup. *Geol. Soc. Am. Bull.* 122, 76–88.
- 1561 Tichomirowa, M., Berger, H.J., Koch, E.A., Belyatski, B., Götze, J., Kempe, U.,  
1562 Nasdala, L., Schaltegger, U., 2001. Zircon ages of high-grade gneisses in the  
1563 Eastern Erzgebirge (Central European Variscides) – constraints on origin of the  
1564 rocks and Precambrian to Ordovician magmatic events in the Variscan foldbelt.  
1565 *Lithos* 56, 303–332.
- 1566 Tichomirowa, M., Sergeev, S., Berger, H.J., Leonhardt, D., 2012. Inferring protoliths of  
1567 high-grade metamorphic gneisses of the Erzgebirge using zirconology,  
1568 geochemistry and comparison with lower-grade rocks from Lusatia (Saxothuringia,  
1569 Germany). *Contrib. Mineral. Petrol.* 164, 375–396.
- 1570 Valverde-Vaquero, P., Dunning, G.R., 2000. New U–Pb ages for Early Ordovician  
1571 magmatism in Central Spain. *J. Geol. Soc. London* 157, 15–26.

- 1572 Valverde-Vaquero, P., Marcos, A., Farias, P., Gallastegui, G., 2005. U–Pb dating of  
1573 Ordovician felsic volcanism in the Schistose Domain of the Galicia-Trás-os-Montes  
1574 Zone near Cabo Ortegal (NW Spain). *Geol. Acta* 3, 27–37.
- 1575 Valverde-Vaquero, P., Farias, P., Marcos, A., Gallastegui, G., 2007. U–Pb dating of  
1576 Siluro–Ordovician volcanism in the Verín synform (Orense, Schistose Domain,  
1577 Galicia-Trás-os-montes Zone). *Geogaceta* 41, 247–250.
- 1578 Vilà, M., Pin, C., Enrique, P., Liesa, M., 2005. Telescoping of three distinct magmatic  
1579 suites in an orogenic setting: Generation of Hercynian igneous rocks of the Albera  
1580 Massif (Eastern Pyrenees). *Lithos* 83, 97–127.
- 1581 Villaseca, C., Castiñeiras, P., Orejana, D., 2013. Early Ordovician metabasites from the  
1582 Spanish Central System: A remnant of intraplate HP rocks in the Central Iberian  
1583 Zone. *Gondwana Res.* 27, 392–409.
- 1584 Villaseca, C., Merino Martínez, E., Orejana, D., Andersen, T., Belousova, E., 2016.  
1585 Zircon Hf signatures from granitic orthogneisses of the Spanish Central System:  
1586 Significance and sources of the Cambro–Ordovician magmatism in the Iberian  
1587 Variscan Belt. *Gondwana Res.* 34, 60–83.
- 1588 Von Quadt, A., 1997. U–Pb zircon and Sr–Nd–Pb whole-rock investigations from the  
1589 continental deep drilling (KTB). *Geol. Rundsch.* 86 (suppl.), S258–S271.
- 1590 Von Raumer, J.F., Stampfli, G.M., 2008. The birth of the Rheic Ocean – early  
1591 Palaeozoic subsidence patterns and tectonic plate scenarios. *Tectonophysics* 461,  
1592 9–20.
- 1593 Von Raumer, J.F., Stampfli, G.M., Borel, G., Bussy, F., 2002. The organization of pre–  
1594 Variscan basement areas at the Gondwana margin. *Int. J. Earth Sci.* 91, 35–52.
- 1595 Von Raumer, J.F., Bussy, F., Schaltegger, U., Schulz, B., Stampfli, G., 2013. Pre–  
1596 Mesozoic Alpine basements: their place in the European Paleozoic framework.  
1597 *Geol. Soc. Am. Bull.* 125, 89–108.

- 1598 Von Raumer, J.F., Stampfli, G.M., Arenas, R., Sánchez Martínez, S., 2015. Ediacaran  
1599 to Cambrian oceanic rocks of the Gondwanan margin and their tectonic  
1600 interpretation. *Int. J. Earth Sci.* 104, 1107–1121.
- 1601 Whalen, J.B., Currie, K.L., Chappell, B.W., 1987. A-type granites: Geochemical  
1602 characteristics, discrimination and petrogenesis. *Contr. Miner. Petrol.* 95, 407–419.
- 1603 Winchester, J.A., Floyd, P.A., 1977. Geochemical discrimination of different magma  
1604 series and their differentiation products using immobile elements. *Chem. Geol.* 20,  
1605 325–343.
- 1606 Zeck, H.P., Whitehouse, M.J., Ugidos, J.M., 2007.  $496 \pm 3$  Ma zircon ion microprobe  
1607 age for pre-Hercynian granite, Central Iberian Zone, NE Portugal (earlier claimed  
1608  $618 \pm 9$  Ma). *Geol. Mag.* 144, 21-31.
- 1609 Zurbruggen, R., 2015. Ordovician orogeny in the Alps – a reappraisal. *Int. J. Earth Sci.*  
1610 104, 335–350.
- 1611 Zurbruggen, R., 2017. The Cenerian orogeny (early Paleozoic) from the perspective of  
1612 the Alpine region. *Int. J. Earth Sci.* 106, 517–529.
- 1613 Zurbruggen, R., Franz, L., Handy, M.R., 1997. Pre-Variscan deformation,  
1614 metamorphism and magmatism in the Strona-Ceneri Zone (southern Alps of  
1615 northern Italy and southern Switzerland). *Schweiz. Miner. Petrograph. Mitteil.* 77,  
1616 361–380.
- 1617 Zwart, H.J., 1979. *The Geology of the Central Pyrenees. Leidse Geol. Meded.* 50, 1–74  
1618

## 1619 FIGURE CAPTIONS

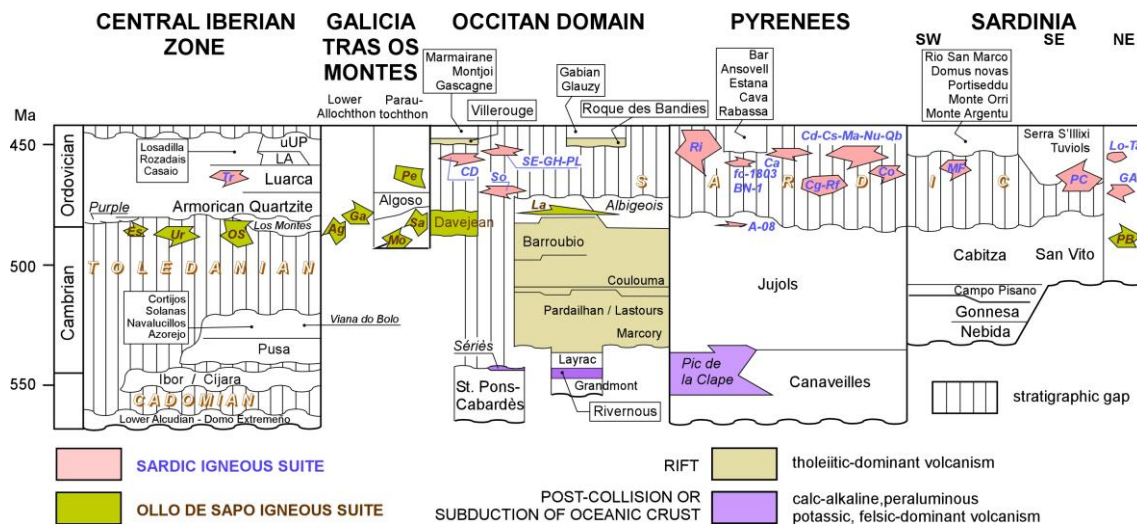


1620

1621

1622 **Figure 1.** A. Pre-Variscan reconstruction of the Variscan tectonostratigraphic units  
 1623 bearing Cambro-Ordovician exposures reported in this work, from the south-western  
 1624 European margin of Gondwana; based on Pouclet et al. (2017) and Álvaro et al.  
 1625 (2020). B. Setting of samples in the Central Iberian and Galicia-Trás-os-Montes zones;

1626 59 Carrascal, 68 Guadarrama, 70 Sanabria, 74 Miranda do Douro, 77 Olo de Sapo, 79  
1627 Portalegre, 82 Saldanha, 84 San Sebastián, 90 Urra, *BCSZ* Badajoz-Córdoba Shear  
1628 Zone, *Ce* Cévennes massif, *CIZ* Central Iberian Zone, *CZ* Cantabrian Zone, *GAPL*  
1629 Grimaud-Asinara-Posada Line, *GTMZ* Galicia-Trás-os-Montes Zone, *ME* Maures-  
1630 Estérel massif, *Mo* Mouthoumet massif, *NPFT* North Pyrenean Fault Thrust, *OD*  
1631 Occitan Domain, *OMZ* Ossa-Morena Zone, *PTFSZ* PYR Porto-Tomar-Ferreira do  
1632 Alentejo Shear Zone, Pyrenean Domain, *Sa* Sanabria, *SAD* South Armorican Domain,  
1633 *SASZs* South-Armorican Shear-Zone southern branch, *SHF* Sillon Houiller Fault, *SISZ*  
1634 South-Iberian Shear Zone, *SPFT* South Pyrenean Fault Thrust, ***SPZ* South Portuguese**  
1635 **Zone** and *WALZ* West Asturian-Leonese Zone; modified from Sánchez-García et al.  
1636 (2019). C. Setting of samples in the Montagne Noire and Mouthoumet massifs; *Am1-2*  
1637 Larroque hamlet (Ambialet), *Stg* St.Géraud, *Sta* St. André, *Mj* Montjoi, *Qu* Quintillan,  
1638 *GL* Roque de Bandies, *VLR* Villerouge-Termenès, *VIN* Le Vintrou, *HER* Gorges d'Héric  
1639 (Caroux massif), *Ax1* S Mazamet (Nore massif), *Ax2* (Rou) S Rouayroux (Agout  
1640 massif); modified from Álvaro et al. (2016). D. Setting of Pyrenean samples; *AB-08-01*,  
1641 *02*, *03* Albera metavolcanics, *AB-08-05* Albera orthogneisses, *BN-1* Andorra rhyolites,  
1642 *fc-1803* Pallaresa rhyolites; modified from Casas et al. (2019). E. Setting of Sardinian  
1643 samples; *CS 2,3,4,8* Spartivento Cap, *T2* Tuerreda, *CC5* Cuile Culurgioni, *MF1* Monte  
1644 Filau, *MFS1* Monte Settiballas, *PB* Punta Bianca; modified from Oggiano et al. (2010).  
1645



1646

1647

1648 **Figure 2.** Cambro-Ordovician lithostratigraphic chart of the areas studied in this work

1649 from the Central Iberian Zone, Galicia Trás-os-Montes Zone, Occitan Domain, Eastern

1650 Pyrenees and Sardinia; modified from Álvaro et al. (2014b, 2016, 2018), Pouclet et al.

1651 (2017) and Sánchez-García et al. (2019); other lithostratigraphic sketches, such as

1652 those of the Ciudad Rodrigo-Hurdes-Sierra de Gata Domain (Díez Balda et al., 1990)

1653 and the Portuguese sector (Medina et al., 1998; Meireles et al., 2013) in the Central

1654 Iberian Zone, the central Pyrenees (Zwart, 1979; Laumonier et al., 1996), the Albigeois

1655 Mountains in the Occitan Domain (Guérangé-Lozes and Alsac, 1986; Pouclet et al.,

1656 2017) and northern Sardinia (Elter et al., 1986), are not included here; abbreviations:

1657 A-08 Albera orthogneisses and metavolcanics (ca. 465–472 Ma; Liesa et al., 2011),

1658 Ag Agualada, BN-1 Andorra rhyolites, Ca Campelles ignimbrites (ca. 455 Ma, Martí et

1659 al., 2014), CD Cadí gneiss (456 ± 5 Ma, Casas et al., 2010), Cg Canigó gneiss (472–

1660 462 Ma, Cocherie et al., 2005; Navidad et al., 2018), Co Cortalets metabasite (460 ± 3

1661 Ma, Navidad et al., 2018), Cs Casemí gneiss (446 ± 5 and 452 ± 5 Ma, Casas et al.,

1662 2010), Es Estremoz rhyolites (499 Ma, Pereira et al., 2012), fc-1803 Pallaresa rhyolites

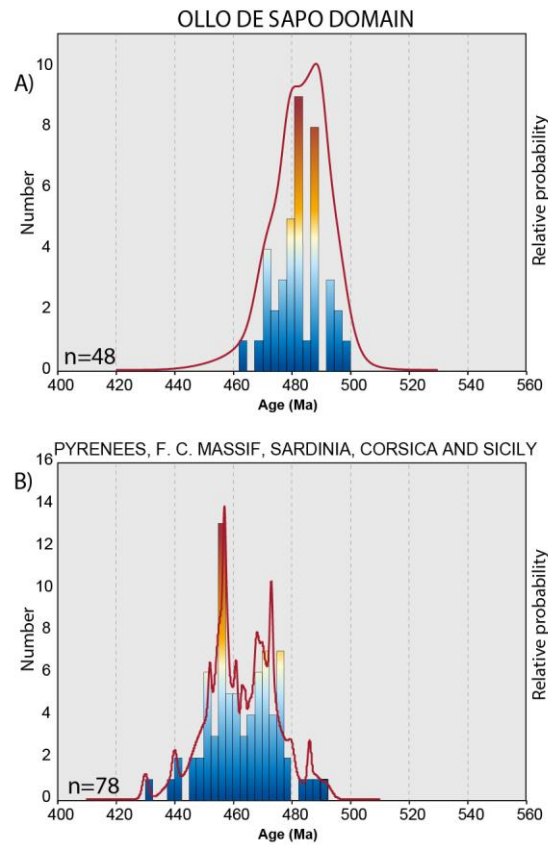
1663 (ca. 453 Ma; Clariana et al., 2018), Ga Galiñero, GA Golfo Aranci orthogneiss (469 ±

1664 3.7 Ma, Giacomini et al., 2006), GH Gorges d'Heric orthogneiss (450 ± 6 Ma, Roger et

1665 al., 2004), La Larroque Volcanic Complex, LA La Aquiana Limestone, Ma Marialles

1666 microdiorite (453 ± 4 Ma, Casas et al., 2010), Lo Lodè orthogneiss (456 ± 14 Ma,

1667 Helbing and Tiepolo, 2005), *MF* Monte Filau-Capo Spartivento orthogneiss ( $449 \pm 6$   
1668 Ma, Ludwing and Turi, 1989;  $457.5 \pm 0.3$  and  $458.2 \pm 0.3$  Ma, Pavanetto et al., 2012),  
1669 *Mo* Mora ( $493.5 \pm 2$  Ma, Dias Da Silva et al., 2014), *Nu* Núria gneiss ( $457 \pm 4$  Ma,  
1670 Martínez et al., 2011), *OS* Olo de Sapo rhyolites and ash-fall tuff beds (ca. 477 Ma.,  
1671 Gutiérrez-Alonso et al., 2016), *Pe* Peso Volcanic Complex, *PL* Pont de Larn  
1672 orthogneiss ( $456 \pm 3$  Ma, Roger et al., 2004), *Qb* Queralbs gneiss ( $457 \pm 5$  Ma,  
1673 Martínez et al., 2011), *PB* Punta Bianca orthogneiss (broadly Furongian–Tremadocian  
1674 in age), *PC* Porto Corallo dacites ( $465.4 \pm 1.9$  and  $464 \pm 1$  Ma, Giacomini et al., 2006;  
1675 Oggiano et al., 2010), *Ri* Ribes granophyre ( $458 \pm 3$  Ma, Martínez et al., 2011), *Rf* Roc  
1676 de Frausa gneiss ( $477 \pm 4$ ,  $476 \pm 5$  Ma, Cocherie et al., 2005; Castiñeiras et al., 2008),  
1677 *So* Somail orthogneiss ( $471 \pm 4$  Ma, Cocherie et al. 2005), *Sa* Saldanha ( $483.7 \pm 1.5$ ;  
1678 Dias da Silva, 2014), *SE* Saint Eutrope gneiss ( $455 \pm 2$  Ma, Pitra et al., 2012), *Ta*  
1679 Tanaunella orthogneiss  $458 \pm 7$  Ma (Helbing and Tiepolo, 2005), *Tr* Turchas, *Ur* Urra  
1680 rhyolites and *uUP* undifferentiated Upper Ordovician.  
1681



1682

1683

1684

**Figure 3.** Relative probability plots of the age of the Cambrian–Ordovician magmatism

1685

for (A) the Ollo de Sapo domain from the Central Iberian Zone; and (B) Pyrenees

1686

(Guilleries and Gavarres massifs), French Central Massif (including Montagne Noire),

1687

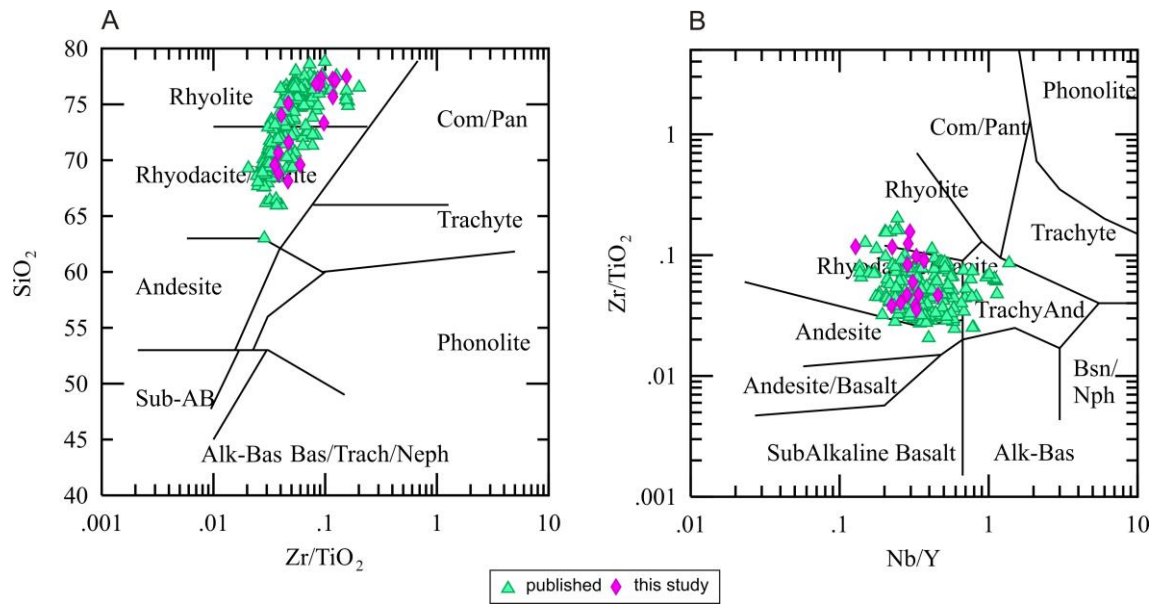
Sardinia, Corsica and Sicily ( $n$  = number of analyses). Data obtained from references

1688

cited in the text.

1689





1690

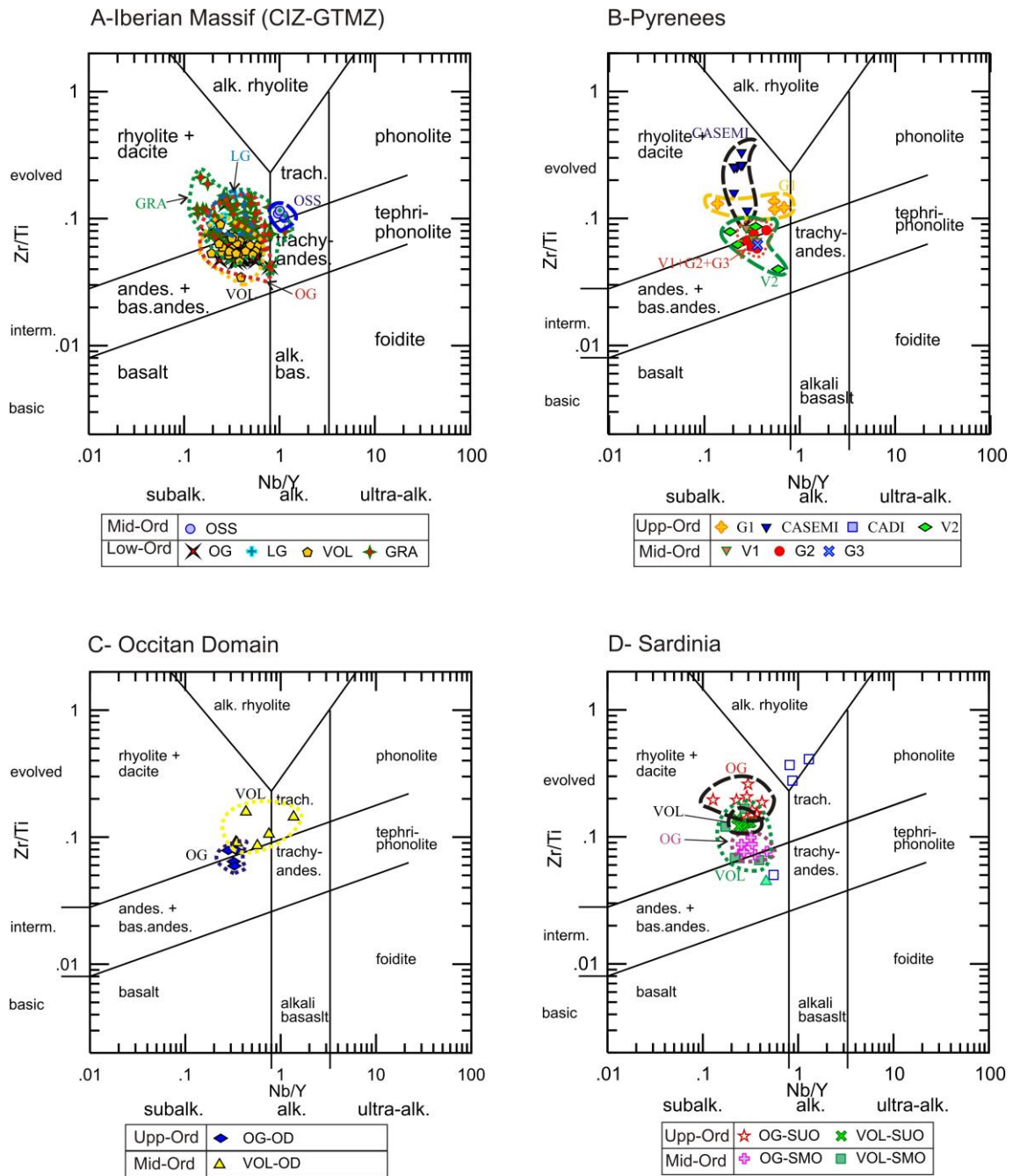
1691

1692 **Figure 4.** SiO<sub>2</sub> vs. Zr/TiO<sub>2</sub> and Zr/TiO<sub>2</sub> vs. Nb/Y plots (Winchester and Floyd, 1977)

1693 showing the composition of new samples (purple diamonds) and those taken from the

1694 literature (green triangles).

1695



1696

1697

1698 **Figure 5.** Zr/Ti vs. Nb/Y discrimination diagram (after Winchester and Floyd, 1977;

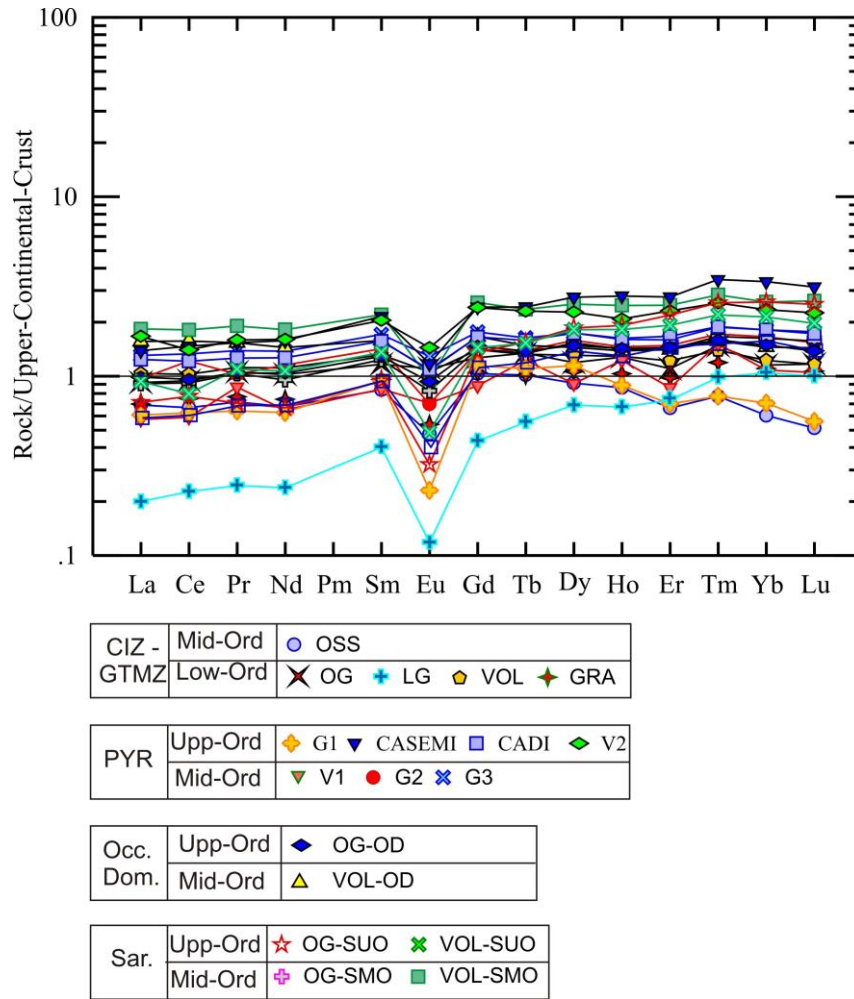
1699 Pearce, 1996). A. Lower–Middle Ordovician rocks of Iberian Massif (Central Iberian

1700 and Galicia-Trás-os-Montes zones). B. Middle–Upper Ordovician rocks of the eastern

1701 Pyrenees. C) Middle Ordovician rocks of the Occitan Domain. C–D. Middle–Upper

1702 Ordovician rocks of Sardinia.

1703

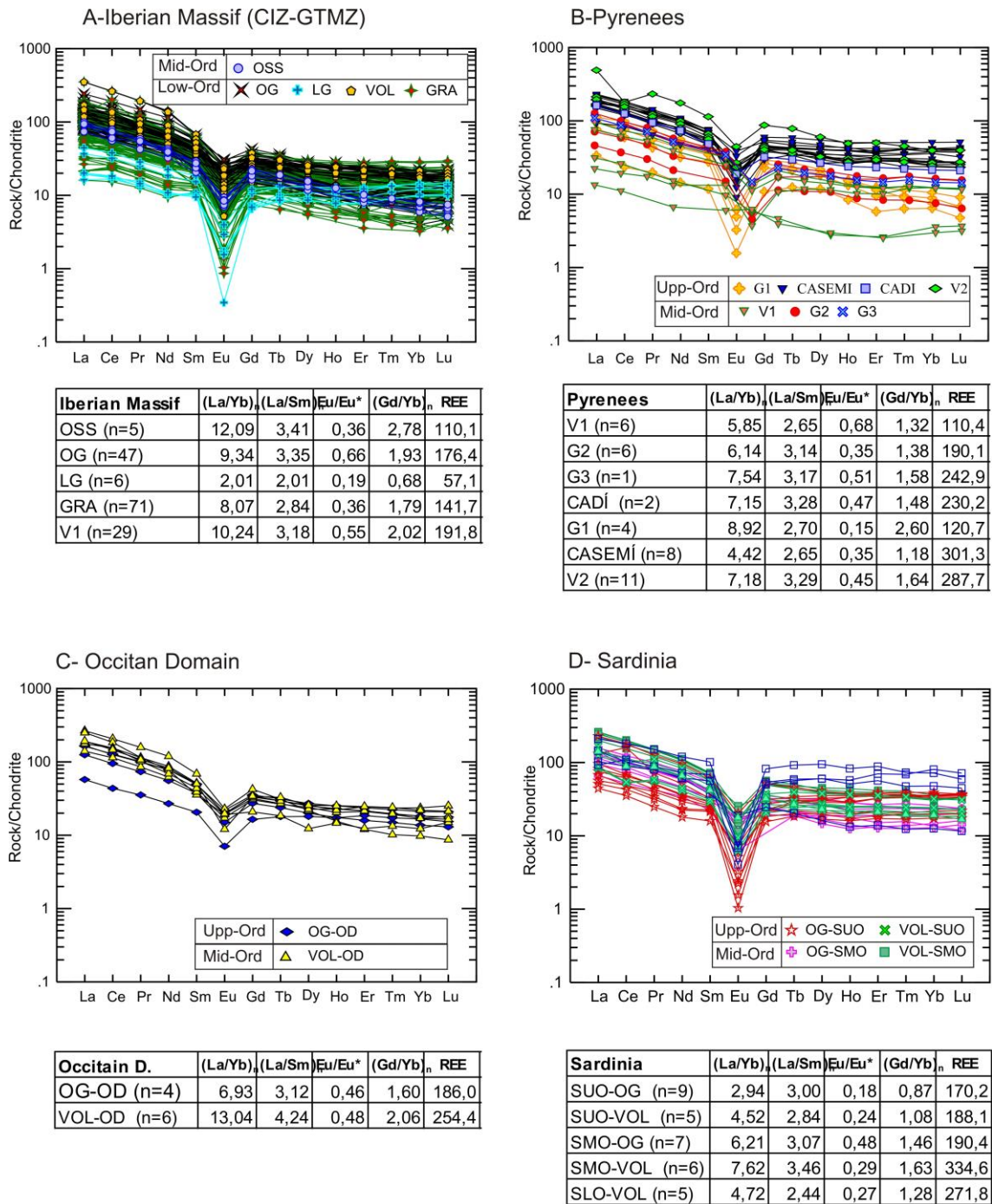


1704

1705

1706 **Figure 6.** Upper Crustal-normalized REE patterns (Rudnick and Gao, 2003) with  
 1707 average values for all distinguished groups; symbols as in Figure 4.

1708



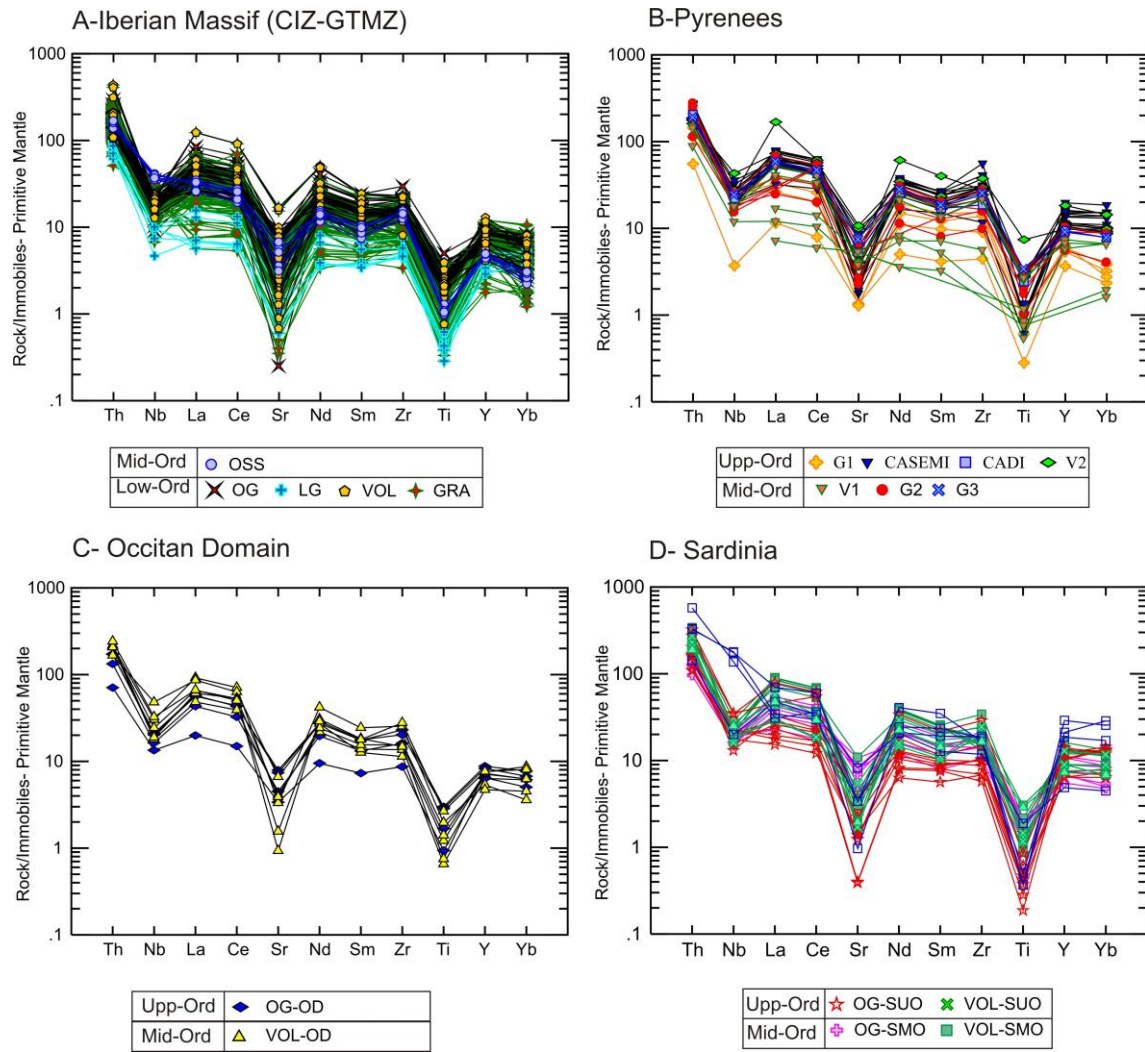
1709

1710

1711 **Figure 7.** Chondrite-normalized REE patterns (Sun and McDonough, 1989) for all

1712 study samples.

1713



1714

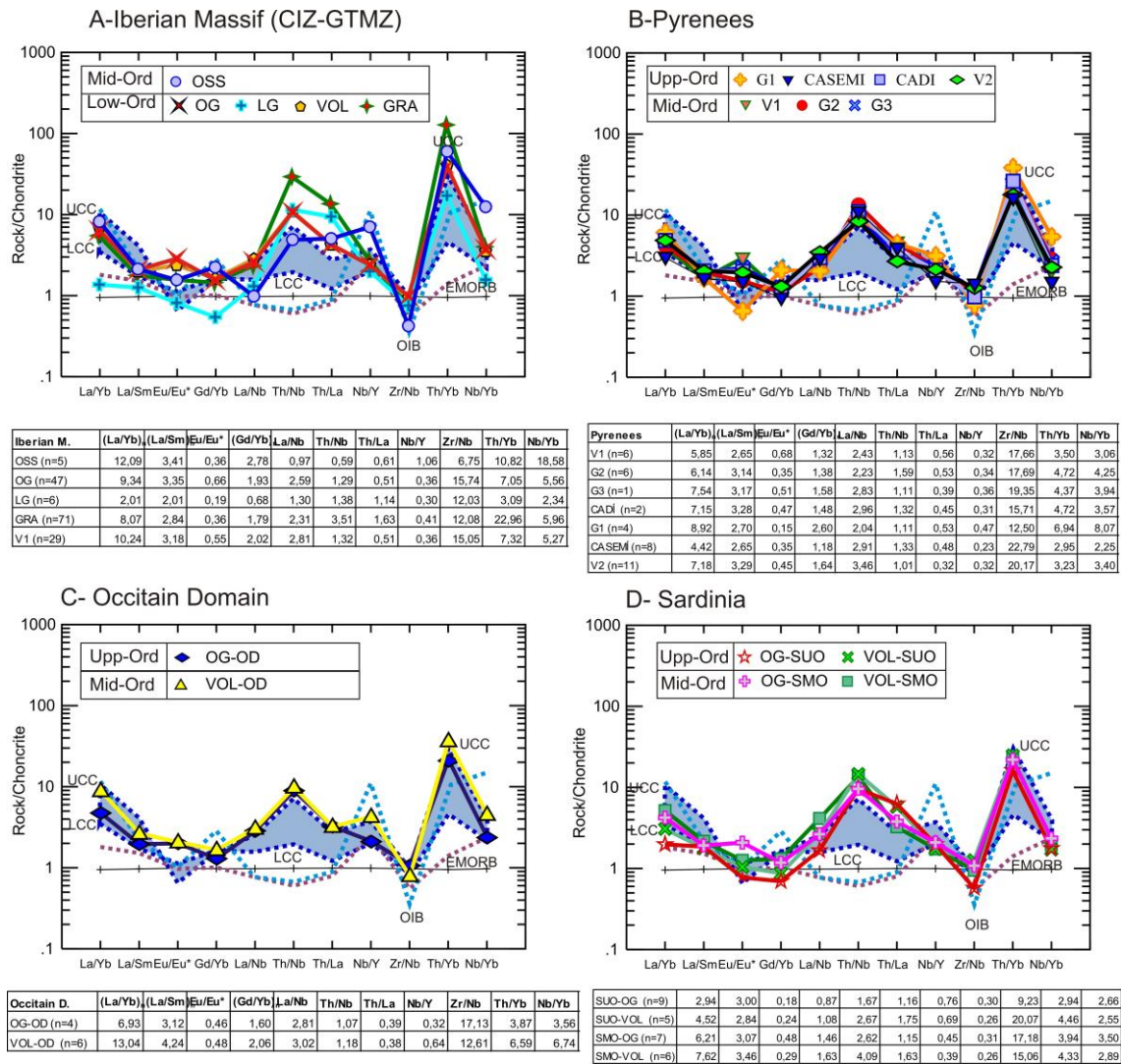
1715

1716 **Figure 8.** Multi-element diagram normalised to Primitive Mantle of Palme and O'Neill

1717 (2004) for all study samples.

1718





## References

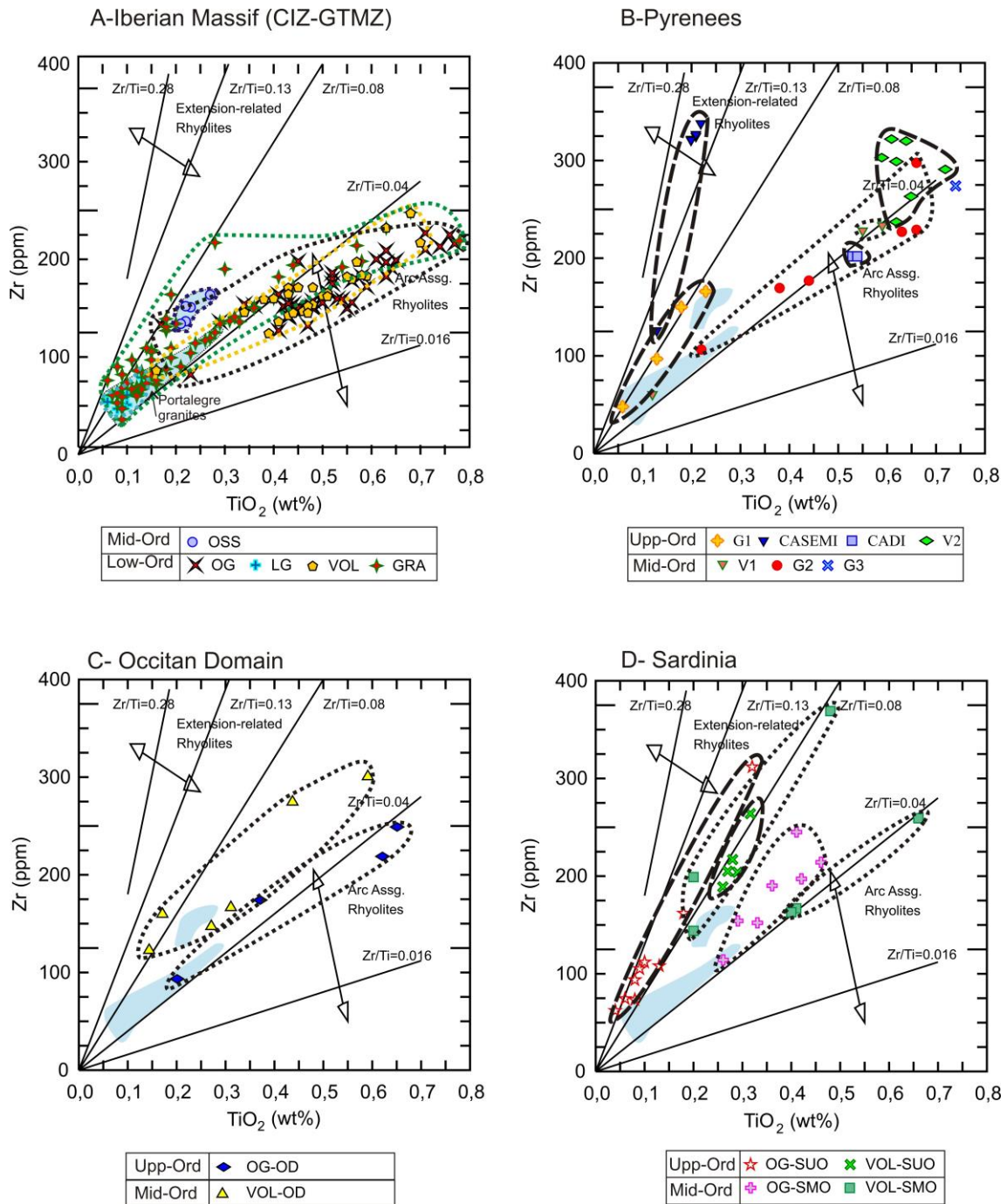
- ..... Continental Crust (limits: upper, UCC and lower, (LCC) of Rudnick and Gao (2004)
- ..... Ocean Island Basalts (OIB) of Sun and McDonough (1989)
- ..... Enriched Mid-ocean ridge basalts (EMORB) of Sun and McDonough (1989)
- Chondrite of Sun & McDonough (1989)

1719

1720

1721 **Figure 9.** Chondrite-normalised isotope ratio patterns (Sun and McDonough, 1989) for  
 1722 standard comparison for all study samples. Blue area: limits of continental crustal  
 1723 values (Lower and Upper) of Rudnick and Gao (2003).

1724

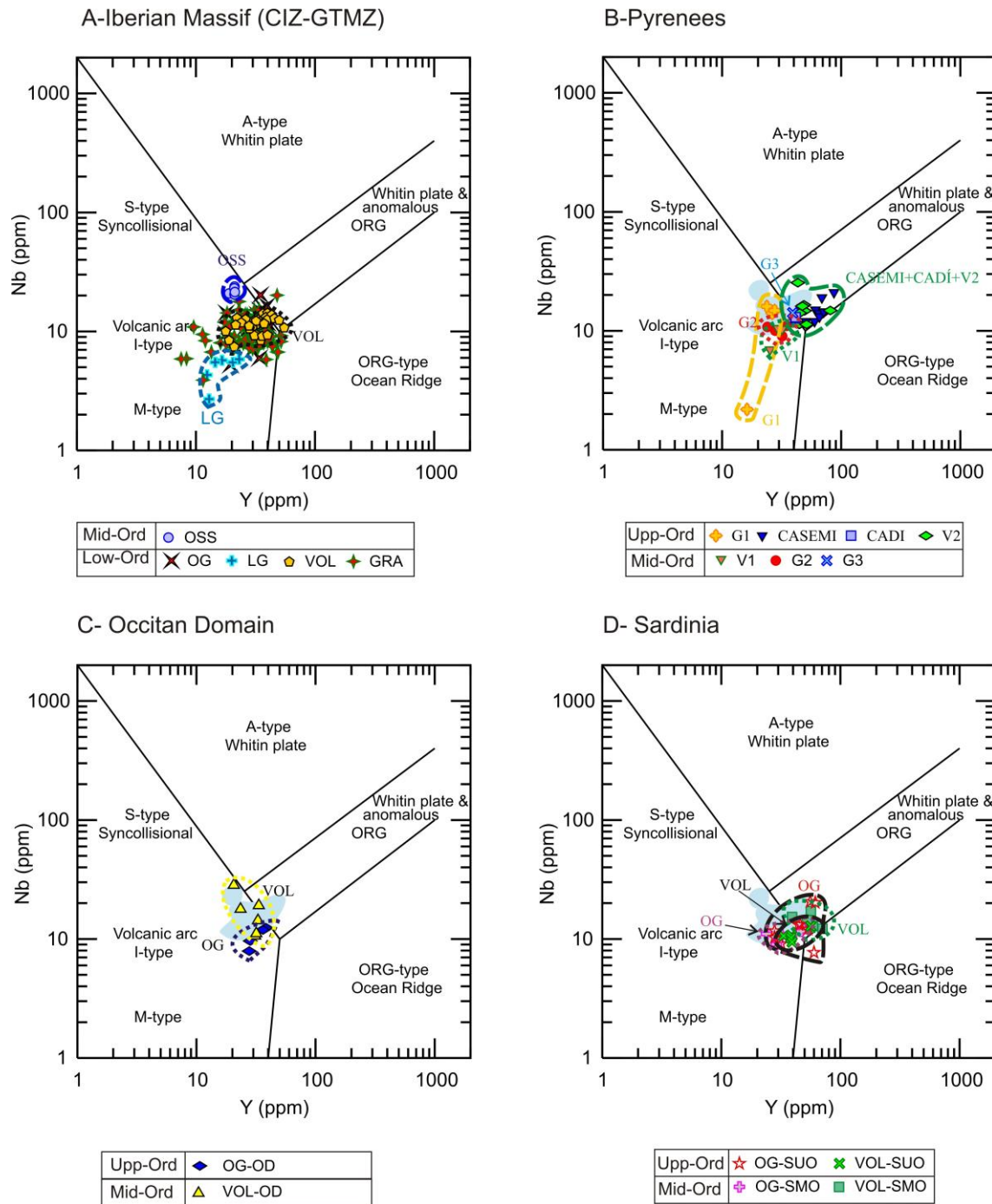


1725

1726

1727 **Figure 10.** Tectonic discriminating diagram of Zr vs. TiO<sub>2</sub> (Syme, 1998) for all study  
 1728 samples. Double-sided arrows indicate ranging of different fields: rhyolites in tholeiitic  
 1729 and calc-alkaline arc suites have Zr/TiO<sub>2</sub> ratios ranging from about 0.016 to 0.04, and  
 1730 extension-related rhyolites from about 0.13 to 0.28 (Syme, 1989).

1731

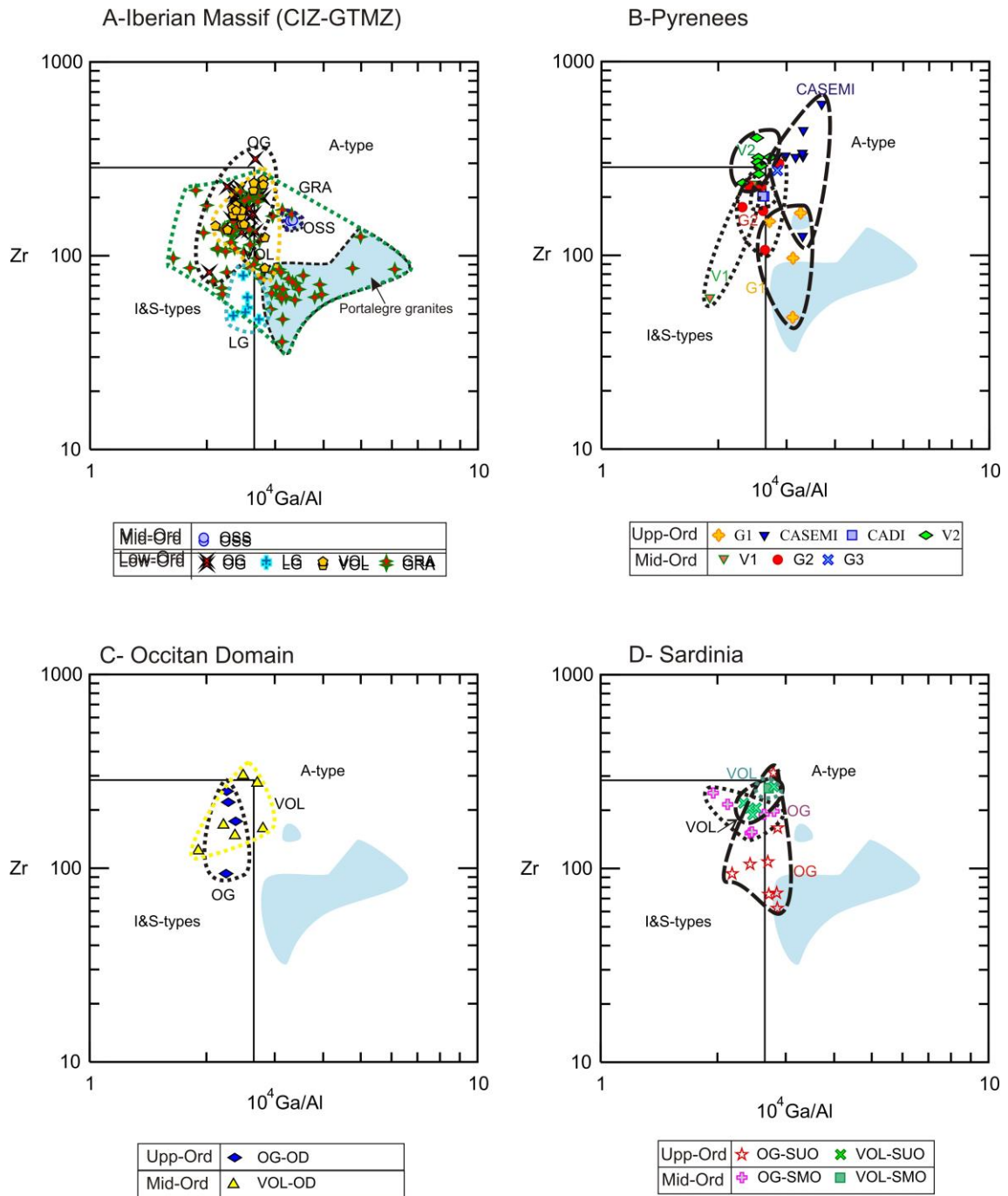


1732

1733 **Figure 11.** Tectonic discriminating diagram of Y vs. Nb (Pearce et al., 1984) for all  
 1734 study samples.

1735



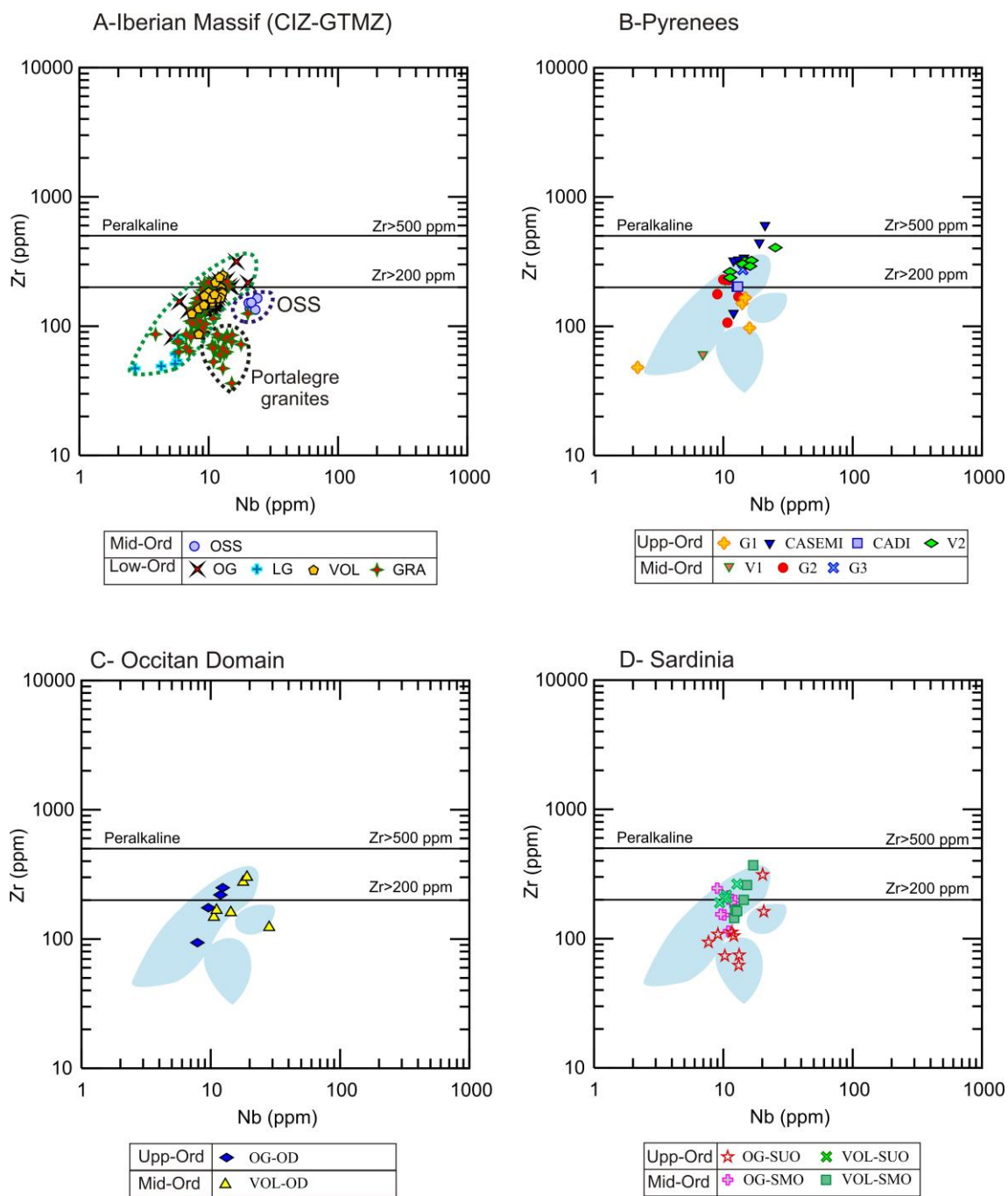


1736

1737

1738 **Figure 12.** Zr vs.  $10^4$  Ga/Al discrimination diagram (Whalen et al., 1987).

1739



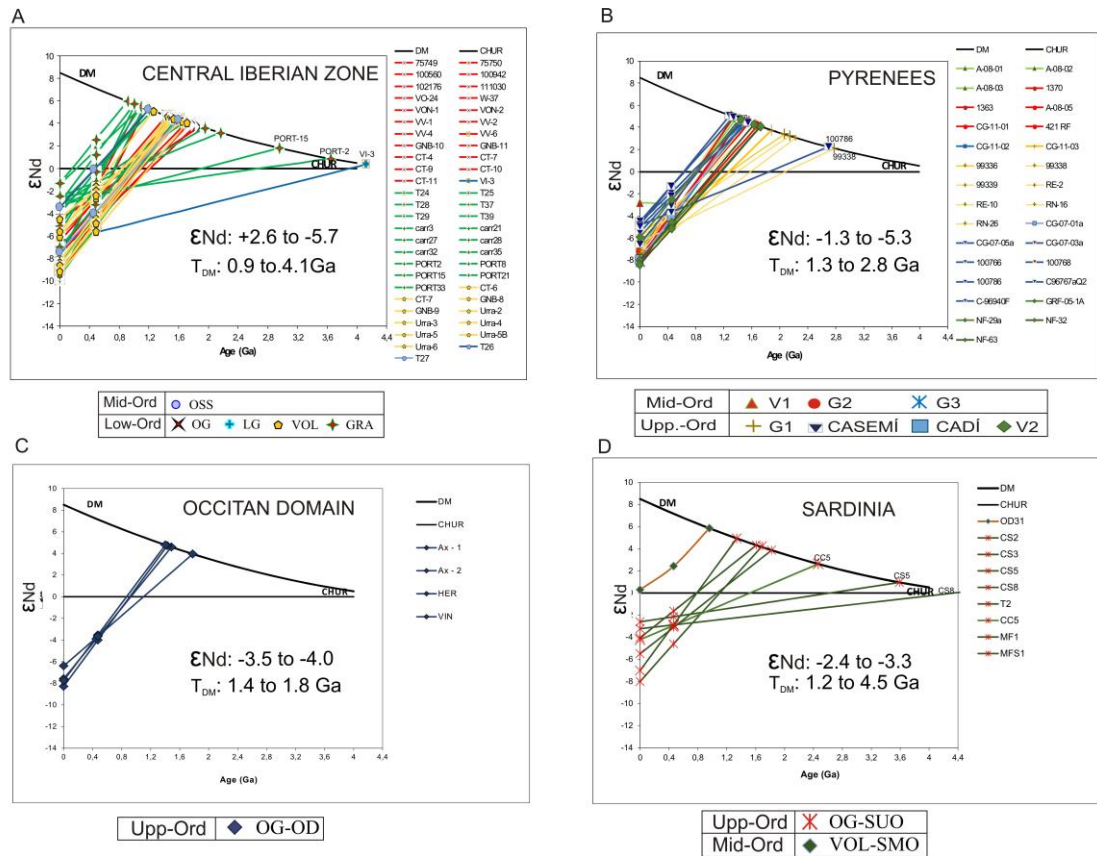
1740

1741

1742 **Figure 13.** Zr–Nb plot diagram (Leat et al.,1986; modified by Piercey, 2011) for all

1743 study samples.

1744



1745

1746

1747 **Figure 14.**  $\epsilon Nd(t)$  vs. age diagram (DePaolo and Wasserburg, 1976; DePaolo, 1981) for  
 1748 study sampled. A. Central Iberian and Galicia-Trás-os-Montes Zones. B. Eastern  
 1749 Pyrenees. C. Occitan Domain. D. Sardinia; see references in the text.

1750

Sample	PYRENEES			MONTAGNE NOIRE				SARDINIA									
	Albera	Pallaresa	Andorra	Axial Zone				External Zone						Inner Zone			
				Ax - 1	Ax - 2	HER	VIN	CC 5	CS 2	CS 3	CS 5	CS 8	MF 1	MFS 1	T 2	PB50	PB100
Long. (E)	3°7'39"	1°27'43"	1°33'29"	2°13'50"	2°33'58"	2°57'58"	2°13'50"	8°50'37"	8°50'35"	8°50'35"	8°50'40"	8°50'35"	8°50'47"	8°52'02"	8°48'54"	9°09'32"	9°09'32"
Lat. (N)	42°25'2"	42°36'1"	42°32'30"	43°34'32"	43°29'3"	43°34'32"	43°17'45"	38°54'16"	38°52'38"	38°52'38"	38°52'36"	38°52'39"	38°54'58"	38°53'57"	38°53'57"	41°11'1"	41°11'04"
SiO <sub>2</sub>	68.38	71.67	69.18	70.38	67.43	68.31	73.97	76.43	75.14	76.52	76.61	76.36	72.13	75.94	75.55	68.93	67.24
TiO <sub>2</sub>	0.57	0.63	0.61	0.36	0.64	0.61	0.20	0.08	0.08	0.09	0.04	0.06	0.31	0.13	0.18	0.41	0.46
Al <sub>2</sub> O <sub>3</sub>	15.68	14.24	15.05	14.90	15.76	15.39	13.82	13.28	12.81	11.80	12.71	12.63	13.80	13.16	12.94	16.32	15.79
Fe <sub>2</sub> O <sub>3</sub>	4.09	4.54	4.20	3.04	4.11	4.19	2.05	0.69	1.39	1.44	1.28	1.35	2.96	1.55	1.62	3.19	4.78
MnO	0.07	0.06	0.05	0.04	0.04	0.04	0.04	0.01	0.01	0.01	0.01	0.01	0.02	0.03	0.04	0.08	0.08
MgO	1.35	0.78	1.16	0.78	1.33	1.34	0.43	0.08	0.15	0.16	0.06	0.05	0.36	0.19	0.08	1.15	1.58
CaO	0.21	0.53	1.78	1.22	1.44	1.58	0.62	0.32	0.25	0.15	0.20	0.35	0.61	0.38	0.17	3.05	2.70
Na <sub>2</sub> O	4.07	1.67	3.40	3.33	2.78	2.93	2.87	3.04	1.71	1.58	2.91	3.35	2.89	2.57	2.53	3.85	3.43
K <sub>2</sub> O	2.84	2.91	2.71	4.35	4.68	4.03	4.55	4.79	7.84	7.43	5.16	4.91	5.47	4.94	5.36	2.26	2.96
P <sub>2</sub> O <sub>5</sub>	0.17	0.24	0.20	0.21	0.2	0.19	0.18	0.15	0.05	0.05	0.03	0.04	0.12	0.11	0.07	0.15	0.14
L.O.I.	2.03	2.60	1.50	1.2	1.3	1.2	1.2	1.1	0.4	0.7	0.9	0.8	1.1	0.9	1.4	0.90	0.70
Total	99.05	99.42	99.42	99.51	99.30	99.39	99.73	99.90	99.69	99.79	99.78	99.78	99.47	99.75	99.78	99.97	99.37
As	77.20	1.70	6.80	2.50	6.00	1.80	1.90	0.70	1.00	0.50	2.80	1.10	1.80	101.10	4.00	5.00	5.00
Ba	742.50	388.00	398.00	499	1050	767	256	60	467	109	21	27	784	194	192	689.00	600.00
Be	2.44	3.00	2.00	4.00	2.00	5.00	3.00	6.00	3.00	1.00	9.00	2.00	7.00	3.00	7.00	3.00	5.00
Bi	0.30	0.20	0.10	0.20	0.20	0.20	0.40	0.30	0.10	0.10	0.10	0.10	0.10	0.70	0.40	4.00	4.00
Cd	0.18	0.10	0.10	0.10	0.10	0.10	0.10	0.10	0.10	0.10	0.10	0.10	0.10	0.10	0.10	0.10	0.10
Co	5.84	4.60	6.20	5.20	5.20	5.40	2.70	0.50	1.60	1.00	0.80	0.60	2.30	1.50	1.20	5.00	14.00
Cs	9.79	5.60	4.90	14.30	7.10	6.80	7.30	4.20	3.40	1.60	4.50	4.60	6.40	3.90	4.10	4.20	9.40
Cu	16.34	13.20	10.30	7.20	7.40	10.10	8.70	4.70	4.60	8.20	26.80	2.50	5.00	5.50	5.00	10.00	60.00
Ga	21.03	19.80	18.80	19.10	19.20	18.90	16.70	19.30	14.90	15.30	19.40	19.20	20.70	19.00	19.90	17.00	18.00
Hf	6.40	7.30	6.40	5.00	6.90	5.70	3.10	3.10	4.10	4.30	3.50	3.80	8.80	3.70	5.80	5.90	5.30
Mo	1.20	0.90	1.00	0.60	0.90	0.60	0.30	0.70	0.70	0.70	0.80	0.50	1.70	0.80	1.60	2.00	2.00
Nb	10.49	11.30	11.30	9.60	12.40	11.90	7.90	10.30	7.70	12.10	13.20	13.30	20.20	9.10	20.60	9.00	11.00
Ni	16.56	8.00	7.70	20.00	20.00	20.00	20.00	20.00	20.00	20.00	20.00	20.00	20.00	20.00	20.00	20.00	80.00
Pb	7.94	9.80	22.90	3.50	4.60	5.10	3.60	2.90	7.40	8.60	4.50	5.50	5.10	6.30	5.50	21.00	24.00
Rb	124.40	123.70	137.20	204.6	161.6	142.2	188.2	289.9	206.1	187.4	294.1	275.1	208.7	256.4	227.1	85.00	118.00
Sb	2.27	0.10	0.30	0.10	0.10	0.10	0.10	0.10	0.10	0.10	0.10	0.10	0.10	0.10	0.10	5.00	5.00
Sc	10.00	10.00	10.00	6.00	9.00	9.00	4.00	3.00	3.00	4.00	4.00	4.00	15.00	4.00	8.00	9.00	12.00
Sn	2.11	5.00	5.00	9.00	3.00	3.00	7.00	9.00	4.00	3.00	13.00	15.00	7.00	15.00	12.00	3.00	3.00
Sr	158.00	201.80	83.70	91.20	160.30	150.10	68.70	30.70	73.90	25.20	7.90	8.10	59.90	45.60	25.00	217.00	167.00
Ta	1.07	1.10	1.10	0.80	1.00	0.80	0.70	2.10	0.90	1.10	3.40	1.70	1.60	1.70	2.30	1.00	1.20
Th	11.90	15.70	13.50	11.10	14.40	14.30	5.90	9.10	14.10	17.00	13.50	13.10	22.80	10.20	26.90	13.30	11.50
U	3.70	5.10	4.60	4.10	3.60	3.20	4.80	3.30	2.90	3.20	3.50	3.50	4.60	8.10	4.90	4.50	2.20
V	44.49	49.00	36.00	36.00	63.00	68.00	22.00	8.00	8.00	8.00	8.00	8.00	15.00	8.00	10.00	62.00	53.00
W	1.80	1.90	2.50	3.20	2.60	1.60	3.00	5.60	0.90	2.10	5.20	3.00	2.40	4.40	3.50	1.00	20.00
Y	29.29	43.90	50.60	28.30	38.40	36.20	27.80	28.00	60.10	53.60	44.40	46.00	61.60	31.80	55.80	29.00	24.00
Zn	63.71	52.00	70.00	55.00	71.00	78.00	46.00	7.00	35.00	39.00	15.00	24.00	37.00	30.00	22.00	70.00	70.00
Zr	233.30	263.20	237.10	174.40	249.20	219.10	93.70	73.50	93.80	105.10	62.20	74.50	311.80	108.10	161.90	245.00	214.00
La	27.90	45.30	38.00	29.60	39.50	38.70	13.60	10.50	22.70	19.50	12.10	13.40	54.20	17.90	31.30	26.90	34.30
Ce	59.00	86.90	75.50	58.10	77.00	78.20	26.70	21.60	42.10	39.70	26.20	29.90	109.80	37.40	97.60	53.20	70.50
Pr	7.26	9.80	8.47	6.99	9.41	9.55	3.36	2.36	4.73	4.85	3.00	3.24	11.94	4.07	6.86	5.88	8.20
Nd	27.83	35.60	31.20	26.00	36.40	36.40	12.60	8.40	16.60	17.10	10.50	10.90	44.70	15.00	24.00	21.60	29.40
Sm	5.80	7.69	7.16	5.70	7.55	7.63	3.15	2.43	4.10	4.41	3.28	3.44	9.37	3.88	4.93	4.70	6.00
Eu	0.98	1.05	1.03	0.87	1.27	1.15	0.41	0.14	0.43	0.13	0.06	0.09	1.17	0.30	0.19	0.95	0.93
Gd	5.22	8.32	7.89	5.59	7.28	7.05	3.38	3.20	5.60	5.50	4.42	4.69	10.60	4.50	6.34	4.00	5.10
Tb	0.87	1.26	1.27	0.89	1.17	1.10	0.67	0.69	1.13	1.18	1.03	1.07	1.70	0.82	1.27	0.70	0.80
Dy	5.30	6.68	8.00	5.09	6.89	6.39	4.59	4.30	7.69	8.23	7.31	7.66	10.28	5.24	9.00	3.70	4.30
Ho	1.06	1.52	1.73	0.99	1.42	1.30	0.98	0.91	1.91	1.91	1.59	1.65	2.13	1.12	2.01	0.70	0.80
Er	2.98	4.52	4.96	2.64	3.92	3.56	3.07	2.85	5.80	6.46	5.35	5.38	6.25	3.64	6.17	2.20	2.10
Tm	0.46	0.60	0.73	0.38	0.57	0.50	0.44	0.43	0.91	1.00	0.85	0.85	0.89	0.52	0.92	0.35	0.32
Yb	3.00	3.98	4.72	2.33	3.56	3.11	2.83	2.95	5.81	6.60	6.10	6.16	5.53	3.70	6.04	2.50	2.20
Lu	0.44	0.58	0.69	0.33	0.53	0.45	0.39	0.44	0.90	0.94	0.92	0.94	0.86	0.56	0.90	0.41	0.36

1751

1752 Table 1. Chemical analyses of magmatic rocks. ICP and ICP-MS methods at ACME-

1753 LABS in Canada.

1754

ORTHOGNEISS FACIES		code	composition	SiO <sub>2</sub> wt. %	Na <sub>2</sub> O wt. %	K <sub>2</sub> O wt. %	A/CNK ratio	εNd	TDM (Ga)	<sup>147</sup> Sm/ <sup>144</sup> Nd	area
<b>(1) Firingtara-Mid Ordovician Suite</b>											
CIZ - Olo de Sapo orthogneiss	OG	K-rich dacite to rhyolite	75-60.3	3.9-0.1	5.9-3.4	3.1-1.0		-5.1 to -1.8	1.8-1.1	0.15-0.09	Sanabria (ca. 472 Ma) and Guadarrama (ca. 488-473 Ma)
CIZ - Leucogneiss	LG	K-rich dacite to rhyolite	75.9-73.6	3.1-2.7	5.3-4.2	1.3-1.1		-5.1 to -4.9	4.1	0.22-0.18	Guadarrama
CIZ - Metagranite	GRA	K-rich dacite to rhyolite	77-64.6	4.8-0.5	6.3-2.5	1.8-1.0		-5.2 to +2.6	3.6-0.9	0.19-0.09	NE Central System, Sanabria, Miranda do Douro (ca. 496-473 Ma), CIZ (496-471 Ma for Carrascal, Fermoselle, Ledesma, Portalegre and Vitigudino granites)
CIZ/GTMZ - Volcanic rocks	VOL	andesite to rhyolite	79.3-64.6	3.2-0.1	6.3-2.2	2.7-1.1		-5.5 to -1.6	1.7-1.3	0.15-0.13	Saldanha Fm. in GTMZ, Olo de Sapo Fm. in Sanabria, and Urta Fm.
CIZ - San Sebastián orthogneiss	OSS	rhyolite	75.4-73.8	3.1-2.5	5.4-4.9	1.2-1.1		-4.0 to 0	1.6-1.2	0.14-0.14	Sanabria (ca. 470-465 Ma)
PYR - augengneiss	G2*	dacite to rhyolite	73.6-68.3	3.9-3.2	4.4-2.5	1.2-1.1		-4.4 to -3.0	1.4-1.2	0.14-0.13	ca. 476-462 Ma
PYR - orthogneiss	G3*	K-rich dacite	73.5-68.4	2.9-2.4	4.4	1.2		-4.2	1.33	0.13	ca. 463 Ma
PYR - volcanic rocks	V1	Na-rich rhyolite	73.5-68.4	7.8-2.4	3.2-1.3	2.0-1.1		-5.1 to -2.6	1.7-1.6	0.19-0.13	Pierreffe Fm. and Albera massif (ca. 472-465 Ma)
OCC - volcanic rocks	VOL-OD	K-rich dacite to rhyolite	75.6-66.7	3.7-0.6	9.3-2.3	2.4-1.3					Saint-Serrin-sur-Rance and Saint-Salvi-de-Carcavés nappes
SAR - orthogneiss	OG-SMO	K-rich rhyolite	74-67.2	3.8-2.6	5.8-2.3	1.3-1.1					ca. 469 Ma
SAR - volcanic rocks	VOL-SMO	K-rich dacite to rhyolite	76.7-67.6	4.7-1.9	5.4-2.9	2.0-1.2				0.16	ca. 464-462 Ma
<b>(2) Upper Ordovician Suite</b>											
PYR - orthogneiss	G1*	K-rich dacite to rhyodacite	76.4-73.4	3.1-2.6	5.3-4.7	1.2-1.1		-5.3 to -3.1	2.7-1.5	0.17-0.12	ca. 457 Ma
PYR - orthogneiss	CADI	K-rich dacite to rhyodacite	69.4	3	4	1.2		-4.1	1.5	0.13	Cadi massif (ca. 456 Ma)
PYR - orthogneiss	CASEMI	K-rich dacite to rhyodacite	76-71.9	4-1.8	6.3-3.2	1.2-0.9		-3.6 to -1.3	2.6-1.3	0.17-0.13	Casemi massif (ca. 451-446)
PYR - volcanic rocks	V2	andesite to rhyodacite	86.1-63	6-0	4.3-0.6	3.6-1		-5.1 to -2.6	1.7-1.6	0.14-0.14	Ribes de Friese, Andorra (ca. 457 Ma), Pallaresa (ca. 453 Ma), Els Meigs (ca. 455.2 Ma)
OCC - orthogneiss	OG-OD	K-rich dacite to rhyolite	73.9-67.4	3.3-2.8	4.7-4	1.3-1.2		-4 to -3.5	1.8-1.4	0.15-0.13	Gorges d'Héric (ca. 450 Ma, Caroux), S Mazamet (Nore), S Rouairoux (Agout), Le Vnitrou
SAR - External Zone orthogneiss	OG-SUD	K-rich dacite to rhyolite	76.6-72.1	3.3-1.6	7.8-4.8	1.3-1.1		-3.3 to -1.6	4.2-1.2	0.19-0.12	Capo Spartivento, Cuile Culurgioni, Tuerredda, Monte Filau, Monte Settblas (ca. 458-457 Ma)
SAR - Nappe Zone volcanic rocks	VOL-SUD	K-rich dacite to rhyodacite	76.7-70.7	3.3-1.6	7.8-4.8	1.3-1.1					Truzzulla Fm. at Monte Grighini

1756 **Table 2.** Summarized geochemical features of the Furongian and Ordovician felsic  
1757 episodes described in the text; data from Lancelot et al. (1985), Calvet et al. (1988),  
1758 Valverde-Vaquero and Dunning (2000), Roger et al. (2004), Vilà et al. (2005),  
1759 Giacomini et al. (2006), Díez-Montes (2007), Montero et al. (2007, 2009), Solá (2007),  
1760 Zeck et al. (2007), Castiñeiras et al. (2008b), Talavera (2009), Casas et al. (2010),  
1761 Navidad et al. (2010, 2018), Liesa et al. (2011), Martínez et al. (2011, 2018), Navidad  
1762 and Castiñeiras (2011), Gaggero et al. (2012), Talavera et al. (2013), Villaseca et al.  
1763 (2016), Pouclet et al. (2017), Cruciani et al. (2018) and this work. Abbreviations: *CIZ*  
1764 Central Iberian Zone, *GTOMZ* Galicia-Trás-os-Montes Zone, *OCC* Occitan Domain,  
1765 *PYR* Pyrenees and *SAR* Sardinia; \* *sensu* Guitard (1970); *A/CNK* ratio is always  
1766 peraluminous.

1767